TÉCNICO LISBOA

CO_2 Separation using Polymeric Ionic Liquids Membranes: the effect of mixing different Cyano Anions

Raquel Marinho Teodoro dos Santos

Thesis to obtain the Master of Science Degree in

Biological Engineering

Supervisor(s):
Prof. Dr. Isabel Maria Delgado Jana Marrucho Ferreira
Prof. Dr. Frederico Castelo Alves Ferreira

Examination Committee

Chairperson: Prof. Dr. Duarte Miguel de França Teixeira dos Prazeres
Supervisor: Prof. Dr. Isabel Maria Delgado Jana Marrucho Ferreira
Members of Committee: Prof. Dr. Eduardo Jorge Morilla Filipe

June 2016

Acknowledgments

To all the people that somehow helped me to elaborate this work: my supervisors Dr. Isabel Marrucho and Liliana Tomé, my laboratory colleagues Andreia, Catarina and David, my family (mom, dad and sister) and all my friends (specially Vitas and Cullen).

“It is not our abilities that show what we truly are. It is our choices.”

Harry Potter and the Chamber of Secrets

I. Abstract

In order to reduce CO_2 emissions and further prevent air pollution and global warming, sustainable and efficient CO_2 separation processes must be developed. Membrane-based technologies represent a simple and environmental friendly alternative to traditional CO_2 separation methods. In the last years, polymeric ionic liquid (PIL) membranes have received enormous attention from the scientific community since they combine the benefits of membrane technology with the unique proprieties of ionic liquids (ILs).

In this work, several PIL-IL composite membranes were prepared and their gas permeation properties measured. Both PIL and IL have cyano-functionalized ($[N(CN)_2]^-$, $[C(CN)_3]^-$ or $[B(CN)_4]^-$) or $[NTf_2]^-$ counter anions, with the anions of the PIL and IL being different from one another. The four synthesized PILs used have a pyrrolidinium polycation backbone, while the five ILs have an imidazolium ($[C_2mim]^+$) or a pyrrolidinium ($[Pyr_{14}]^+$) based cation. Several experimental conditions were tested in order to achieve the maximum number of homogenous and free standing PIL-IL composite membranes possible. The CO_2 and N_2 separation properties (permeability, diffusivity and solubility) of suitable membranes were evaluated at a fixed temperature (20 ºC) and constant trans-membranar pressure differential (100 kPa) using a time-lag method, so that trends regarding the different counter anions could be evaluated.

From all 42 PIL-IL composite membranes prepared, 21 were suitable for gas permeation experiments and 3 surpassed the 2008 Robeson upper bound for CO_2/N_2 separation performance. These high performance membranes contain $[C(CN)_3]^-$ and $[B(CN)_4]^-$ counter anions, enlightening the promise these anions entail for fabrication of high CO_2 separation performances membranes.

Keywords: CO_2 Separation, Ionic Liquids, Polymeric Ionic Liquids, Composites, Cyano-based Anions, Gas Permeation

II. Resumo

Processos eficientes e sustentáveis para a separação de CO_2 devem ser desenvolvidos de modo a reduzir emissões de CO_2, prevenindo a poluição do ar e aquecimento global. As tecnologias baseadas em membranas constituem uma alternativa simples aos métodos tradicionais de separação de CO_2. Tendo recebido atenção nestes últimos anos, as membranas poliméricas de líquidos iónicos (PILs) combinam as vantagens da tecnologia de membranas com as propriedades únicas dos líquidos iónicos (LIs).

Neste trabalho, várias membranas compósitas PIL-LI foram preparadas. Ambos o PIL e o LI têm aniões funcionalizados com grupos ciano ($[N(CN)_2]^-$, $[C(CN)_3]^-$ or $[B(CN)_4]^-$) ou $[NTf_2]^-$, sendo os aniões no PIL e no LI diferentes ente si. Os quatro PILs usados têm um policatião de pirrolidinio, enquanto que os cinco LIs têm um catião imidazólio ($[C_2mim]^+$) ou pirrolidinio ($[Pyr_{14}]^+$). Diferentes condições experimentais foram testadas para obter o maior número possível de membranas homogéneas e estáveis. Para estas últimas mediram-se as propriedades de transporte do CO_2 e N_2 (permeabilidade, difusão e solubilidade), a uma temperatura e diferencial de pressão trans-membranar constantes (20ºC e 100 kPa), usando um método de time-lag, de modo a avaliar tendências para os diferentes aniões.

Das 42 membranas PIL-IL compósitas preparadas, 21 foram consideradas aptas para efectuar estudos de permeação de gás e destas últimas, 3 superaram o Robeson upper bound de 2008 para a separação CO_2/N_2. Estas membranas de alta performance contêm os aniões $[C(CN)_3]^-$ e $[B(CN)_4]^-$, ilustrando assim o seu uso promissor na fabricação de novas membranas de alta performance para separação de CO_2.

Palavras-Chave: Separação de CO_2, Líquidos Iónicos, Polímeros de Líquidos Iónicos, Compósitos, Ciano, Permeação de Gases

III. Table of Contents

IV. List of Figures

V. List of Tables

VI. List of Abbreviations

IL	Ionic Liquid
PIL	Polymeric Ionic Liquid
CCS	Carbon Capture Storage
IGCC	Integrated Gasification Combined Cycle
CLC	Chemical looping combustion
MOF	Metal Organic Framework
T_g	Glass Transition Temperature
MMM	Mixed Matrix Membrane
RTIL	Room Temperature Ionic Liquid
TSIL	Task Specific Ionic Liquid
SILM	Supported Ionic Liquid Membrane
$[NTf_2]^-$	Bis(trifluoromethylsulfonyl)imide
$[N(CN)_2]^-$	Dicyanamide
$[C(CN)_3]^-$	Tricyanomethane
$[B(CN)_4]^-$	Tetracyanoborate
$[C_2mim]^-$	1-Ethyl-3-Methylimidazolium
$[Pyr_{14}]^+$	1-Butyl-1-Methylpyrrolidinium
DMSO	Dimethylsulfoxide
DMF	Dimethylformamide
PTFE	Poly(tetrafluoroethylene)

VII. List of Symbols

$\boldsymbol{J}$	Gas Flux
$\boldsymbol{\Delta p}$	Pressure Difference
$\boldsymbol{l}$	Thickness
$\boldsymbol{P}$	Permeability
$\boldsymbol{D}$	Diffusivity
$\boldsymbol{S}$	Solubility
$\boldsymbol{C}$	Gas Concentration
$\boldsymbol{p}$	Gas Pressure
$\boldsymbol{\alpha_{i/j}}$	Permselectivity
$\boldsymbol{n}$	Upper Bound Slope
$\boldsymbol{\theta}$	Time-Lag
$\boldsymbol{M}$	Molecular Weight
$\boldsymbol{\eta}$	Dynamic Viscosity
$\boldsymbol{\rho}$	Density
$\boldsymbol{V_M}$	Molar Volume

1. Introduction

1.1 Motivation

Since the industrial revolution until the present time there has been an increased need for electricity generation and consumption. Despite the existence of cleaner alternative energy sources, fossil fuels are still the world's primary energy source and are expected to remain so for the next couple of years. One concern of the burning of these fuels is the emission of anthropogenic carbon dioxide (CO_2) which, in turn, is largely responsible for air pollution and global warming.[1] The consequences of global warming consist of several environment problems including enhancement of heat stress, increased number of diseases, severity of tropical storms, ocean acidity, melting of glaciers, snow pack and sea ice, as well as harm to ecosystems and animals habitats.[2]

One of the solutions proposed to reduce the emission of CO_2 to the atmosphere consist of Carbon Capture and Storage (CCS) systems. While being a short term solution, CCS systems represent the most promising solution to deal with the steep rising of anthropogenic CO_2 emissions, while humanity tries to come up with efficient and cost effective technologies for energy production that can compete with fossil fuels. Carbon Capture and Storage systems can be defined as a set of technologies that allow the capture of CO_2 emitted from the burning of fossil fuels in power plants (like coal and natural gas), as well as from other industrial processes such as cement, iron and steel manufacture. After the separation of the CO_2 at these point sources, the gas is then pressurized in order to be transported to a storage site. These sites are carefully selected in geological formations (like depleted oil fields or deep saline aquifers), where the CO_2 is injected, usually several kilometers below the surface of the earth, and where it remains trapped, therefore preventing the emission of the gas to the atmosphere.[3,4] Although CO_2 transportation and storage present some technological and economic challenges, it is the capture of CO_2 that still needs an additional effort in research and development so that alternative economic, energetic and environmental viable methods can be implemented.[5]

Another example of CO_2 separation occurs in natural gas and biogas processing prior to its transport and use (Table 1). Natural gas and biogas, before being transported through pipelines, must abide to pipeline specifications in order to reduce corrosion in the pipes and other equipment. For this purpose, and also to upgrade (increase methane concentration) the gas stream, especially in the case of biogas, methane must be separated from CO_2, which is a common contaminant.[6]

These different processes involve streams with distinct gas compositions (Table 1), as well as different temperature and pressure conditions. Consequently, the efficient separation of CO_2 from other gases, namely methane (CH_4), nitrogen (N_2) and hydrogen (H_2), represents a major technical, economic and environmental challenge. Since power plants are unquestionably the major source of anthropogenic CO_2, the majority of the studies addresses power plant CO_2 streams conditions. Within a power plant, four main strategies for CO_2 capture have been proposed, depending on the different

point sources: pre-combustion, post-combustion, oxy-fuel combustion and chemical looping combustion.[3, 4] A detailed analysis of these four approaches follows next.

Table 1 - Typical gas stream compositions of CO_2 separation processes.

Natural Gas and Biogas	Pre-Combustion	Oxy-Fuel Combustion	Chemical Looping Combustion	Post-Combustion
CO_2/CH_4	CO_2/H_2	CO_2/H_2O	CO_2/H_2O	CO_2/N_2

1.1.1 Pre-Combustion Capture

In this approach, CO_2 is removed before combustion takes place (Figure 1). First, the fuel is reacted with oxygen or air, at high pressure and temperature, resulting in a stream mainly composed of H_2 and carbon monoxide (CO). This stream is often called synthesis gas or syngas. The syngas enters a catalytic reactor, entitled a shift reactor, where CO reacts with steam resulting in a stream composed of CO_2 and H_2. These two gases are then separated resulting in a hydrogen rich stream, which can later be used in numerous applications, including chemical feedstock for other industries processes or for power generation using fuel cells or turbines.

The main advantage of this approach is the reduced energy capture penalty of the process (±20%) when compared with post-combustion capture (±30%).[7] The high pressure of the stream that leaves the shift reactor, as well as its high concentration in CO_2, allows for the reduced energy capture penalty of the process. The gas stream conditions of pre-combustion also allow for a more favorable CO_2 separation. Despite its advantages, this approach has fuel conversion steps more complex and expensive than in post-combustion systems. Although pre-combustion systems are already employed in some Integrated Gasification Combined Cycle (IGCC) power plants, introducing them in already existing power plants is more complex and costly than the implementation of post-combustion systems.[8]

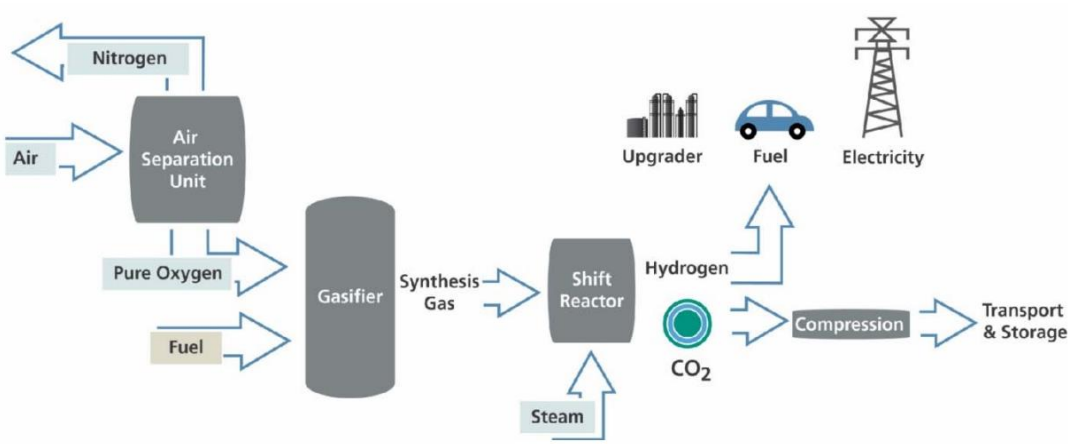

Figure 1 – CO_2 capture in pre-combustion processes.[68]

1.1.2 Oxy-Fuel Combustion

In power plants, where oxy-fuel or oxy-firing combustion is employed, the fuel is combusted in the presence of nearly pure oxygen (O_2), instead of ambient air (Figure 2). Recycling CO_2 from the combustion reactor allows, to some extent, to overcome the high flame temperature required in pure oxygen combustion. Due to the absence, or very low concentration, of nitrogen, a stream with high concentration of CO_2, along with water (H_2O), is obtained. This stream is then cooled and compressed in order to condense and remove water, resulting in a very pure (high concentration) CO_2 stream.

One of the most critical steps of this capture method is the separation of ambient air into its two main components, O_2 and N_2. Four main technologies have been used for this separation namely, polymeric membranes and molecular sieves, oxygen production by chemical air separation, high temperature ceramic membranes and cryogenic air separation. The last is currently the most used method in the industry.

One of the main advantages of this technology is the high concentration and pressure of CO_2 in the stream resulting from the combustion reactor, whose conditions facilitate the CO_2 separation from water. Consequentially, a very pure CO_2 stream suitable for further processing (transport and storage) can be obtained. The main disadvantage is the significant high energy demand, as well as high capital cost of the air separation techniques.[5, 7]

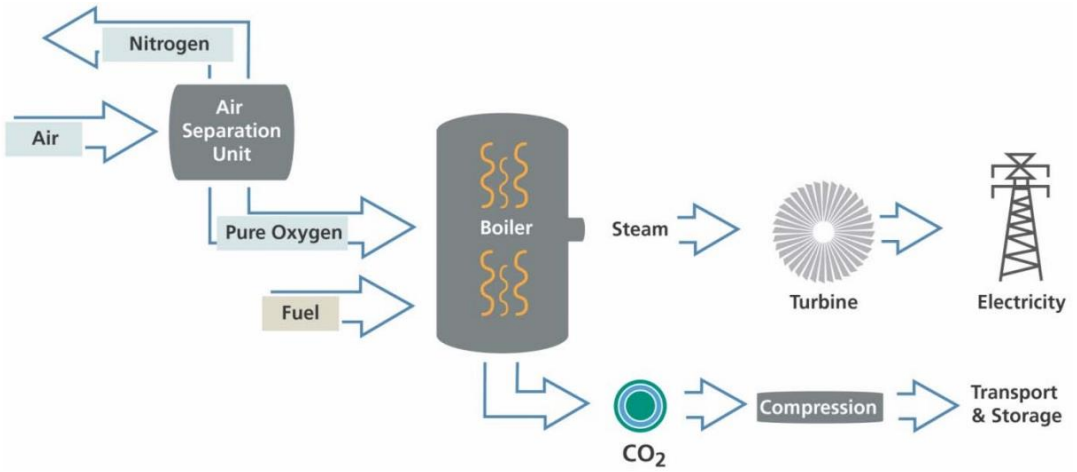

Figure 2 - CO_2 capture in oxy- fuel combustion processes.[68]

1.1.3 Chemical Looping Combustion

Chemical looping combustion (CLC) is a new emerging technology, suggested in 2000 by the CO_2 Capture Project as one of the best alternatives to reduce the cost of CO_2 capture.[9] Both gaseous and solid fuels have already been tested for this emerging process.

In CLC processes direct contact between fuel and air is avoided through the use of a solid oxygen carrier (Figure 3). This solid carrier acts as the intermediary between the fuel and air by caring

oxygen, which then reacts with the fuel. Several materials based on metals Ni, Cu, Fe, Mn and Co have been used as solid oxygen carriers. Other mixed oxides and cheap materials have also been tested.

The first step of CLC consists on the oxidation of the fuel to CO_2 and H_2O by means of reduction of the solid oxygen carrier, usually a metal oxide (MeO is reduced to Me). The stream obtained after combustion is mostly composed by CO_2 and H_2O. Just like in oxy-fuel combustion, H_2O is removed by cooling and compressing the stream, leading to water condensation and resulting in a stream with a high concentration of CO_2. In the second step, the previously reduced metal is now oxidized when in contact with air (Me is oxidized to MeO) and is ready to be used in another CLC cycle. The stream obtained in this step consists of N_2 and O_2 that did not react in the first step.

The separation of CO_2 from H_2O is relatively simple and, just like in oxy-fuel combustion, obtaining a stream with mostly these two components (after combustion) is a huge advantage. In the end, a high concentrated CO_2 stream is obtained, which is ready for transport and storage.

The main disadvantages of this method are related with the high cost of the metal solid oxygen carriers. Being a relatively new technology, more research is needed to find suitable solid oxygen carriers that can balance the cost of raw materials, preparation and lifetime, with the environmental costs.[9]

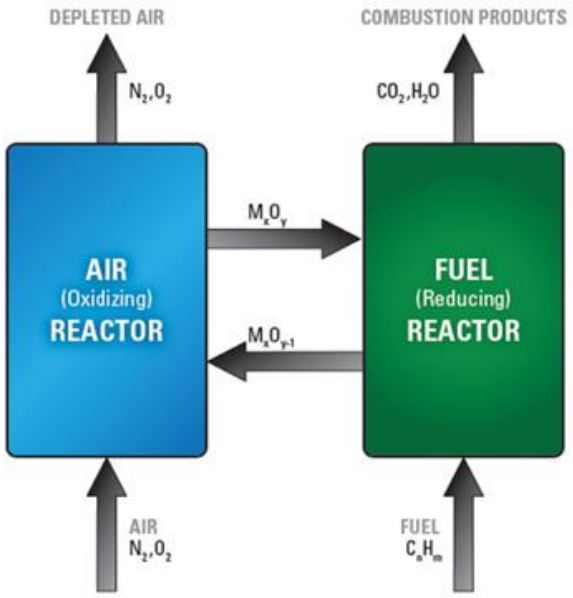

Figure 3 - CO_2 capture in chemical looping combustion processes.[69]

1.1.4 Post-Combustion Capture

In this approach, the CO_2 is removed after combustion of fossil fuels (Figure 4). The obtained stream is composed primarily by N_2, with CO_2 present in low concentration, which are then separated. The main advantage of post-combustion systems is the maturity of this technology and its easiness to retrofit in already existing power plants. However, the low pressure of the post-combustion resulting

stream does not facilitate CO_2 separation. This stream also has a high volume, due to the unreacted N_2, which is another disadvantage of this process.[7]

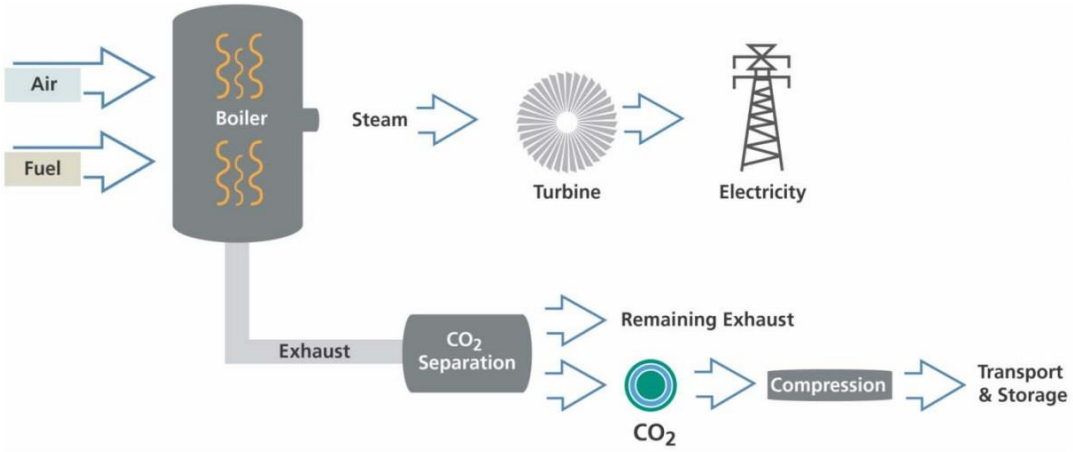

Figure 4 - CO_2 capture in post-combustion processes.[68]

Since in post-combustion systems, new technologies can more easily be retrofitted in already existing power plants, this work will focus on the CO_2/N_2 gas pair separation. The disadvantages associated with post-combustion processes, especially the high energy requirement for solvent regeneration of current CO_2/N_2 separation technologies, prompt for new and more energy efficient solutions for this gas pair separation.

1.2 Main CO_2 Separation Technologies

Different CO_2 emission point sources lead to different stream's conditions and compositions. The diversity of CO_2 streams demands for the development of efficient and sustainable separation technologies. Among all the technologies used so far for CO_2 separation, four stand out as the most relevant: solvent chemical absorption, psychical/chemical adsorption, cryogenic distillation and membranes. A more detailed analysis of each one follows next.

1.2.1 Absorption

In this process, the gas stream comes into contact with a liquid phase, usually named solvent or absorbent. The different gases that compose the gas stream are selectively dissolved in the solvent by mass transfer (Figure 5) via chemical or physical interactions. The solvent is later regenerated by means of a stripping column and the CO_2 stream is released. Several absorbents exist, but only four are largely employed at the industrial level: amines, aqua ammonia, dual-alkali and sodium carbonate. From these four, absorption using amines is the preferred technology in post-combustion processes. Amine absorption is a highly efficient and mature technology to process streams with low CO_2 partial

pressure. However, the amines employed require high energy for regeneration, are volatile and will eventually degrade and corrode the equipment over time.[10]

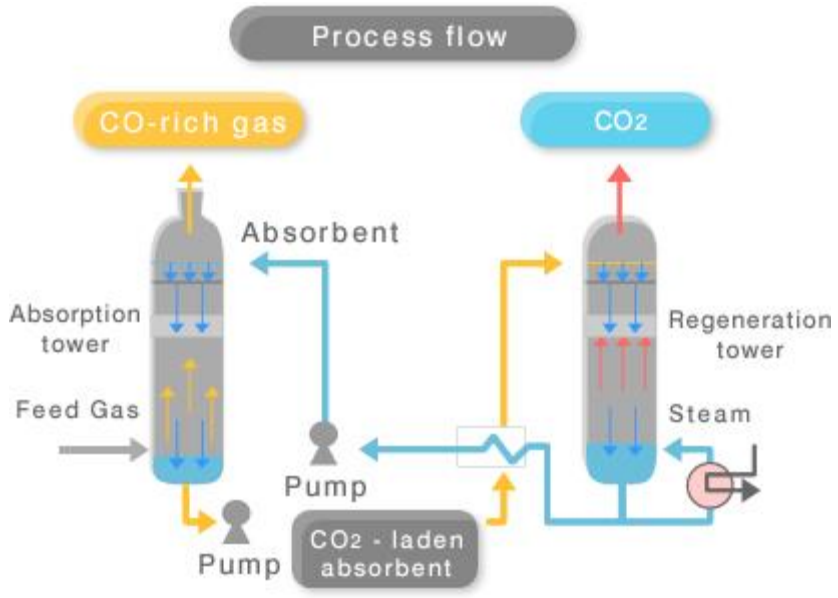

Figure 5 - Schematic representation of absorption used for CO_2 separation.[70]

1.2.2 Adsorption

In this process, the gas stream comes into contact with a solid material, usually named adsorbent. Weak physical interactions or strong chemical interactions, depending on the adsorbent used, selectively adsorb the different gases that compose the gas stream (Figure 6). The adsorbent is then regenerated by pressure swing, temperature swing or electrical swing adsorption and the CO_2 is desorbed. Typical materials used as adsorbents include zeolites (like aluminosilicates), activated carbons, metal organic frameworks (MOFs) and amine functionalized adsorbents. Solid sorbents are more environmental friendly and can be used with a wider temperature range than liquid sorbents. They are also not corrosive, require lower energy for regeneration and are fairly easy to operate. Despite all this, additional cost reduction and improved stability and selectivity is needed for these materials to become a reality in industrial CO_2 separation.[11]

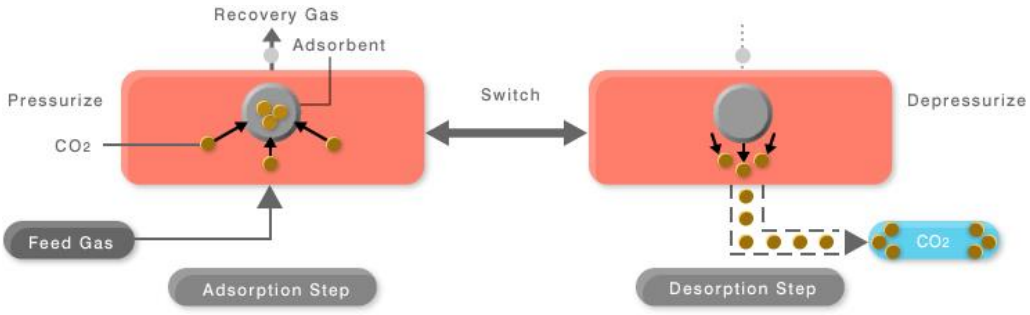

Figure 6 - Schematic representation of adsorption used for CO_2 separation.[70]

1.2.3 Cryogenic Distillation

Cryogenic distillation makes use of extreme low temperatures, usually around -110 ºC, to cool and condensate CO_2. Other light gases, like N_2, do not condensate under these conditions and thus the different gas components of the stream are separated. Despite being a relatively new CO_2 separation technology, cryogenic distillation has been used to separate air into O_2 and N_2 for years. The absence of chemical absorbents is the main advantage of this process. However, the use of refrigerants and the low temperatures employed require high energy and high costs. Also, in order to avoid formation of ice, and consequently plugging and decrease in the efficiency, traces of water must also be removed during this process, which accounts for a large increase operational costs.[10]

1.2.4 Membranes

A membrane can be defined as a thin and discrete interface which regulates permeation of different chemical species (in this case gases) that interact with it. The differences in physical and/or chemical interactions between these chemical species and the membrane allow for the selective permeation of certain chemical species in detriment of others (Figure 7). Membranes can be divided into porous or non-porous, which discern gases through different mechanisms. Non-porous (or dense) membranes have interfaces that are uniform in both structure and composition and its separation ability follows the sorption-diffusion mechanism. On the contrary, porous membranes present a heterogeneous interface. These membranes can have, for example, pores or holes that separate gases according to their size (molecular sieving mechanism). Because of its simplicity, membranes have many benefits including reduced environmental impact, low operation costs and energy requirements, small scale of equipments and easiness of integration into already existing processes.[15] Taking into account the material they are made off, membranes can be classified into one of three categories: inorganic, organic or inorganic-organic composites.[12]

Inorganic membranes comprise ceramic, metallic and silica membranes, carbon molecular sieves, zeolites and MOFs. They possess great advantages such as high thermal and chemical stability, high selectivity and resistance to harsh environments (like high pressure). However, they have some drawbacks like complex and expensive fabrication procedures and high brittleness.[13]

Organic membranes, also known as polymeric membranes, can either be glassy or rubbery depending on their glass transition temperature (T_g) relative to working temperature. For glassy polymers, the T_g value is higher than the working temperature value, which makes these membranes structurally rigid.[14] The majority of commercially available membranes are polymer based and for CO_2 separation applications most have glassy characteristics. Applications regarding CO_2 separation, using commercially available membranes, include post-combustion (CO_2/N_2), pre-combustion (CO_2/H_2) and biogas (CO_2/CH_4) separation.[12] Their high selectivity and enhanced mechanical properties make these glassy polymeric membranes advantageous and some of the commercial available membranes include polyamides, polycarbonates, polyimides and others. Rubbery polymers

have a T_g value lower than the working temperature, which grants them rubber/elastic like features. These polymers usually have higher gas permeability but lower selectivity.[14] The already existence of commercially available polymer membranes reflects the great potential of these materials for CO_2 separation. However, CO_2 separation efficiency requires improvement in order to compete with well-established technologies like amine absorption. The combination of these polymer membranes with new and promising materials like ionic liquids (ILs) holds a great promise for CO_2 capture technologies with competitive CO_2 separation efficiencies.

Inorganic-organic composite membranes, also known as mixed matrix membranes (MMMs), combine the benefits of polymeric membranes, like flexibility, with the benefits of inorganic membranes, like enhanced separation efficiency, and are a recent alternative to enhance polymer membranes properties. A typical MMM has a dispersed inorganic particle phase embebed within a continuous polymer phase.[16] Major drawbacks for the use of MMMs include defects in the organic-inorganic interface, which lead to lower gas selectivities, and also the lack of information on their manufacture resulting in difficult and expensive fabrication methods.[17]

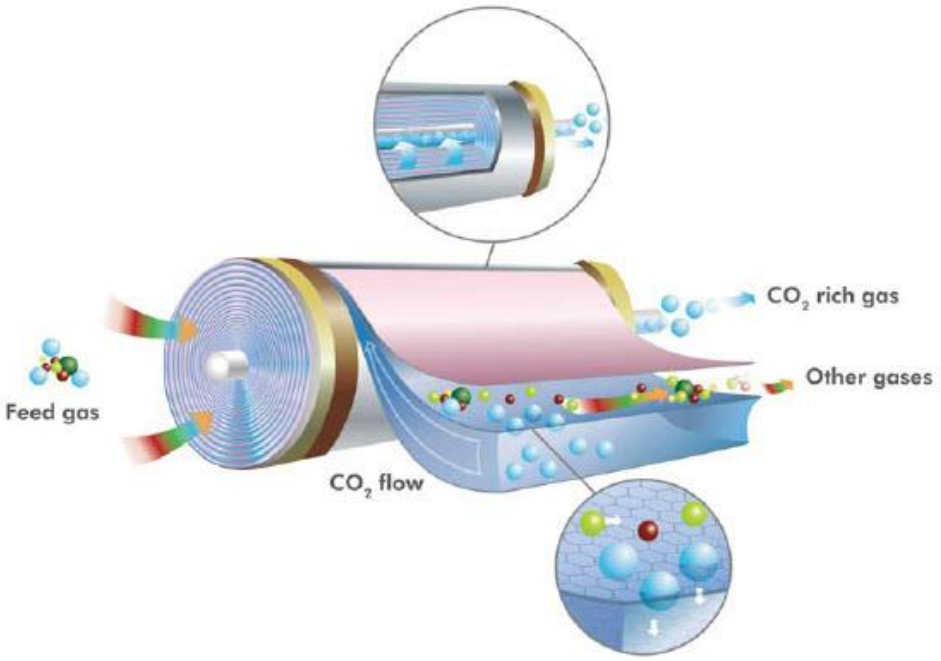

Figure 7 - Schematic representation of membrane CO_2 separation.[43]

Due to the advantages presented by membrane´s processes, this work focuses on the fabrication of polymer based membranes and the evaluation of their CO_2/N_2 separation performances. Consequently, from here on, a discussion on the mechanism that governs gas transport in dense membranes will be presented, followed by a literature review on the materials used for membrane´s fabrication.

1.3 Gas Transport in Dense Membranes

Non-porous (or dense) membranes separate gases through the solution-diffusion mechanism. Adolph Fick's law of diffusion, which relates the diffusion flux of a substance to that substance concentration gradient across a certain length, is the basis for this solution-diffusion model first mentioned in 1866.[14] The concepts used to describe gas transport in dense membranes and evaluate their performance are illustrated and discussed below.

1.3.1 Permeability, Diffusivity and Solubility

Gas permeability (Eq.1) of a pure gas passing through a dense membrane is defined as the thickness normalized steady-state gas flux (J) under a transmembrane pressure difference ($\Delta p = p_1 - p_2$):

$$P = J\frac{l}{\Delta p} \quad (1)$$

where l is the membrane thickness and p_2 and p_1 are the upstream and downstream pressure, respectively. Permeability is a propriety of the membrane material and is usual to express it in Barrer (Eq.2):

$$1\ Barrer = \frac{10^{-10} cm^3\ (STP)\ cm}{cm^2\ s\ cmHg} \quad (2)$$

Gas permeability (Eq.3) reflects the ability of a gas to permeate the membrane. According to the solution-diffusion model, gas permeability is the product of gas diffusivity (D) and solubility (S) across that membrane:

$$P = S \times D \quad (3)$$

Diffusivity is usually expressed in $cm^2.s^{-1}$ and it accounts for the gas ability to move through the membrane material. Several properties of the membrane material are directly related with gas diffusivity including the polymer free volume and chain flexibility.

Solubility (Eq.4) is often expressed in cm^3 (STP).cm^{-3}.$cmHg^{-1}$ and, as given by Henry's law, it is influenced by the gas concentration in the membrane at a given pressure and temperature:

$$S = \frac{C}{p} \quad (4)$$

where C is the gas concentration in the membrane at a given temperature and p the pressure of gas contiguous to the membrane. Solubility is mainly dependent on gas molecule condensability, but gas-polymer interactions and polymer morphological features, like crystallinity, also influence solubility.[14]

Two important assumptions underline the solution-diffusion model. The first entails that on both sides of the membrane, at the interface, the gas is in equilibrium with the membrane material. The second states that at a constant gas pressure, a gas concentration gradient exists inside the membrane and only this concentration gradient is responsible for the difference in pressure and concentration across the membrane.[18]

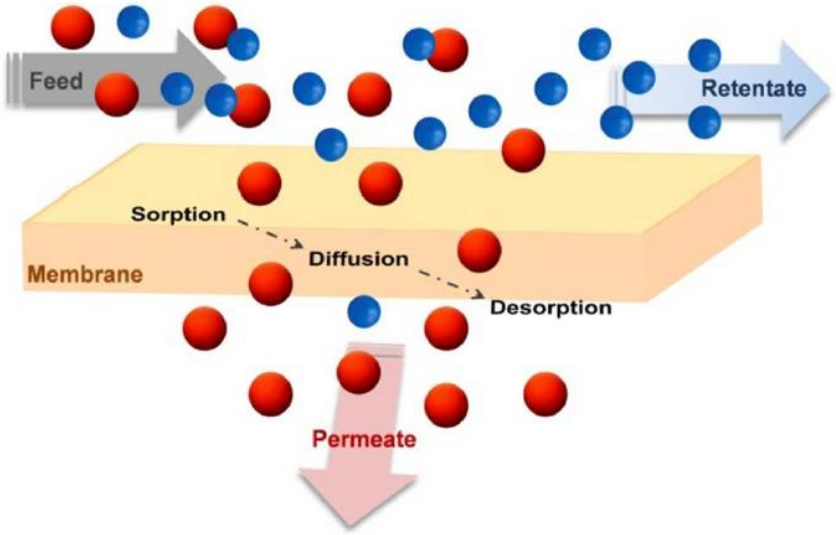

Figure 8 - Schematic illustration of the solution-diffusion model governing gas separation in dense membranes.[22]

The solution-diffusion model can be summarily illustrated in three steps (Figure 8):[12]

1. The gas particles are adsorbed on the upstream side of the membrane;
2. The concentration gradient inside the membrane drives the diffusion of the gas particles through the membrane;
3. The gas particles are desorbed on the downstream side of the membrane;

1.3.2 Selectivity

Different gases have specific chemical and physical affinities to a certain membrane material. The different gas-membrane affinities allow some gases to permeate faster than others, providing the selectivity basis for using dense membranes in gas separation applications.

The ideal selectivity (Eq.5), also known as permselectivity or permeability selectivity ($\alpha_{i/j}$), is a measure of how well a membrane material discerns one gas from another. Like permeability, it's a property of the membrane material and it can be determined by dividing the permeability of most permeable gas *i* (P_i) by the permeability of the least permeable gas *j* (P_j):

$$\alpha_{i/j} = \frac{P_i}{P_j} \qquad (5)$$

Permselectivity (Eq.6) can also be expressed as the product of the diffusivity selectivity and solubility selectivity, by combining Eq.5 with Eq.3.[14]

$$\alpha_{i/j} = \left(\frac{D_i}{D_j}\right) \times \left(\frac{S_i}{S_j}\right) \quad (6)$$

1.3.3 Separation Performance

The two fundamental parameters that characterize the separation performance of a membrane are the permeability of gases, specially the permeability of the most permeable gas, and permselectivity. Membranes with better gas separation performance have higher permeability values for a single gas specie within a gas mixture and a higher permselectivity value as well. Membranes with high permeability require less membrane area to process a certain volume of a gas mixture, therefore, they also require less membrane material. Higher permselectivity values result in purer separated gas streams. Although this is the desired scenario, it has been proven that a trade-off relationship exists between these two parameters, meaning, membranes that are more selective are usually less permeable and vice versa.[19]

This trade-off was described in 1991 by Robeson. By plotting the permeability of the most permeable gas against the permeability selectivity, on a log-log scale, the existence of an upper bound was shown.[20] Since 1991 many new membranes were obtained and tested, and their respective data released, and so the upper bound was revised by Robeson in 2008 for numerous gas pairs (CO_2/N_2, CO_2/CH_4, O_2/N_2, etc.). This data can be graphically represented (Figure 9) in the so called Robeson plot and the upper bound (Eq.7) described as:[21]

$$P_i = k\alpha_{i/j}^{n} \quad (7)$$

where P_i is the permeability of the most permeable gas in the gas mixture, $\alpha_{i/j}$ represents the gas pair permselectivity and *n* is the upper bound slope. The upper bound represents an empirical correlation based on the compilation of extensive experimental results for several membranes. Membranes with the best separation performance fall into the upper-right corner of the Robeson plot (Figure 9). Obtaining membranes that fall in this region is difficult and rare and most membranes fall below the upper bound. The use of Robeson plots to evaluate membranes gas pairs separation performance is currently widely used since it allows the evaluation of the progress made in membrane technology for gas separation.[19]

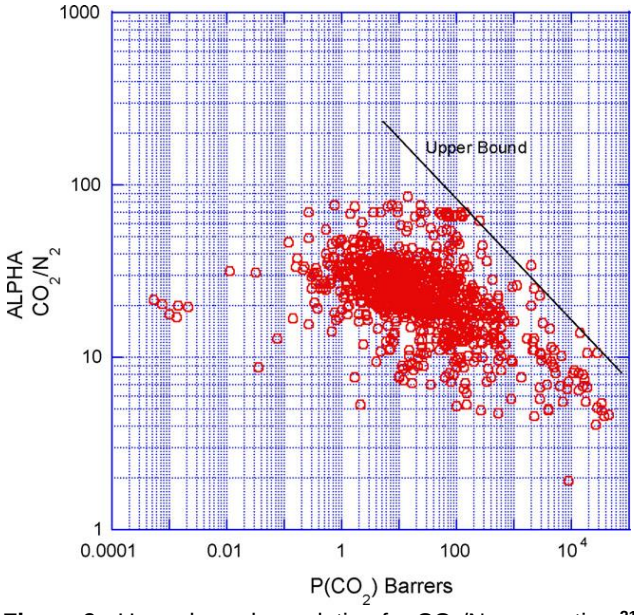

Figure 9 - Upper bound correlation for CO_2/N_2 separation.[21]

1.4 Ionic Liquid-Based Materials

Ionic Liquids (ILs) are salt comprised by organic cations and inorganic or organic anions. Unlike most conventional salts, ILs have cations (many with delocalized charges) and anions that are highly asymmetrical, which leads to weak intermolecular interactions and consequently ILs are poorly packed. This results in one of the main properties of ILs which is their low melting point that, usually, falls below 100 ºC. The melting point of ILs distinguishes them from conventional salts that usually present higher melting points (e.g. sodium chloride melting point is 801 ºC) making them solid at room temperature, unlike several ILs.[24]

In 1914, Paul Walden published the first article on ILs. Even though it did not attract much attention at the time, a growing interest in ILs has resurfaced in the last couple of decades.[23]

A set of unique chemical and physical properties makes ILs alternative solvents (to the conventional organic solvents) that have been used for numerous applications. These properties include low volatility and flammability, high thermal stability and electric conductivity. However, the most important feature of ILs is perhaps their tunability, which allows for the design ILs that can be tailored to fit in a particular technology application. By combining different anions and cations, or adding different functional groups, countless new ILs can be obtained.[22, 24]

Although ILs were first introduced as alternative green solvents to conventional organic solvents, their toxicities and potential environmental effects are still unclear. Many ILs are also highly viscous and their production cost is high.[25] Nevertheless, ILs unique advantages make them promising materials and they have already found use in catalysis and chemical synthesis.[22] Other potential applications of ILs include: alternative solvents for CO_2 absorption, use as lubricants and additives, use in fuel cells and batteries as electrolytes and use in separation technologies, including membranes, extraction and gas separation, among others.[26]

As mentioned before, ILs also possess high CO_2 solubility and selectivity values. Along with their tunable nature, ILs offer a novel platform for CO_2 separation technologies and in 2001 they were first proposed as alternative solvents for CO_2 separation by Blanchard.[27] Since then, the most widely studied and successful applications for CO_2 separation using ILs regard the gas pairs CO_2/N_2, CO_2/CH_4, CO_2/H_2.[22] Amines used in CO_2 absorption require high energy for solvent regeneration and are volatile, and therefore using ILs as amine alternatives would reduce environmental concerns and possibly reduce energy needs.

Regarding the behavior of ILs in CO_2 separation through absorption processes, two different types of ILs can be considered: room temperature ionic liquids (RTILs), which exhibit the typical behavior of a physical solvent (CO_2 is captured in between the free volume of the ILs' ions) and task specific ionic liquids (TSILs) that make use of the tunability of ILs to incorporate suitable functional groups that increase absorption capacity. Through these functional groups, TSILs are able to absorb CO_2 physically, like RTILS, but also chemically, through a chemical reaction or chemical bonding. Even though RTILs are usually less viscous and more thermally stable than TSILs, they also require higher CO_2 partial pressure values to absorb CO_2 while TSILs can absorb at lower CO_2 partial pressures.[28] In addition, the CO_2 absorption capacity of TSILs can be three times higher than that of the corresponding alkyl-functionalized RTILs. This has prompted several research groups to study the influence of CO_2 solubility in ILs with different moieties like cyano, amine, fluorine, hydroxyl, ether, etc.[25] Additionally, other parameters have also been evaluated, including the influence of the cation versus the influence of the anion[48] and the length of the alkyl side chain.[73] It was concluded that CO_2 molecules are more attracted to the anions than the cations, and that the anions influence CO_2 solubility the most.[29] Increasing the length of the alkyl side chain also increases CO_2 solubility in ILs due to the increase of free volume between cations and anions.[29]

In order to advantageously integrate ILs in already existing absorption industrial processes it is necessary to find solutions for two of the major ILs disadvantages: high viscosity and high production costs. In the meantime, other technologies, such as membranes, are becoming relevant in CO_2 separation context.[30] The combination of membrane technology with ILs results in different membrane configurations and morphologies. These configurations can be classified into one of four main categories: supported ionic liquid membranes (SILMs), polymer-ionic liquid composite membranes, gelled ionic liquid membranes and polymeric ionic liquid (PIL) membranes.

In a supported ionic liquid membrane capillary forces immobilize the IL, which was previously impregnated inside the pores of an inert solid membrane support. SILMs usually wield good CO_2 separation results, high permeability and permselectivity values, and often stay on top or above the 2008 Robeson upper bound for CO_2/N_2 separation.[21] However, their long term stability is compromised and in high pressure conditions the immobilized IL can come out of the pores.[31]

In the second configuration, polymer-ionic liquid composite membranes, the free IL is incorporated inside a (conventional) polymer matrix.[74, 75] The IL, entrapped within the polymer chains, cannot leach as easily as it happens with SILMS, allowing for higher pressure to be employed during the gas mixture separation. Despite the good mechanical and thermal stability offered by the polymer,

the permeability and permselectivity obtained in these membranes are inferior to those obtained in SILMs.[22]

Gelled ionic liquid membranes can be prepared by mixing a low quantity of an organic gelator[76] or polymer[77] with the desired ionic liquid. The gelator solidifies the ionic liquid forming, at the end, a gelled ionic liquid structure that is mainly liquid at a microscopic scale but overall is practically solid and stable. The gelator allows for a more mechanically stable membrane and thus higher pressure differences can be employed. It also exhibits good CO_2 separation performances, similar to SILMs. The CO_2 separation performance is still, however, limited by the membrane thickness.[22]

The final configuration, polymeric ionic liquid membranes, is the membrane type prepared and evaluated in this work, therefore it will be analyzed with more detail in the next chapter.

1.5 Polymeric Ionic Liquid (PIL) Membranes

Polymeric ionic liquids (PIL), polymerized ionic liquids or poly(ionic liquid)s belong to a subclass of polyelectrolytes. The polymeric backbone is formed by monomer repeating units, each one containing one ionic liquid specie (anion and cation), that overall form a macromolecular architecture.

PILs are obtained through the polymerization of an IL monomer. More than one polymerizable unit can be incorporated into the IL specie and the unit(s) can be located on the anion, cation or both (Figure 10). It should be noted that the IL is in the liquid state but most PILs are solid.[32]

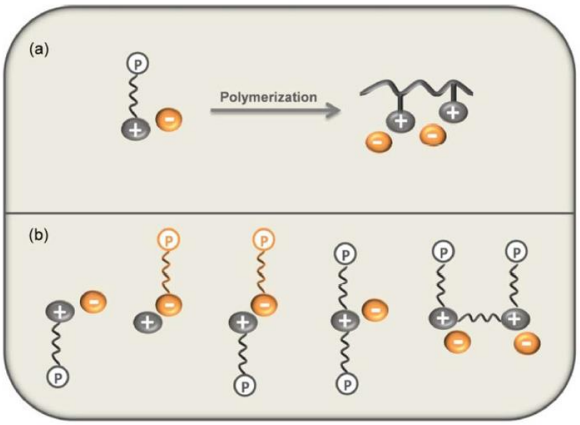

Figure 10 – Schematic illustrations of (a) the polymerization of an IL monomer and (b) several IL monomers configurations.[22]

The synthesis of PILs can be carried out by one of two main methods. In the first one, IL monomers with polymerizable groups, compressing the desired anion and cation, are synthesized, followed by direct polymerization (in bulk, UV, etc.) of the monomers. In the second route, an already existing PIL is subjected to an ion exchange reaction, using a salt, and/or an *N*-quaternization reaction. Depending on the target PIL, both methods present advantages and disadvantages. Overall, the first method allows for the synthesis of several PILs with different anions and cations combinations

but it takes longer, is more complicated and the polymer chain length (molecular weight) is harder to control. The second method is simpler because already existing polymers are used, therefore the molecular weight is controlled by the supplier, but it has more limitations regarding anion-cation combinations.[33]

Polymeric ionic liquids combine the advantages of both polymers and ionic liquids. The polymer macrostructure not only improves processability and durability but also enhances the mechanical stability of the membrane. The tunability of ILs is present in PILs, allowing for the tailoring of the PIL chemical and physical properties.[33] Thus, PILs have also been finding applications in different technological fields, including analytical chemistry,[34] biotechnology,[35] materials science,[36] and gas separation,[37] among others.

PIL-based membranes can have different configurations, by blending them with free IL and/or inorganic materials, for example. Therefore, PIL-based membranes can fit in one of four categories: neat PIL, PIL-IL composites, PIL copolymers or PIL-IL-zeolite mixed matrix membranes (MMM).

Neat PIL membranes represent the simplest configuration of a PIL based membranes. Noble's group synthesized the first five neat PIL membranes in 2007.[38] Since then, numerous neat PIL membranes have been studied and synthesized, all with cations tethered to the polymeric backbones and free anions as the counter ion. Among some of the different polycations studied are the ones based on the imidazolium,[38-42] pyrrolidinium[55] and ammonium[44] moieties. The influence of different counter anions was also studied, being the bis(trifluoromethylsulfonyl)imide anion, $[NTf_2]^-$, the most used due to its high CO_2 affinity.[38, 41, 42] Tomé and coworkers concluded that neat PILs with a pyrrolidinium-based backbone did not outperform the imidazolium analogues. Despite this, the CO_2 separation performance stayed in the same order of magnitude.[55]

The permeability, diffusivity and permselectivity greatly decreases from SILMs to the respective PIL membranes. On the other hand, PIL membranes allow for a more mechanical and thermal stable membrane. A possible alternative to neat PILs include the synthesis of PIL copolymers that have at least one PIL monomeric unit. Although some PIL copolymers are on top or even surpass the 2008 Robeson upper bound, there is still considerable research that needs to be done in order to truly understand these membranes gas permeation properties.[51] The other alternative include PIL-IL-zeolite MMMs. These membranes incorporate an inorganic phase and a certain percentage of free IL within a polymeric matrix. All the membranes fabricated so far did not, however, surpass the 2008 Robeson upper bound.[52]

Aiming at creating a membrane with the best of both SILMs and neat PIL membranes configurations, Bara and coworkers synthesized in 2008 the first PIL-IL composite membrane.[30] A PIL-IL composite membrane contains a PIL framework in which a certain percentage of free IL is incorporated. For instance, by incorporating 20 mol% of imidazolium based free IL in an imidazolium based PIL Bara and coworkers increased the CO_2 permeability by approximately 400% when compared with the respective neat membrane.[45] After this, several polycations and counter anions variations, with different percentages of free ILs, were studied. Polymer backbones with imidazolium,[45-49] pyrrolidinium,[48] pyridinium,[48] ammonium,[48] and cholinium[48] based moieties were

some of the cations variations studied so far. The $[NTf_2]^-$ anion was, just like in the neat PIL membranes, the most used counter anion.[44, 48, 49]

Ionic liquids bearing cyano-functionalized anions are reported to have low viscosity values. What is more, the CO_2 solubility in SILMs containing immobilized ILs with cyano anions was shown to be high and the CO_2 separation performance was on top or above the 2008 Robeson upper bound.[50] In 2015, Tomé and coworkers, synthesized pyrrolidinium-based neat PIL membranes, with three different cyano counter anions: dicyanamide ($[N(CN)_2]^-$), tricyanomethane ($[C(CN)_3]^-$) and tetracyanoborate ($[B(CN)_4]^-$). All the three membranes obtained were very brittle and broke easily. Afterwards, PIL-IL composite membranes were prepared by incorporating different percentages of free IL (20 wt%, 40 wt% and 60 wt%) into the prepared PILs. The ILs used had the same counter anions as the PIL but the cation was the 1-ethyl-3-methylimidazolium ($[C_2mim]^+$), due to their commercially availability. The PIL-IL composite membranes containing the $[N(CN)_2]^-$ and $[B(CN)_4]^-$ counter anions were not stable due to their brittle nature. Only the membrane with 20 wt% of the IL with the $[N(CN)_2]^-$ anion was stable and homogenous and only this membrane was used in gas permeation experiments. However, for the $[C(CN)_3]^-$ counter anion, the incorporation of all the three different percentages of free IL resulted in stable and homogenous membranes. By increasing the amount of free IL, the CO_2 permeability increased and for 60 wt% of free IL the 2008 Robeson upper bound for CO_2/N_2 pair was surpassed. This work reported, for the first time, a PIL-IL composite membrane that achieved such high CO_2/N_2 separation performance.[53]

Giving the outstanding results obtained by Tomé et al., cyano-functionalized counter anions seem to hold a great promise to obtain stable and over performing CO_2 separation membranes. The work carried out in this thesis is a continuation of their work where the novelty here is the preparation of membranes with different counter anions in the PIL (Figure 11) and the IL (Figure 12).

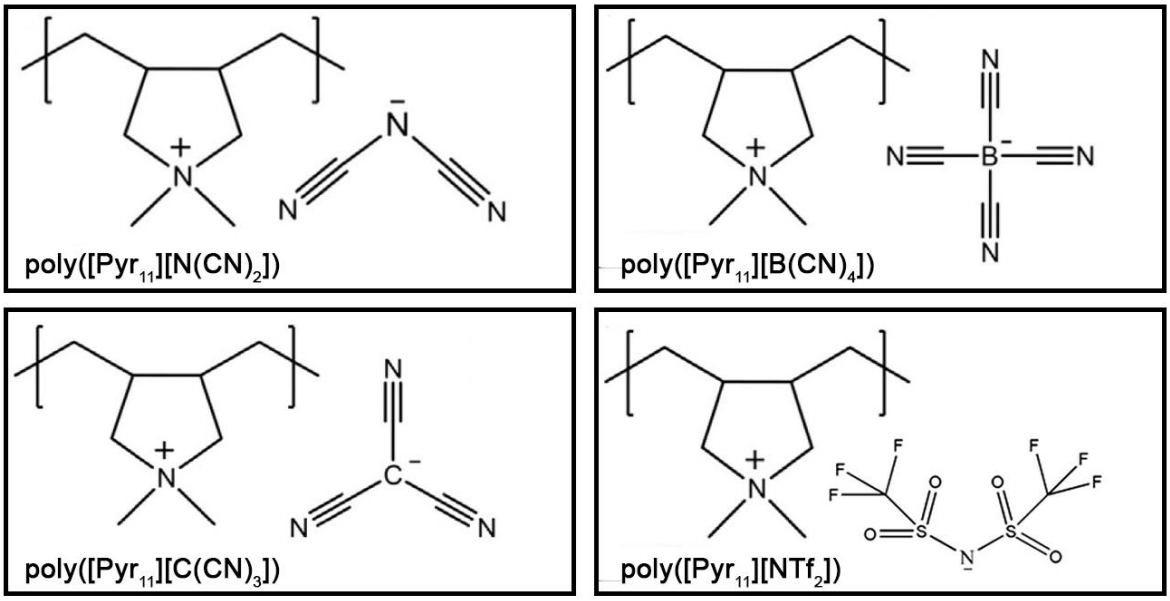

Figure 11 – Chemical structure of the four PILs used in this work.

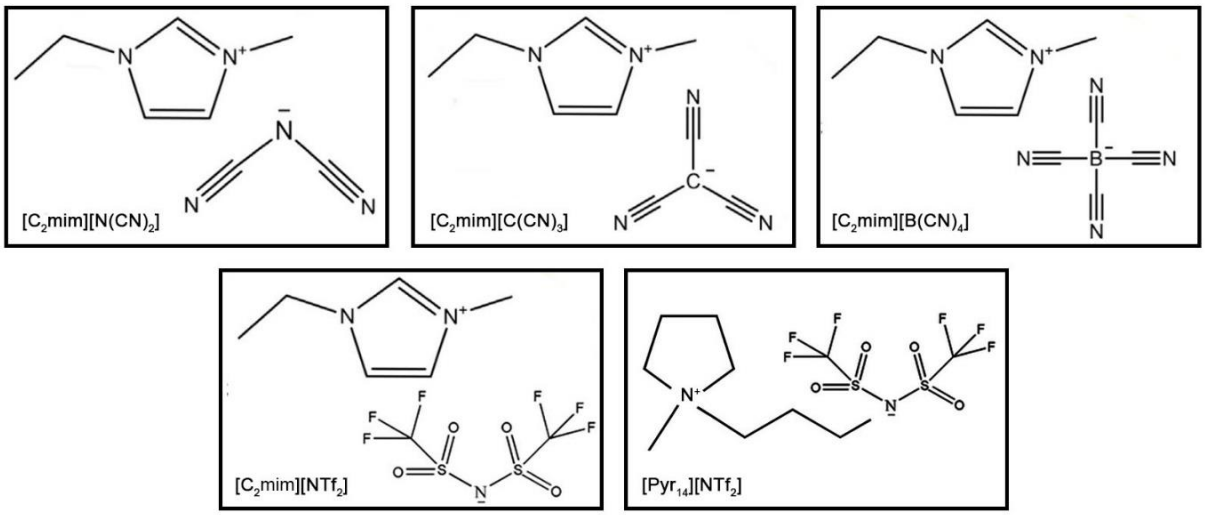

Figure 12 – Chemical structure of the five ILs used in this work.

1.6 Objectives

The two main objectives of this work are: i) preparation and evaluation of the mechanical stability and chemical compatibility of different PIL-IL composite membranes having different cyano counter anions in both the PIL and IL; and, ii) measurement of the gas (CO_2 and N_2) permeation properties of the prepared membranes and evaluation of their CO_2 separation performance.

For all the composite prepared membranes, the PIL backbone is based on the pyrrolidinium polycation, while the free IL cation is the 1-ethyl-3-methylimidazolium ($[C_2mim]^+$). The three cyano counter anions used, for both the PIL and IL, are: dicyanamide ($[N(CN)_2]^-$), tricyanomethane ($[C(CN)_3]^-$) and tetracyanoborate ($[B(CN)_4]^-$).

Dense membranes were prepared on a mass basis for three different percentages of free IL (20, 40 and 60 wt%) using a solvent casting method. The CO_2 and N_2 permeation properties (permeability, diffusivity and solubility) through the obtained stable and homogenous membranes were then determined using a time-lag apparatus.

In parallel, PIL-IL composite membranes with the bis(trifluoromethylsulfonyl)imide ($[NTf_2]^-$) as a counter anion, in both the PIL and IL, were also synthesized and their CO_2 separation performance evaluated using the same procedures as those used for the cyano-based membranes. The main purpose of this extra work is to evaluate the influence of the free IL cation. The PIL polycation backbone here used is based on pyrrolidinium moities, but two different free IL were tested, one with the $[C_2mim]^+$ cation and the other with the 1-butyl-1-methylpyrrolidinium cation ($[Pyr_{14}]^+$).

2. PIL Synthesis and Membranes Preparation

In this work, four PILs were used, namely poly([Pyr_{11}][$N(CN)_2$]) (PIL $N(CN)_2$), poly([Pyr_{11}][$C(CN)_3$]) (PIL $C(CN)_3$), poly([Pyr_{11}][$B(CN)_4$]) (PIL $B(CN)_4$) and poly([Pyr_{11}][NTf_2]) (PIL NTf_2). Since all these polymers have a pyrrolidinium-based polycation, from here onwards PIL will be used to refer to poly([$Pyr_{11}]^+$), followed by the respective counter anion, eg., PIL $N(CN)_2$ refers to poly([Pyr_{11}][$N(CN)_2$]). The same rationale will be applied to the ionic liquids containing cyano functionalized anions used in the preparation of composite membranes. For example, [C_2mim][$N(CN)_2$] will be referred to as IL $N(CN)_2$. Regarding [C_2mim][NTf_2] and [Pyr_{14}][NTf_2], these ILs will continue to be referred using the common ILs nomenclature.

In this work, PIL-IL composite membranes containing different weight percentages of free IL (20, 40 and 60 wt%) were prepared by a solvent casting method. Different experimental conditions (solvent, evaporation time and temperature) for the casting process were tested in order to obtain stable and homogenous membranes. The PIL-IL composite membranes will make use of the above introduced PIL and IL acronyms. For instance, the membrane constituted by PIL $C(CN)_3$ and 20 wt% of free IL $B(CN)_4$ will be referred to as PIL $C(CN)_3$ - 20 IL $B(CN)_4$.

2.1 Materials

Poly(diallydimethyammonium) chloride solution (average Mw 400,000-500,000, 20 wt% in water) was supplied by Sigma-Aldrich. The salts sodium dicyanamide ($NaN(CN)_2$, >97 wt%), sodium tricyanomethane ($NaC(CN)_3$, 98 wt%), and lithium bis(trifluoromethylsulfonyl)imide ($LiNTf_2$, 99%), as well as the ionic liquids 1-ethyl-3-methylimidazolium dicyanamide ([C_2mim][$N(CN)_2$], >98 wt%), 1-ethyl-3-methylimidazolium tricyanomethane ([C_2mim][$C(CN)_3$], >98 wt%), 1-ethyl-3-methylimidazolium bis(trifluoromethylsulfonyl)imide ([C_2mim][NTf_2], 99 wt%) and 1-butyl-1-methylpyrrolidinium bis(trifluoromethylsulfonyl)imide ([Pyr_{14}][NTf_2], 99 wt%) were purchased from IoLiTec GmbH. Merck KGaA (Germany) provided the 1-ethyl-3-methylimidazolium tetracyanoborate ([C_2mim][$B(CN)_4$], >98 wt%), while the potassium tetracyanoborate ($KB(CN)_4$) was synthesized as reported elsewhere.[54]

2.2 PILs Synthesis

The four polymeric ionic liquids with a pyrrolidinium-based polycation and cyano functionalized or $[NTf_2]^-$ counter anions (Figure 13), were obtained by anion exchange reaction from the commercially available polyelectrolyte precursor, poly(diallyldimethylammonium chloride), followed by further purification steps.[53]

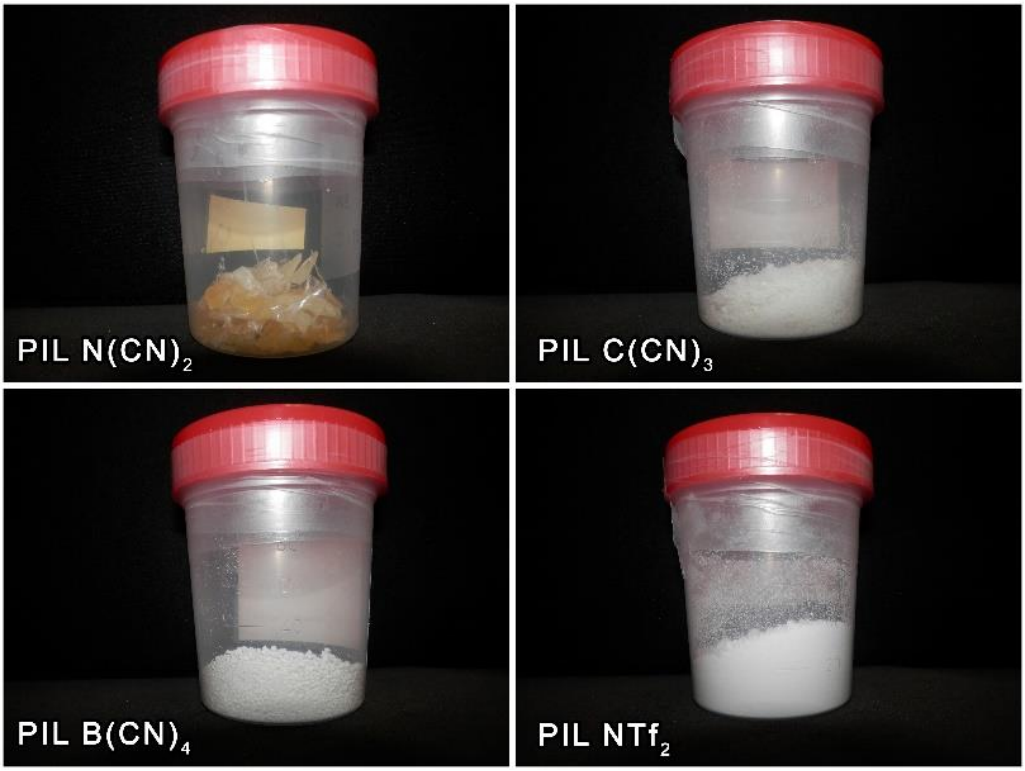

Figure 13 – The four PILs synthesized in this work.

In a typical procedure, for instance to obtain approximately 15 g of PIL $C(CN)_3$, an aqueous solution of poly(diallyldimethylammonium chloride) (55 g, 0.068 mol, 150 mL of distilled water) was added and mixed to an aqueous solution of $NaC(CN)_3$ (8.5 g, 0.071 mol, 20 mL in distilled water) in a round bottom flask. The final solution was stirred for, at least, 30 minutes at room temperature. Note that 5 wt% excess of $NaC(CN)_3$ salt was added to the solution to ensure equimolar anion exchange (Figure 14). Due to its hydrophobic nature, PIL $C(CN)_3$ precipitated as a white solid in the aqueous media, just as soon as it was formed. The polymer was then washed with distilled water, filtered (Sartorius Stedim, Germany) and dried at 45 ºC in an oven with forced air convection (VENTI-Line), until constant weight was obtained. The other two polymers, PIL $B(CN)_4$ and PIL NTf_2, were obtained using the same procedure, but with the respective salts $KB(CN)_4$ and $LiNTf_2$, as illustrated in Figure 14. On the other hand, the hydrophilic polymer PIL $N(CN)_2$ did not precipitate in water and thus required a different purification method. After removing the water by rotary evaporation (VWR, IKA RV 10, Figure 15) at 45 ºC, PIL $N(CN)_2$ and NaCl, a byproduct of the anion exchange reaction, are left behind in the solid state (Figure 14). In order to dissolve the polymer and precipitate the NaCl, 250mL of ethanol were added. The excess of precipitated salt was filtered and the filtrate was kept at -5 ºC overnight to complete the NaCl precipitation. The remaining NaCl in suspension was filtrated in the next day. This procedure was repeated until no more NaCl precipitate was observed. After evaporation of ethanol, a dark yellow solid corresponding to PIL $N(CN)_2$ was finally obtained (Figure 13).

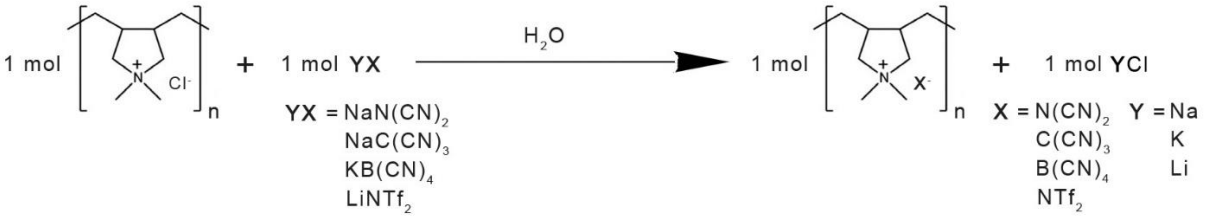

Figure 14 – Anion exchange reaction used to synthesize the four different PILs studied in this work.

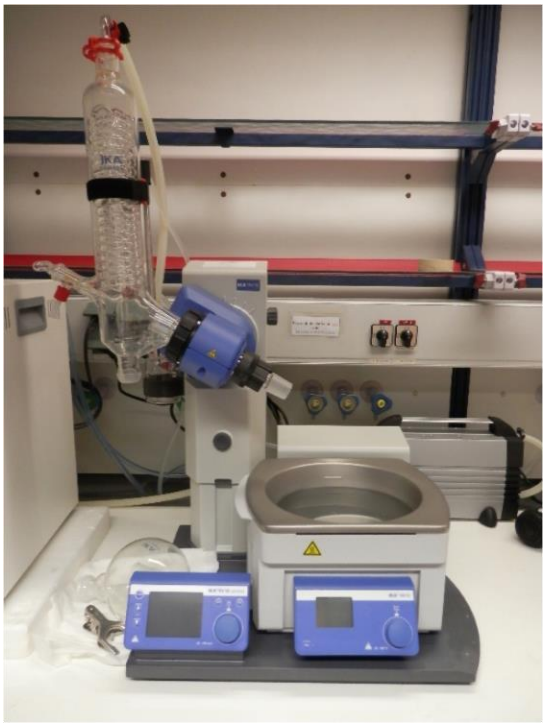

Figure 15 - Rotary evaporator used in the purification of PIL $N(CN)_2$.

2.3 Membrane Preparation Method

The preparation of PIL-IL composite membranes was attempted by a solvent casting method combining the synthesized PILs (Figure 13) with commercial ILs (Figure 16). First, solvent screening for both PILs and ILs was carried out. Second, solutions containing the PIL and the corresponding amount of free IL were prepared using the appropriated solvents. Afterwards, the prepared solutions were stirred until both PIL and IL were completely dissolved and a homogeneous solution was obtained. The PIL and IL solutions were then poured into dishes and left for slow evaporation of the solvents (Figure 17). The different solvent casting conditions used for each of the membranes are discussed in more detail below. Finally, to ensure that the solvent was completely evaporated, the membranes were dried at 45 ºC before gas permeation measurements.

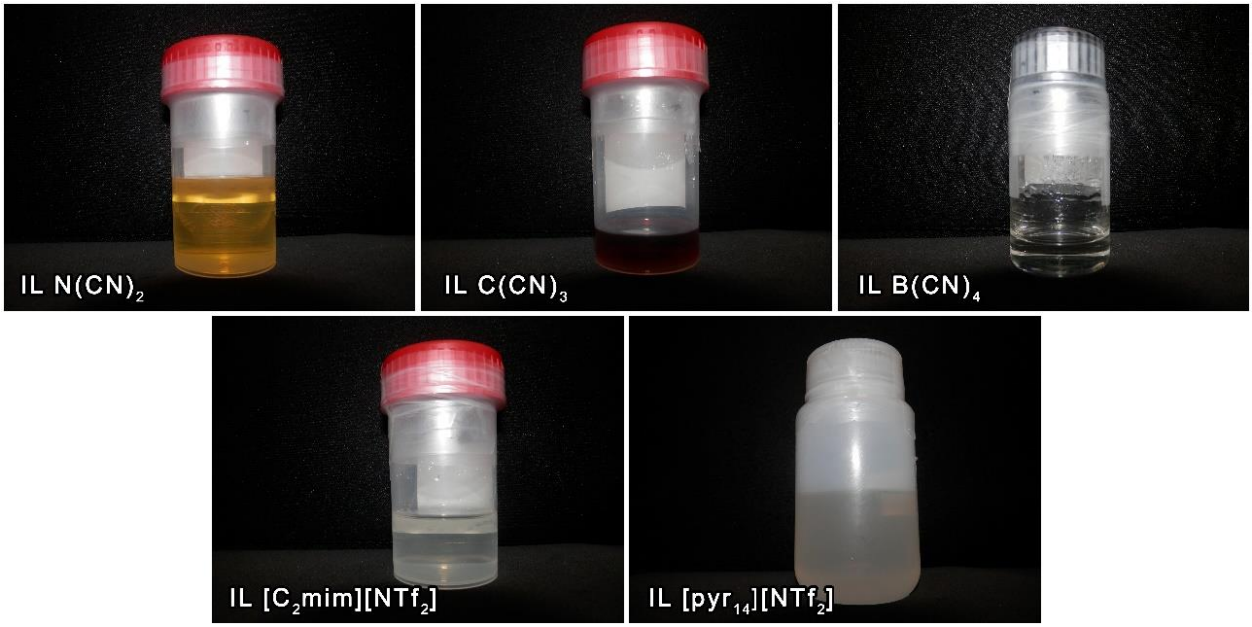

Figure 16 – The five ILs used in this work and their respective acronyms.

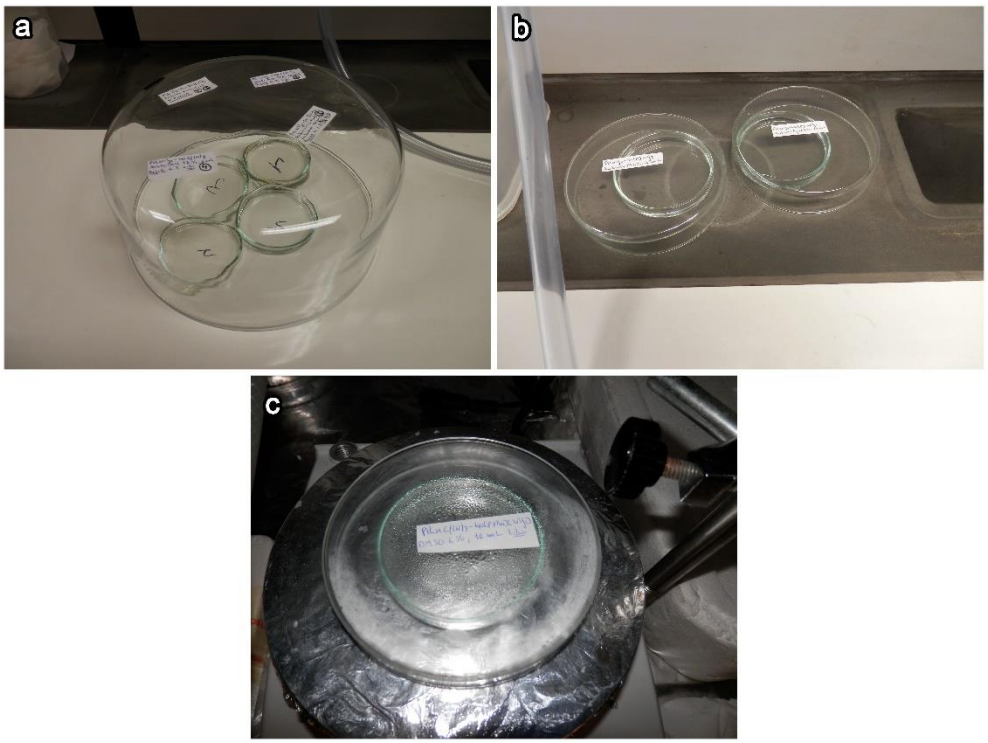

Figure 17 – Solvent evaporation (**a** and **b**) at room temperature and (**c**) above room temperature during the casting procedure used to prepare PIL-IL composite membranes.

Table 2 summarizes all the membranes prepared in this work as well as their stability and homogeneity.

Table 2 - Summary of all the membranes prepared in this work. Cells with a gray background represent membranes already reported in previous works.[53, 55] N.S stands for "not synthesized". Membranes denoted with a √ mark are stable and homogenous, while those with the mark X are non-stable and/or heterogeneous membranes.

		IL													
		$[C_2mim][N(CN)_2]$			$[C_2mim][C(CN)_3]$			$[C_2mim][B(CN)_4]$			$[C_2mim][NTf_2]$			$[pyr_{14}][NTf_2]$		
	IL wt%	20	40	60	20	40	60	20	40	60	20	40	60	20	40	60
PIL	PIL $N(CN)_2$	√	X	X	√	√	√	X	X	X	X	X	X	N.S		
	PIL $C(CN)_3$	√	√	X	√	√	√	√	√	√	√	√	X	√	√	X
	PIL $B(CN)_4$	X	X	X	X	√	√	X	X	X	√	√	X	N.S		
	PIL NTf_2	√	X	X	√	X	X	√	X	X	√	√	X	√	√	√

In order to obtain stable and homogenous membranes, different solvent casting conditions were tested including the use of different solvents, PIL and IL (w/v)% concentrations, evaporation times and temperatures, as well as different plate materials. The different solvents tested include acetone, acetonitrile, ethanol, dimethyl sulfoxide (DMSO) and dimethylformamide (DMF). Plates made of two different materials, polytetrafluoroethylene (PTFE) and glass (Petri dishes), were used.

The initial casting conditions were taken from Tomé et al. previous study, who prepared free standing and homogenous membranes with a final thickness between 120 and 200 µm.[53] As a starting point, the membranes were prepared in either acetone or acetonitrile, using 6 (w/v)% PIL and IL solutions, and left to evaporate in Petri dishes between 2 to 4 days at room temperature. Due to the high number of PIL-IL membrane combinations planned in this work (42), the different casting experimental conditions used for each membrane are divided into two tables: the first one (Table 3) contains the conditions used to obtain the 21 stable and homogenous membranes (membranes marked with √ on Table 2), while the second one (Table 4) contains the conditions tested to obtain the other 21 membranes, which after many trials, were either non-stable, non-homogenous (heterogeneous) or both (membranes marked with X on Table 2).

Table 3 – Experimental conditions of the solvent casting procedure used to prepare the PIL-IL composite membranes. In all these cases, the obtained membranes were stable and homogenous.

Composite Membrane	Solvent	PIL-IL Solutions (w/v)%	Evaporation Time (days)	Evaporation Temperature (ºC)	Petri Dish Material
PIL $N(CN)_2$-20 IL $C(CN)_3$	Ethanol	6	4	45	PTFE
PIL $N(CN)_2$-40 IL $C(CN)_3$					
PIL $N(CN)_2$-60 IL $C(CN)_3$		9	3		
PIL $C(CN)_3$-20 IL $N(CN)_2$	Acetonitrile	6	3	20	Glass
PIL $C(CN)_3$-40 IL $N(CN)_2$					
PIL $C(CN)_3$-20 IL $B(CN)_4$	Acetonitrile	6	4	20	Glass
PIL $C(CN)_3$-40 IL $B(CN)_4$			3		
PIL $C(CN)_3$-60 IL $B(CN)_4$					PTFE
PIL $C(CN)_3$-20 IL $[C_2mim][NTf_2]$	Acetonitrile	6	3	20	Glass
PIL $C(CN)_3$-40 IL $[C_2mim][NTf_2]$					
PIL $C(CN)_3$-20 IL $[Pyr_{14}][NTf_2]$	Acetonitrile	6	4	20	Glass
PIL $C(CN)_3$-40 IL $[Pyr_{14}][NTf_2]$					
PIL $B(CN)_4$-40 IL $C(CN)_3$	Acetone	6	2	20	Glass
PIL $B(CN)_4$-60 IL $C(CN)_3$					
PIL $B(CN)_4$-20 IL $[C_2mim][NTf_2]$	Acetone	6	2	20	Glass
PIL $B(CN)_4$-40 IL $[C_2mim][NTf_2]$					PTFE
PIL NTf_2-20 IL $N(CN)_2$	Acetone	6	1	20	Glass
PIL NTf_2-20 IL $C(CN)_3$	Acetone	6	1	20	Glass
PIL NTf_2-20 IL $B(CN)_4$	Acetone	6	2	20	Glass
PIL NTf_2-20 IL $[C_2mim][NTf_2]$	Acetone	6	2	20	Glass
PIL NTf_2-40 IL $[C_2mim][NTf_2]$					

The membranes containing PIL $N(CN)_2$ posed a number of challenges in their preparation due to the high hydrophilic nature of the polymer. For example, it was impossible to peel them out from the Petri dish. To overcome this problem, a plate made of a more hydrophobic material (PTFE) was used instead. Moreover, the evaporation of the solvent for these membranes was carried out at 45º C, inside an oven, to minimize the quantity of water absorbed by the polymer. For some of the prepared membranes with higher amounts of free IL, it was also difficult to peel out the membranes from Petri dishes due to their gel-like nature, although they were stable enough to be handled. Nevertheless, PTFE plates were also used in these cases (Table 3).

Table 4 – Experimental conditions tested/used during the solvent casting procedure to prepare PIL-IL composite membranes. In these cases, and after many trials, all the obtained membranes were non-stable and/or heterogeneous.

Composite Membrane	Solvent	PIL-IL Solutions (w/v)%	Evaporation Time (days)	Evaporation Temperature (ºC)	Petri Dish Material
PIL $N(CN)_2$-20 IL $B(CN)_4$ *PIL $N(CN)_2$-40 IL $B(CN)_4$* *PIL $N(CN)_2$-60 IL $B(CN)_4$*	Ethanol	6	5 7	45	Glass PTFE
PIL $N(CN)_2$-20 IL $[C_2mim][NTf_2]$ *PIL $N(CN)_2$-40 IL $[C_2mim][NTf_2]$* *PIL $N(CN)_2$-60 IL $[C_2mim][NTf_2]$*	Ethanol Acetonitrile DMSO	6	5 7	45	Glass PTFE
PIL $C(CN)_3$-60 IL $N(CN)_2$	Acetonitrile	6 7	4	20	Glass PTFE
PIL $C(CN)_3$-60 IL $[C_2mim][NTf_2]$	Acetonitrile Acetone DMF	6 12	2 7	20 35	Glass PTFE
PIL $C(CN)_3$-60 IL $[Pyr_{14}][NTf_2]$	Acetonitrile Acetone DMF DMSO	6 7	2 7	20 35 40 50	Glass PTFE
PIL $B(CN)_4$-20 IL $N(CN)_2$ *PIL $B(CN)_4$-40 IL $N(CN)_2$* *PIL $B(CN)_4$-60 IL $N(CN)_2$*	Acetonitrile Acetone	6	2 5	20 45	Glass PTFE
PIL $B(CN)_4$-20 IL $C(CN)_3$	Acetonitrile Acetone	6 12	2 5	20	Glass PTFE
PIL $B(CN)_4$-60 IL $[C_2mim][NTf_2]$	Acetone	6	2	20	Glass PTFE
PIL NTf_2-40 IL $N(CN)_2$ *PIL NTf_2-60 IL $N(CN)_2$*	Acetonitrile Acetone DMF	6 12	2 7	20 35	Glass PTFE
PIL NTf_2-40 IL $C(CN)_3$ *PIL NTf_2-60 IL $C(CN)_3$*	Acetonitrile Acetone	3 6 12	2 5	20	Glass PTFE
PIL NTf_2-40 IL $B(CN)_4$ *PIL NTf_2-60 IL $B(CN)_4$*	Acetone	6	2	20	Glass PTFE
PIL NTf_2-60 IL $[C_2mim][NTf_2]$	Acetone	6	2	20	Glass PTFE

2.4 Results and Discussion

This section contains the results obtained during the PIL-IL membranes preparation, including figures, remarks and conclusions. The presentation and discussion of the results will be done for each one of the different PILs studied (PIL $N(CN)_2$, PIL $C(CN)_3$, PIL $B(CN)_4$ and PIL NTf_2) individually, followed by an overall comparison and discussion.

2.4.1 PIL $N(CN)_2$

Figure 18 shows the PIL-IL composite membranes bearing PIL $N(CN)_2$ and different amounts of free IL $C(CN)_3$, IL $B(CN)_4$ and IL $[C_2mim][NTf_2]$. Note that the composite membranes made of PIL $N(CN)_2$ and free IL $N(CN)_2$ were previously reported by Tomé et al.[53]

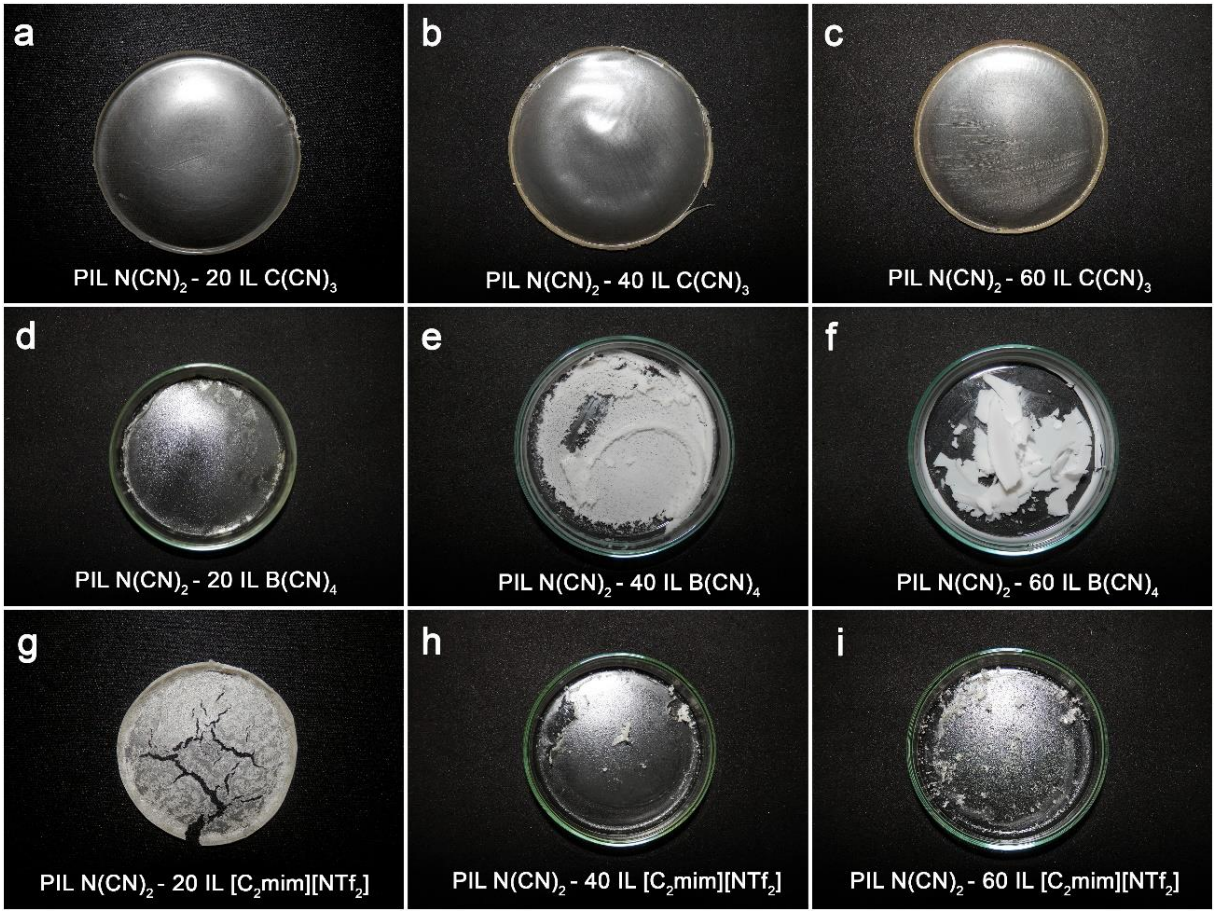

Figure 18 - Pictures of the prepared PIL-IL composite membranes containing PIL $N(CN)_2$ with different amounts of three different free ILs.

The incorporation of 20 wt% of free IL $N(CN)_2$ into PIL $N(CN)_2$ allows the formation of a stable and homogenous membrane (Table 2). Nevertheless, for higher wt% of this free IL, the membranes become gel-like materials, probably due to the hydrophilic nature of the $[N(CN)_2]^-$ anion present in both

components, PIL and IL.[53] Stable and homogeneous PIL-IL composite membranes containing PIL $N(CN)_2$ with 20, 40 and 60 wt% of free IL $C(CN)_3$ were obtained (Figure 18 – a to c). The chemical similarity of $[C(CN)_3]^-$ and $[N(CN)_2]^-$ anions coupled with the lower hydrophilicity of IL $C(CN)_3$ (when compared to that of the IL $N(CN)_2$) allows for more stable membranes instead of gel-like ones, resulting in homogenous PIL-IL membranes.

In contrast, what concerns the PIL-IL composite membranes bearing PIL $N(CN)_2$ with different amounts of free IL $B(CN)_4$, all the obtained membranes were heterogeneous and non-stable (Figure 18 – d to f). This is probably due to the different geometries of both anions: the rigid trigonal bipyramidal geometry of the $[B(CN)_4]^-$ anion does not "adjust" to the trigonal planar geometry of $[N(CN)_2]^-$ anion. These two anions differ from each other in the number (2) of cyano groups and thus volume effects should also be taken into account. Conversely, $[N(CN)_2]^-$ and $[B(CN)_4]^-$ anions are both more similar to $[C(CN)_3]^-$ anion, since both of them only differ from $[C(CN)_3]^-$ by one cyano group.

The composite membranes prepared with PIL $N(CN)_2$ and free IL $[C_2mim][NTf_2]$ are entirely heterogeneous (Figure 18 – g to i). This can probably be attributed to the different nature of both anions, since $[NTf_2]^-$ anion is the most hydrophobic, while the $[N(CN)_2]^-$ anion is the most hydrophilic, and also to volume and geometry effects.

Overall, it was difficult to obtain stable and homogenous composite membranes using PIL $N(CN)_2$, essentially due to its hydrophilic nature, being the membranes with free IL $C(CN)_3$ an exception due to its excellent compatibility with the $[N(CN)_2]^-$ anion.

2.4.2 PIL $C(CN)_3$

The PIL-IL composite membranes bearing PIL $C(CN)_3$ polymer with different amounts of free IL $N(CN)_2$, IL $B(CN)_4$, IL $[C_2mim][NTf_2]$ and $[Pyr_{14}][NTf_2]$ – are shown in Figure 19. Pictures of the composites membranes containing the PIL $C(CN)_3$ and free IL $C(CN)_3$ can be found in a previous work of our group.[53]

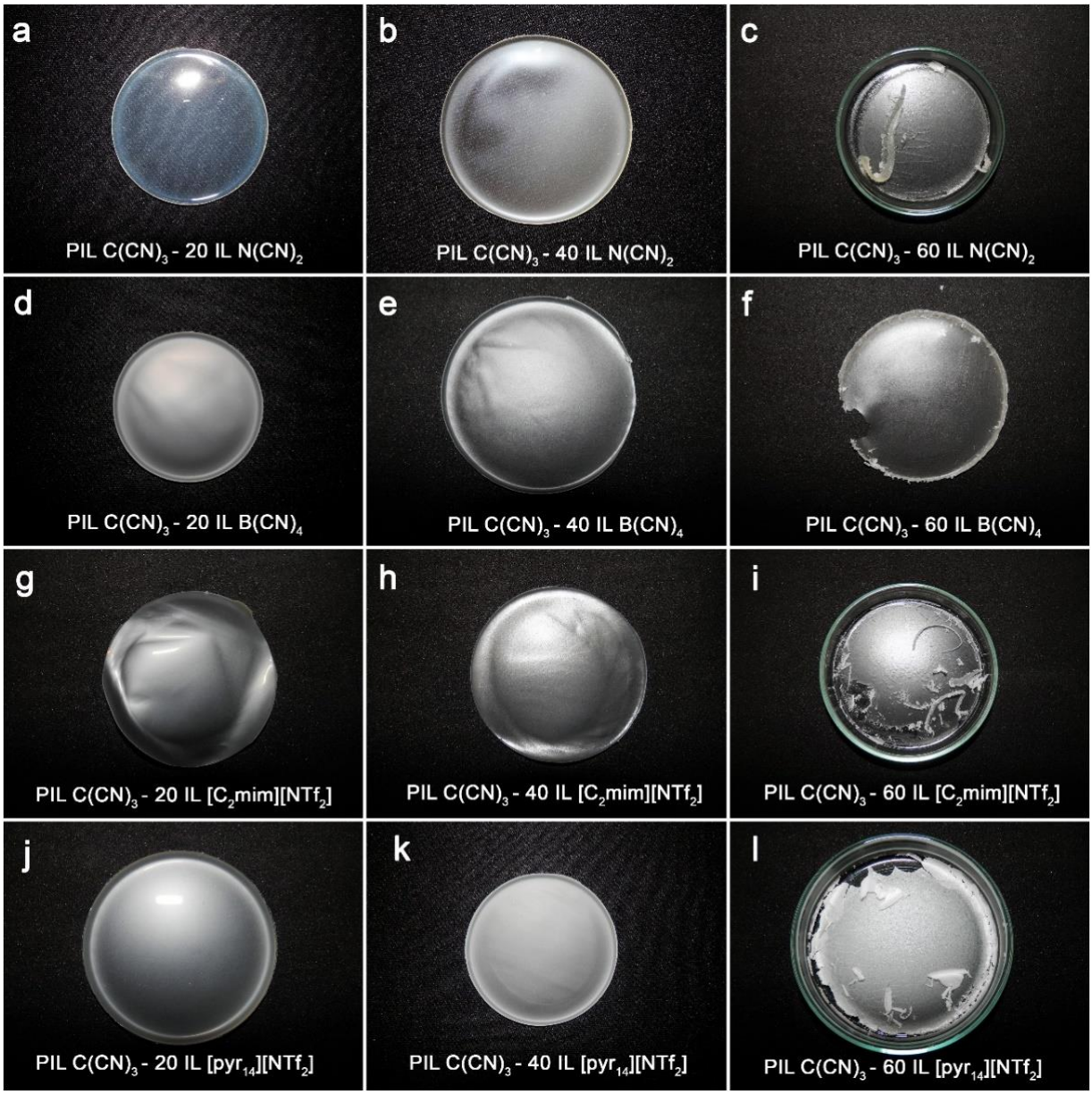

Figure 19 - Pictures of the prepared PIL-IL composite membranes containing PIL $C(CN)_3$ and different amounts of four different free ILs.

Similar to what was previously observed by Tomé et al. for PIL-IL composite membranes bearing PIL $C(CN)_3$ and free IL $C(CN)_3$,[53] the membranes prepared in this work with PIL $C(CN)_3$ and free IL $B(CN)_4$ are homogenous and mechanically stable, as it can be seen in Figure 19 – d to f. As aforementioned, the $[C(CN)_3]^-$ and $[B(CN)_4]^-$ anions differ only in a cyano group, which makes them more similar in terms of volume, allowing the formation of stable and homogenous membranes. The $[C(CN)_3]^-$ and $[N(CN)_2]^-$ anions also differ in a cyano group, which also makes them similar, but the hydrophilic nature of the $[N(CN)_2]^-$ anion compromises the membranes mechanical stability. For instance, regarding composite membranes with PIL $C(CN)_3$ and free IL $N(CN)_2$, stable and homogenous materials can be obtained up to 40 wt% of free IL incorporated (Figure 19 – a and b). The addition of 60 wt% of IL $N(CN)_2$ leads to the formation of a gel-like material, probably due to the

higher amount of $[N(CN)_2]^-$ anions present into the composite, which can effectively absorb more moisture from the atmosphere (Figure 19 – c).

It is interesting to compare the membrane formation ability of the composite membranes with PIL $C(CN)_3$ and 20, 40 and 60 wt% of IL $N(CN)_2$ to those with PIL $N(CN)_2$ and 20, 40 and 60 wt% IL $C(CN)_3$ already discussed in section 2.4.1. For both PIL-IL combinations, stable and homogeneous membranes were obtained for 20 and 40 wt% of free IL incorporated, as it can be respectively seen in Figures 18 – a and 19 – a and Figures 18 – b and 19 – b. The PIL $N(CN)_2$ – 60 IL $C(CN)_3$ composite membrane (Figure 18 – c) is also homogenous and free standing, whereas PIL $C(CN)_3$ – 60 IL $N(CN)_2$ composite is a gel-like material (Figure 19 – c). These results can be probably attributed to the presence of a higher amount of free $[N(CN)_2]^-$ anions from the free IL component. Albeit PIL $N(CN)_2$ – 20 IL $C(CN)_3$ composite also has a high amount of $[N(CN)_2]^-$ anions$^-$ anions, they do not come from the free IL component but from the PIL, a solid macromolecule that is less flexible than the free IL component and thus the respective $[N(CN)_2]^-$ counter anions have lower mobility, aiding in the mechanical stability of the membrane. In this discussion we are considering that there is no interchange of anions between the PIL and IL, a topic that has never been studied before but that deserves to be explored in future works.

Regarding the composite membranes comprising PIL $C(CN)_3$ and free ILs $[C_2mim][NTf_2]$ and $[Pyr_{14}][NTf_2]$, segregation occurs only when 60 wt% of free IL is incorporated, resulting in heterogeneous membranes, as it can be observed in Figures 19 – i and l. Despite the chemical and geometrical differences between $[NTf_2]^-$ and $[C(CN)_3]^-$ anions, the $[NTf_2]^-$ anion (either combined with $[C_2mim]^+$ or $[Pyr_{14}]^+$ cations) is highly flexible and thus allow for the dispersion between PIL $C(CN)_3$ chains and can prompt the formation of homogeneous membranes until 40 wt% of free IL incorporated (Figure 19 – g, h, j and k). This behavior is consistent with the well-known high conformational structural flexibility of the $[NTf_2]^-$ anion.[45, 48, 49]. Nevertheless, when 60 wt% of free IL, either $[C_2mim][NTf_2]$ or $[Pyr_{14}][NTf_2]$, is incorporated into PIL $C(CN)_3$ chains phase separation occurs (Figure 19 – i and l).

2.4.3 PIL $B(CN)_4$

Figure 20 shows PIL-IL composite membranes bearing PIL $B(CN)_4$ and different amounts of free IL $N(CN)_2$, IL $C(CN)_3$ and IL $[C_2mim][NTf_2]$. Composite membranes combining PIL $B(CN)_4$ and free IL $B(CN)_4$ were previously studied by our group[53] and heterogeneous membranes were obtained for all the compositions tested (20, 40 and 60 wt% of free IL), due to the occurrence of segregation between both components, PIL $B(CN)_4$ and IL $B(CN)_4$.

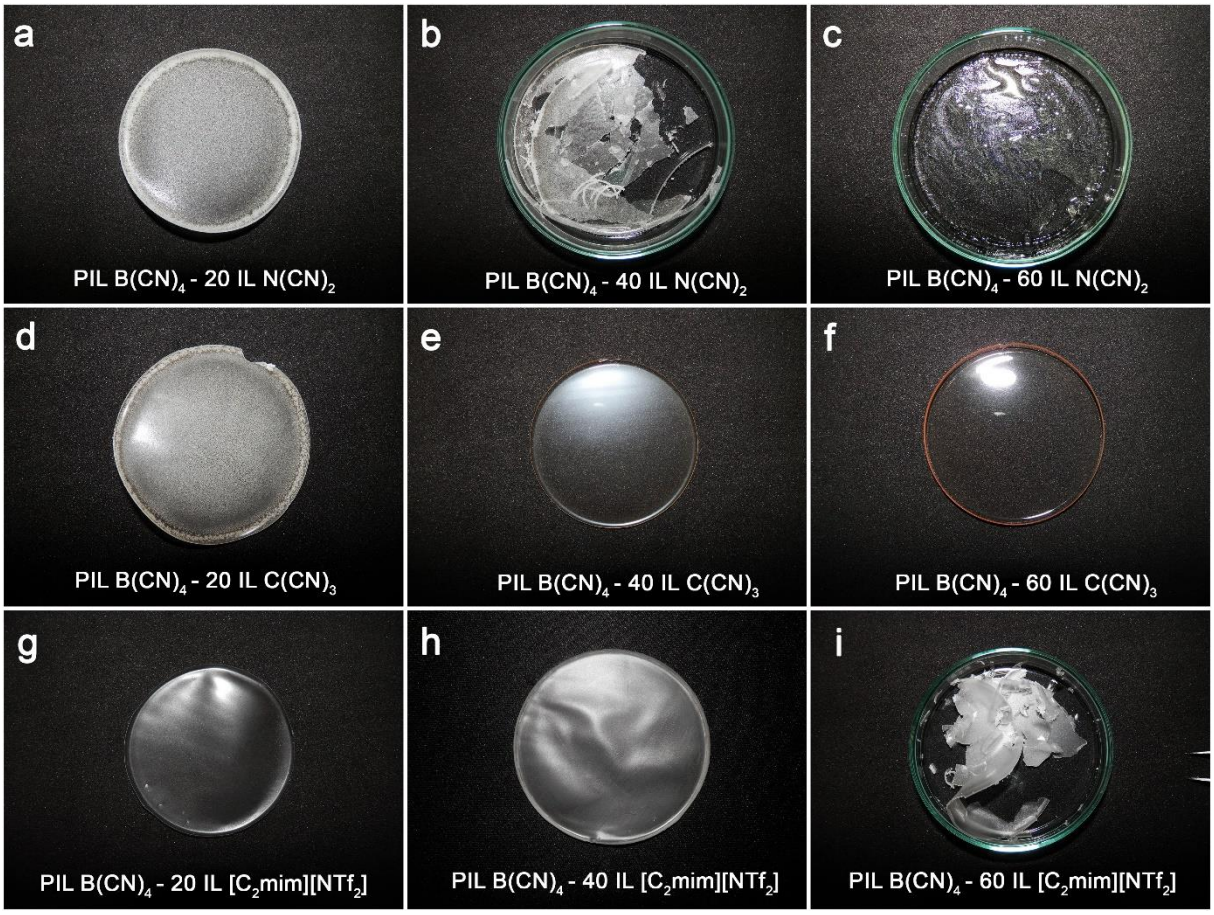

Figure 20 - Pictures of the prepared PIL-IL composite membranes containing PIL $B(CN)_4$ and different amounts of three different free ILs.

As mentioned in section 2.4.1., the obtained composite membranes made of PIL $N(CN)_2$ and 20, 40 and 60 wt% of IL $B(CN)_4$ were all heterogeneous and non-stable. This was attributed to the rigid geometry of the $[B(CN)_4]^-$ anion and its incompatibility with the $[N(CN)_2]^-$ anion (Figure 18 – d to f). In the same line, the prepared composite membranes containing PIL $B(CN)_4$ and 20, 40 and 60 wt% of IL $N(CN)_2$ were also found to be heterogeneous, as shown in Figure 20 – a to c. This means that, when combining $[B(CN)_4]^-$ and $[N(CN)_2]^-$ anions, the origin of the anions (either from PIL or from IL) does not significantly influence membrane forming ability and segregation.

In contrast to what was observed for composite membranes of PIL $C(CN)_3$ and IL $B(CN)_4$, where stable and homogenous membranes were obtained until 60 wt% of free IL incorporated (Figure 19 – d to f), an unexpected result was found amongst the composites bearing PIL $B(CN)_4$ and IL $C(CN)_3$. In general, if a PIL is able to incorporate 60 wt% of a certain free IL, this PIL should also be able to incorporate 40 and 20 wt% of the same free IL. From Figure 20 – e and f, it can be observed that both PIL $B(CN)_4$ – 40 IL $C(CN)_3$ and PIL $B(CN)_4$ – 60 IL $C(CN)_3$ membranes are homogenous, transparent and free standing, but the PIL $B(CN)_4$ – 20 IL $C(CN)_3$ membrane is heterogeneous, and a white precipitate is clearly visible at naked eye (Figure 20 – d), even after distinct casting process conditions were attempted (Table 4). The membrane PIL $B(CN)_4$ – 20 IL $B(CN)_4$ was reported by Tomé et al. to be heterogeneous and brittle[53] and, as stated before, the $[C(CN)_3]^-$ and $[B(CN)_4]^-$ anions

are very similar. The chemical similarity between these two membranes, PIL $B(CN)_4$ – 20 IL $C(CN)_3$ and PIL $B(CN)_4$ – 20 IL $B(CN)_4$, could explain the segregation of the PIL $B(CN)_4$ – 20 IL $C(CN)_3$ membrane. It seems that for composites of PIL $B(CN)_4$ with higher amounts (40 and 60 wt%) of free IL $C(CN)_3$, the presence of higher amount of $[C(CN)_3]^-$ anions increases the compatibility of the starting materials and thus homogeneous membranes can be obtained. Nonetheless, after a couple of weeks of storage, PIL $B(CN)_4$ – 60 IL $C(CN)_3$ composite membrane started to leek small amounts of free IL $C(CN)_3$, indicating that 60 wt% is an approximated value of the maximum amount of free IL $C(CN)_3$ wt% possible that can be incorporated into the PIL $B(CN)_4$.

The results obtained for composites made of PIL $B(CN)_4$ and 20, 40 and 60 wt% of free IL $[C_2mim][NTf_2]$ are similar to those of composites having PIL $C(CN)_3$ combined with the same IL, showing again that, despite the chemical differences between $[NTf_2]^-$ and $[B(CN)_4]^-$ anions, the structural flexibility of the $[NTf_2]^-$ anion is essential for the successful incorporation of 20 and 40 wt% of this free IL between the rigid polymeric chains of PIL $B(CN)_4$ (Figure 20 – g and h). Segregation between both phases was only observed for the composite membrane with 60 wt% of free IL $[C_2mim][NTf_2]$ (Figure 20 – i). Interestingly, free IL $[C_2mim][NTf_2]$ is the only IL that can be successfully incorporated, at a concentration of 20 wt%, within the PIL $B(CN)_4$ chains, resulting in a free standing and homogenous membrane. This was not possible when using IL $C(CN)_3$, neither IL $N(CN)_2$ due to the differences in anions' geometry and conformational structures.

2.4.4 PIL NTf_2

PIL-IL composite membranes bearing PIL NTf_2 and different amounts of free IL $N(CN)_2$, IL $C(CN)_3$, IL $B(CN)_4$ and IL $[C_2mim][NTf_2]$ are depicted in Figure 21. Composite membranes containing PIL NTf_2 and different amounts (0, 40 and 60 wt%) of free IL $[Pyr_{14}][NTf_2]$ were previously studied by our group and can be found elsewhere.[55]

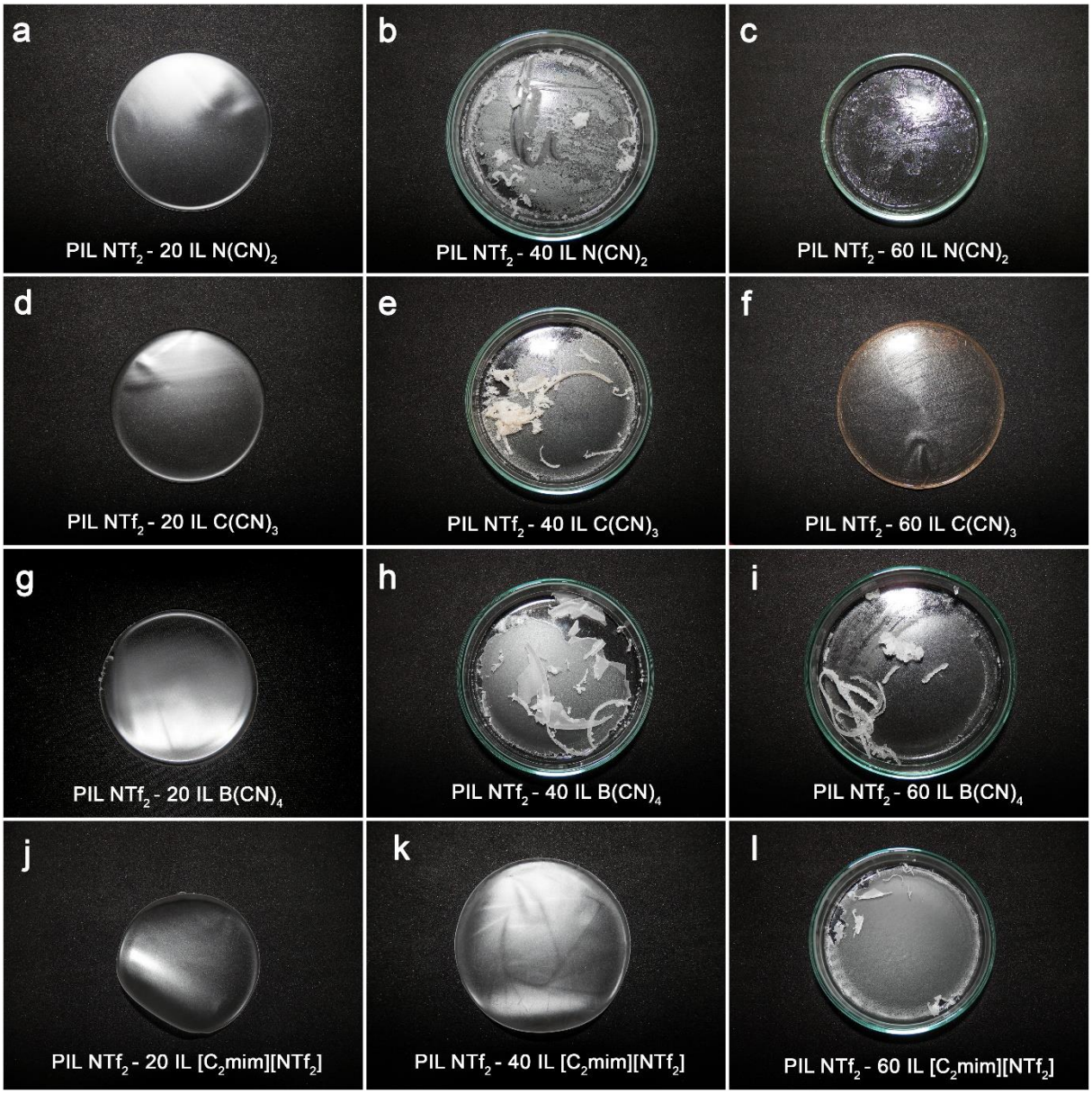

Figure 21 - Pictures of the prepared PIL-IL composite membranes containing the PIL NTf_2 and different amounts of four different free ILs.

The first thing to be noted for the PIL NTf_2 composite membranes is that, for all the studied ILs having cyano-functionalized anions (IL $N(CN)_2$, IL $C(CN)_3$ and IL $B(CN)_4$), only 20 wt% of these free IL can be incorporated into PIL NTf_2 so that mechanically stable and homogenous membranes (Figure 21 – a, d, g and j) can be obtained. This is in contrast to what was found for composite membranes of PIL $C(CN)_3$ or PIL $B(CN)_4$ combined with IL $[C_2mim][NTf_2]$, respectively shown in Figures 19 (g to h) and 20 (g to h), where it can be seen that stable and homogenous membranes were obtained at 20 and 40 wt% of free IL. These results clearly indicate that the source component (either PIL or IL) of the $[NTf_2]^-$ anion is crucial for the membrane formation ability: when the $[NTf_2]^-$ anion is in the PIL, it is difficult to incorporate each one of the three ILs containing cyano-functionalized anions within the PIL chains. A possible explanation might be that $[NTf_2]^-$ anions can be more strongly connected to the PIL polycation (due to the localized charge of the PIL polycation, in contrast with the delocalized charge of

the IL's cation), somehow allowing for less polymer chain mobility and thus for a more packed macromolecular structure with little space for entrapping the free IL's cations and anions, allowing for, in general, only 20 wt% of the three free ILs containing cyano-functionalized anions to be incorporated within the polymeric chains of PIL NTf_2. An unexpected behavior was observed when the IL $C(CN)_3$ is added to PIL NTf_2: PIL NTf_2 – 60 IL $C(CN)_3$ (Figure 21 – f) does not present a phase separation behavior as clear as that found for PIL NTf_2 – 40 IL $C(CN)_3$ (Figure 21 – e). However, the membrane PIL NTf_2 – 60 IL $C(CN)_3$ leaches IL after some days of storage, suggesting that the free IL was not stably arranged within the PIL chains.

Conversely, when the source of $[NTf_2]^-$ anions is the free IL, it is possible to incorporate up to 40 wt% of $[C_2mim][NTf_2]$ within the chains of both the PIL $C(CN)_3$ and PIL $B(CN)_4$ (Figure 20 – g and h and Figure 19 – g and h). In addition, it is also possible to incorporate up to 40 wt% of the free IL $[Pyr_{14}][NTf_2]$ into PIL $C(CN)_3$ (Figure 19 – j and k). At 60 wt% of each one these two free ILs ($[C_2mim][NTf_2]$ and $[Pyr_{14}][NTf_2]$), PILs and ILs become incompatible no matter what the source of the $[NTf_2]^-$ anions is.

Although Tomé et al. reported the incorporation of 60 wt% of the free IL $[Pyr_{14}][NTf_2]$ into PIL NTf_2 and obtained a stable and homogenous membrane,[55] in the present work only up to 40 wt% of the free IL $[C_2mim][NTf_2]$ could be incorporated inside the same PIL (Figure 21 – j and k). In this case, the differences in the PIL and IL's cations seem to be the key factor regarding the membranes forming ability. For the composite membranes of PIL NTf_2 and 20, 40 and 60 wt% of IL $[Pyr_{14}][NTf_2]$ prepared by Tomé et al,[55] both the PIL cation and the IL cation are based on pyrrolidinium moieties, while for the composite membranes of PIL NTf_2 and 20, 40 and 60 wt% of IL $[C_2mim][NTf_2]$ the IL cation is based on imidazolium moieties. Due to the higher chemical similarity between their respective PIL and IL cations, it was possible to incorporate a higher 60 wt% of the free IL $[Pyr_{14}][NTf_2]$ inside the PIL NTf_2 chains when compared to that of free IL $[C_2mim][NTf_2]$ (only 40 wt%). As it can be seen in Figure 19 – g to l, such cation difference was not relevant for composite membranes combining PIL $C(CN)_3$ and each one of the free ILs $[C_2mim][NTf_2]$ and $[Pyr_{14}][NTf_2]$, since in both combinations only the incorporation of 40 wt% of free IL resulted in homogenous free standing membranes.

2.4.5 Final Remarks

In summary, it can be observed that despite the chemical similarities between some of the anions present in either the IL or the PIL studied in this work, a large variety of behaviors was obtained. It is useful to provide a perspective on all the prepared membranes and compare results obtained among the different PILs.

It can be observed that it is possible to incorporate 20 wt% of the free IL $N(CN)_2$ into PIL $N(CN)_2$,[53] PIL $C(CN)_3$ and PIL NTf_2, but not into PIL $B(CN)_4$. Despite the fact that both anions $[N(CN)_2]^-$ and $[B(CN)_4]^-$ are cyano functionalized, they are not compatible (at the three free IL concentrations tested), as their geometries are significantly different. Surprisingly, the $[N(CN)_2]^-$ anion is even more compatible with the $[NTf_2]^-$ anion than with $[B(CN)_4]^-$, allowing at least the formation of the PIL NTf_2 – 20 IL $N(CN)_2$ composite membrane. On the other hand, a closer similarity between the $[N(CN)_2]^-$ and

$[C(CN)_3]^-$ anions allowed the incorporation of 20 and 40 wt% of the free IL $N(CN)_2$ into the PIL $C(CN)_3$. In general, the incorporation of 60 wt% of free IL $N(CN)_2$ in all four PILs used lead to the formation of composite membranes that are gel-like materials (Figures 19, 20 and 21 - c), essentially due to the hydrophilic nature of the $[N(CN)_2]^-$ anion.

The free IL $C(CN)_3$ is highly compatible with PIL $N(CN)_2$, forming stable and homogenous membranes at all three wt% of free IL tested. Also, IL $C(CN)_3$ is compatible with the PIL $B(CN)_4$, with the only exception being PIL $B(CN)_4$ – 20 IL $C(CN)_3$. As previously reported by Tomé et al.,[53] the IL $C(CN)_3$ can also be used to prepare homogenous composite membranes with the PIL $C(CN)_3$. In fact, this IL is very versatile and compatible with, at least, the three PILs also bearing a cyano-functionalized counter anion.[53] Despite the versatility of the IL $C(CN)_3$, it cannot be incorporated into PIL NTf_2 chains at free IL concentrations higher than 20 wt% (Figure 21 – e and f).

In what concerns the incorporation of the free IL $B(CN)_4$ into PIL $N(CN)_2$, heterogeneous membranes were obtained for all concentrations of free IL tested. It was also found that is not possible to incorporate any amount of the free IL $B(CN)_4$ into the PIL $B(CN)_4$.[53] Overall, it can be concluded that the incorporation of the free IL $B(CN)_4$ into different PILs is not easy, probably due to the $[B(CN)_4]^-$ anion's rigid geometry and conformational structure. Only PIL NTf_2 – 20 IL $B(CN)_4$ and composites of PIL $C(CN)_3$ and 20, 40 and 60 wt% of free IL $B(CN)_4$ could be successfully prepared.

Regarding the incorporation of IL $[C_2mim][NTf_2]$ in the studied PILs, it can be concluded that this IL can be incorporated at 20 and 40 wt% into PIL $C(CN)_3$, PIL $B(CN)_4$ and PIL NTf_2, probably due to the high structural flexibility of the $[NTf_2]^-$ anion in the free IL. It is interesting to notice that both PIL NTf_2 and the free IL $[C_2mim][NTf_2]$ share the same anion, but no distinction can be made (regarding membrane formation and stability) between the PIL NTf_2 and the PIL $C(CN)_3$ and PIL $B(CN)_4$ when the IL $[C_2mim][NTf_2]$ is used. This lack of distinct behavior is probably a result of the difference between the imidazolium based cation of the free IL $[C_2mim][NTf_2]$ and the pyrrolidinium based cation of all three PILs. This difference in the cation moieties is only relevant when incorporating 60 wt% of free IL, even for PIL NTf_2 - 60 IL $[C_2mim][NTf_2]$ since, even though the PIL and IL's anions are the same, an heterogeneous membrane was obtained.

The preparation of composite membranes through the incorporation of free IL $[Pyr_{14}][NTf_2]$ was performed only PIL $C(CN)_3$ and PIL NTf_2.[55] In this case, both the PIL and IL components share a pyrrolidinium-based cation, while the anions can be either different or equal. It can be concluded that having the same anion in both the PIL and the IL allows the formation of homogenous composite membranes of PIL NTf_2 and 20, 40 and 60 wt% of free IL $[Pyr_{14}][NTf_2]$, whereas the use of PIL and IL components having different anions only results in homogenous membranes up to 40 wt% of free IL (PIL $C(CN)_3$ – (20 and 40) IL $[Pyr_{14}][NTf_2]$).

In order to have a better grasp of the easiness of preparation of the composite membranes studied in this work, Table 5 presents a summary of the number of all membranes prepared, including the success rate of membrane formation for the different anions. From the 21 prepared composite membranes containing the $[C(CN)_3]^-$ anion (either as PIL $C(CN)_3$ or free IL $C(CN)_3$)), 15 (71 %) of them formed free standing and homogeneous. The three composite membranes based on PIL $C(CN)_3$ and different amount of free IL $[Pyr_{14}][NTf_2]$ (20, 40 and 60 wt%) will be considered as extra materials,

since no other PIL was studied along with this free IL and thus comparisons/discussions cannot be established. Taking into account this fact, the success rate percentage of membranes containing the $[C(CN)_3]^-$ anion is now 66 %. By applying the same statistics to the other anions, a 45 % success rate is achieved for the composite membranes containing $[NTf_2]^-$ anion, 44 % for membranes bearing $[B(CN)_4]^-$ anion and only 33% for the composite membranes combining $[N(CN)_2]^-$ anions. These simple statistic calculations show that PIL-IL composites containing $[C(CN)_3]^-$ anions are the most successful in the preparation of stable and homogenous composite membranes, due to the better structural and/or chemical compatibility of the $[C(CN)_3]^-$ anion with the other cyano-functionalized anions, and also with the $[NTf_2]^-$ anion, as well as its geometrical flexibility. At the other end, membranes bearing the $[N(CN)_2]^-$ anion are the most difficult to prepare. In general, the high hydrophilic nature of this anion result in phase separated and/or gel-like membranes, impossible to be manipulated, bringing the success rate to the lowest (33 %) amongst the four anions studied in this work.

Table 5 – Summary of the number of membranes studied in this work. The membrane formation success rate (%) was calculated by dividing the number of stable and homogenous membranes by the number of total membranes.

	Number of Membranes
Stable and Homogenous	21
Non-Stable and/or Heterogeneous	21
TOTAL	42

		Number of Membranes			
		Stable and Homogenous	Non-Stable and/or Heterogeneous	TOTAL	**Membrane Formation Success Rate (%)**
Membranes containing the anion:	**$[N(CN)_2]^-$**	6	12	18	**33**
	$[C(CN)_3]^-$	15	6	21	**71**
	$[B(CN)_4]^-$	8	10	18	**44**
	$[NTf_2]^-$	11	13	24	**45**

3. Gas Permeation Experiments

The single CO_2 and N_2 permeation properties (permeability, diffusivity and solubility) determined through all the prepared 21 stable and homogenous composite membranes are presented in this chapter. The gas permeation experiments were carried out, at 293 K, with a trans-membrane pressure differential of 100 kPa and in single gas feed conditions, using the time-lag method. This equipment allows for the simultaneous determination of permeability and diffusivity. Assuming that the gas transport through the prepared dense composite membranes occurs via a solution-diffusion mechanism, gas solubility values were estimated from the measured permeability and diffusivity data using Eq. 3.

3.1 Gas Permeation Measurements

Three methods have been commonly used to measure the permeation properties of gases through dense polymeric membranes: a differential method, an integral method (also known as the time-lag) and a sorption method.[56] Experiments using the sorption method usually take longer than the other two methods and thermal effects can account for potential error sources. The differential method has the advantage of minimizing gas leakages, but for low permeation flow rates it requires very sensitive on-line detection systems.[57] The time-lag method was first proposed in 1920 by Daynes,[58] and despite the advantages and disadvantages of the other two methods, it is undoubtedly the most frequently used.[57] In the time-lag method, a practically constant pressure difference is applied to both sides of the membrane and the gas accumulated on the permeate side is measured over time. A schematic representation of the time-lag apparatus used in this work is depicted in Figure 22.

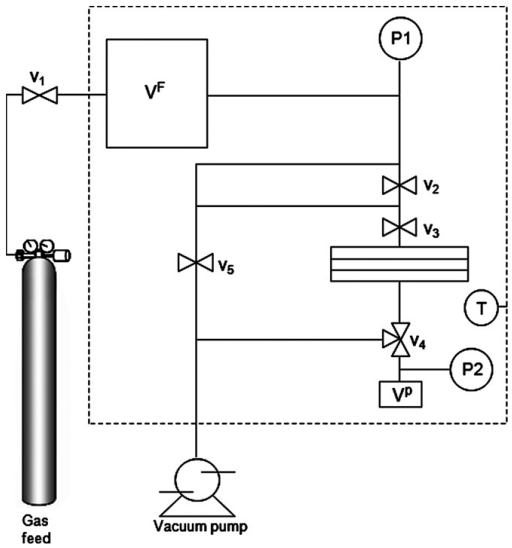

Figure 22 – Schematic representation of the time-lag apparatus. *P* represents the pressure sensors, *V* the manual valves, V^F the feed tank, V^P the permeate tank and *T* a thermostatic air bath.[55]

The apparatus is composed by two stainless steel tanks, the feed tank (5 dm^3) and the permeate tank (34.2 ± 0.2) cm^3, both connected to a flat-type permeation cell with an effective area of 13.9 cm^2. The PIL-IL composite membranes were first positioned on the permeation cell (Figure 23), where a highly porous sintered disk supports the membranes, and then a Viton O-ring was used to seal the permeation cell.

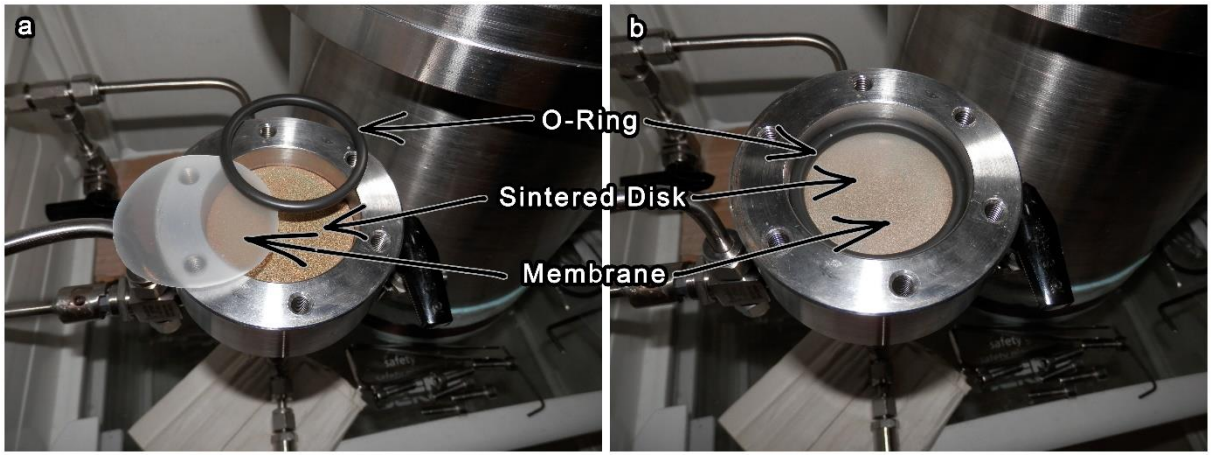

Figure 23 – Flat-type permeation cell used in this work. In the left picture (a) the components are separated. In the right picture (b) the components are assembled and ready to sell the permeation cell.

To ensure gas permeation experiments took place under constant temperature, the time-lag apparatus is positioned inside a thermostatic cabinet, where temperature is controlled with a precision of ±0.05 K. All manual valves (Figure 22 - V_1, V_2, V_3, V_4 and V_5) and gas bottles are placed outside this cabinet so they can be manipulated without compromising the thermostatic conditions. The pressure on the feed tank was monitored using a suitable sensor (S-10 WIKA, 600 kPa ±0.05% FS, Figure 22 - P1), while the pressure variations on the permeate tank were measured using a high precision absolute pressure sensor (MKS e-Baratron, ref. 628C, 13.33 kPa, 0.001% FS, Figure 22 - P2). A rotatory high vacuum pump (BOC Edwards, RV3) guaranteed vacuum conditions. Air Liquide supplied the carbon dioxide (CO_2) and nitrogen (N_2) with, at least, 99.99% purity. These gases were used with no further purification.

In a typical procedure, vacuum is first applied to the whole system (at least for 12h) to ensure that possible traces of water and gases are removed from the feed and permeate side, as well from the membrane itself. Second, the vacuum (<0.1 kPa) is isolated on the permeate side, to ensure the initial gas concentration on this side is approximately null ($C_0 \approx 0$), and on the feed side the desired gas (CO_2 or N_2) is introduced until the desired feed pressure (100 kPa) is achieved. Finally, the single gas permeation experiments were conducted at 293 K with a tans-membrane pressure differential of 100 kPa against initial vacuum downstream (< 0.1 kPa). At least three separate experiments of each gas on a single membrane sample were carried out. Between each run, the permeation cell and lines were evacuated, on both upstream and downstream sides until the pressure was below 0.1 kPa. The thicknesses of the PIL-IL composite membranes measured in this work (120 to 200 μm) were measured before and after testing using a digital micrometer (Mitutoyo, model MDE-25PJ, Japan).

Average thickness was calculated from six measurements taken at different locations of each membrane sample. At the end of the gas experiments, no residual IL was found inside the permeation cell and similarly, the membranes mass remained constant.

The time-lag method assumes that the volume of the feed chamber is large enough to allow the feed pressure to remain approximately constant during the experiment. This method also neglects the influence of permeate pressure build up on the trans-membrane driving force, meaning that this force is considered constant during the experiment.[59] The determination of the mass transport parameters by the time-lag method is based on the downstream pressure history, monitored herein by the pressure sensor P2 (Figure 22). Accordingly, the permeate pressure built up follows the behavior illustrated in Figure 24. In the first state, also known as the transient state or non-steady state, the flow rate of the gas specie through the membrane is non-steady, it increases over time. After a certain time, the "time lag" (θ), a steady state is achieved and the flow rate of the gas specie through the membrane is steady.[60]

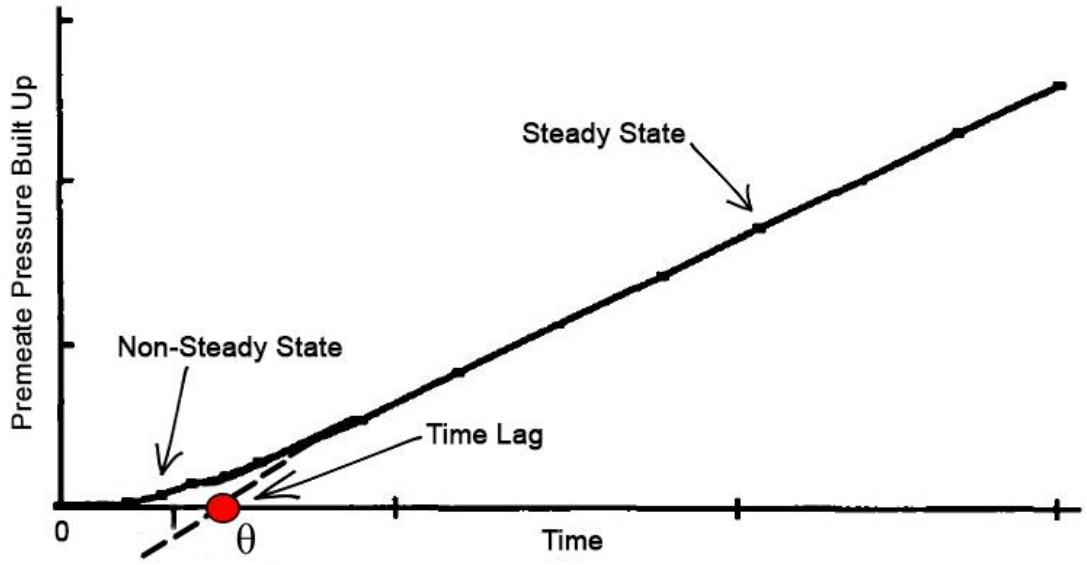

Figure 24 – Permeate pressure built up across time, for gas permeation experiments on dense membranes, according to the time-lag method. Picture adapted from[60].

The permeability of the gases through the 21 stable and homogenous membranes was determined using Eq. 1 (Introduction – 1.3 Gas Transport in Dense Membranes) and Eq. 8: [55]

$$J = \frac{V^p \Delta P}{AtRT} \quad (8)$$

where V^p is the permeate volume, ΔP the variation of the downstream pressure, A the effective area of the membrane, t time, R the gas constant and T is the absolute temperature.

The diffusivity was determined using Eq. 9: [55]

$$D = \frac{l^2}{6\theta} \quad (9)$$

where l is the membrane thickness and θ the time lag parameter (Figure 24). Finally, the solubility values were obtained through Eq. 3 (Introduction – 1.3 Gas Transport in Dense Membranes) using the previously obtained permeability and diffusivity data.

3.2 Results and Discussion

The following chapter contains the final results of the gas permeation experiments for all the 21 stable and homogenous PIL-IL composite membranes. The presentation and discussion of the results are divided into the different PILs (PIL $N(CN)_2$, PIL $C(CN)_3$, PIL $B(CN)_4$ and PIL NTf_2) and ILs (IL $N(CN)_2$, IL $C(CN)_3$, IL $B(CN)_4$, IL $[C_2mim][NTf_2]$ and IL $[Pyr_{14}][NTf_2]$) studied, followed by a final discussion regarding the CO_2 separation performance of all the membranes and final remarks.

For comparative and discussion purposes, Table 6 presents a summary of the thermophysical properties of the five ILs used in this work, as well as their CO_2 and N_2 permeabilities and respective permselectivities.

Table 6 – Thermophysical properties of the ILs used in this work, as well as their CO_2 and N_2 permeabilities and respective CO_2/N_2 permselectivities through the respective SILMs. The data of the ILs containing cyano anions were taken from Tomé et. al,[61] while data for the ILs having the $[NTf_2]^-$ anion was taken from Tomé et al.[62]. All the gas permeation data were obtained at 293.15 K and 100 kPa.

IL	M (g/mol)	η (MPa.s)	ρ (g/cm^3)	V_M (cm^3/mol)	PCO_2 (Barrer)	PN_2 (Barrer)	$\alpha CO_2/N_2$
IL $N(CN)_2$	177.21	18	1.11	160.24	476	7	68
IL $C(CN)_3$	201.23	17	1.09	185.54	667	12	57
IL $B(CN)_4$	226.05	21	1.04	226.89	742	15	49
IL $[C_2mim][NTf_2]$	391.30	27	1.51	258.40	589	17	36
IL $[pyr_{14}][NTf_2]$	422.40	60	1.39	303.95	340	12	28

It should be noted that the error of the permeability, diffusivity and solubility values represent standard deviations based on three experimental replicas (error bars in Figures 25 to 49). The error of permselectivity values was determined by the error propagation method (Eq. 10): [72]

$$\Delta S = \left(\frac{1}{P_{N_2}}\right)\Delta P_{CO_2} + \left(\frac{P_{CO_2}}{P_{N_2}^2}\right)\Delta P_{N_2} \qquad (10)$$

3.2.1 PIL $N(CN)_2$

Figure 25 shows that the CO_2 permeability values are always higher than those of N_2 permeability ($PCO_2 >> PN_2$) for all the composite membranes of PIL $N(CN)_2$ with 20, 40 and 60 wt% of IL $C(CN)_3$. The differences between CO_2 and N_2 solubilities (Figure 27), being the CO_2 solubility values higher than the N_2 solubility values, justify the use of these membranes in CO_2/N_2 separation due to their selective separation behavior. By increasing the amount of free IL incorporated into the PIL, both the CO_2 and N_2 permeabilities increase (Figure 25). This increment in gas permeability can be attributed to the increase of both gas solubility and diffusivity, being the increase of gas diffusivity more significant, as it can be seen in Figures 26 and 27. The larger contribution of diffusivity to the increase in the permeability values indicates an increase in free volume of these PIL-IL composite

membranes, which enhances the polymer chain mobility, thanks to the presence of the free ions pairs. Both these trends have been observed for other PIL-IL composite membranes[53, 71].

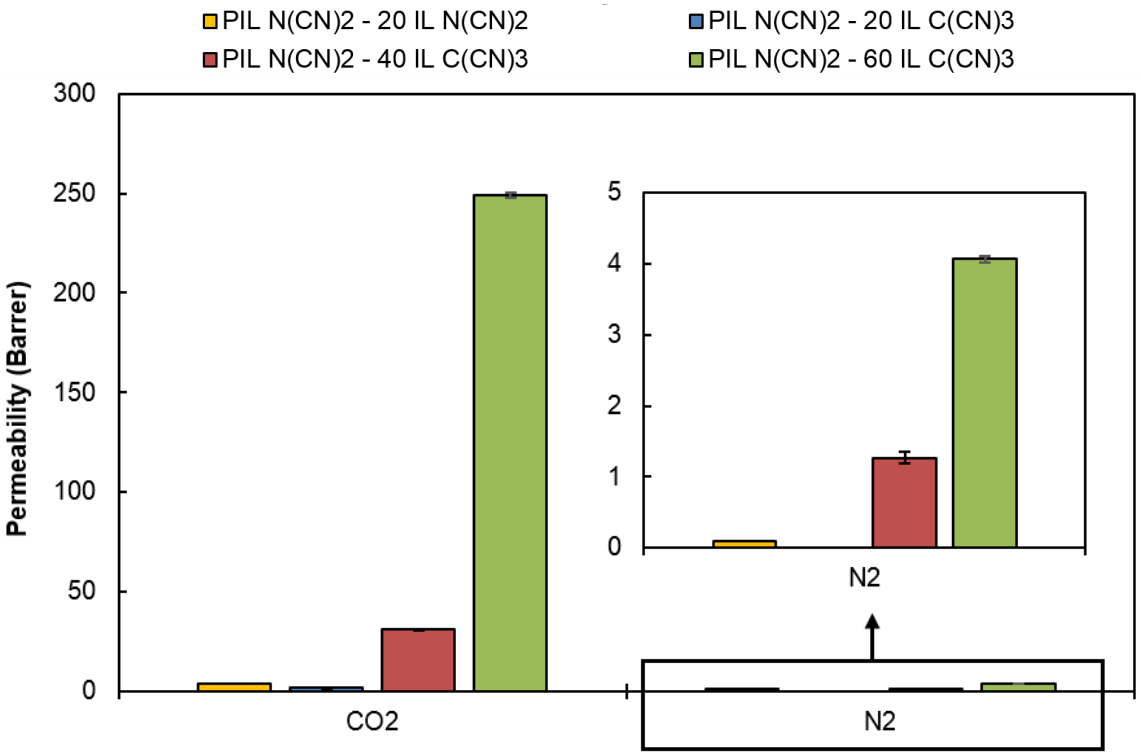

Figure 25 - Gas permeabilities through composite membranes bearing the PIL $N(CN)_2$. Sensitivity of the time-lag apparatus prevented a reliable measurement of the N_2 flux through the prepared PIL $N(CN)_2$ - 20 IL $C(CN)_3$ membrane. The data regarding the PIL $N(CN)_2$ - 20 IL $N(CN)_2$ membrane was taken from Tomé et al.[53]

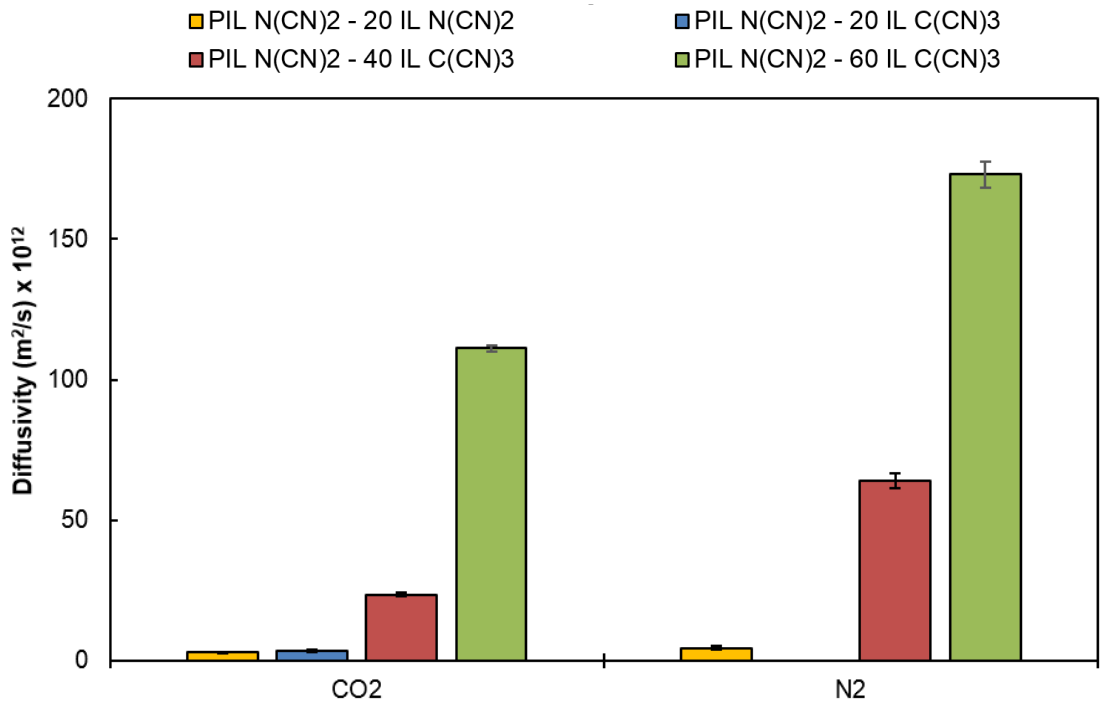

Figure 26 - Gas diffusivities through composite membranes bearing the PIL $N(CN)_2$. Sensitivity of the time-lag apparatus prevented a reliable measurement of the N_2 time-lag through the prepared PIL $N(CN)_2$ - 20 IL $C(CN)_3$ membrane and, consequently, the determination of diffusivity and estimation of solubility. The data regarding the PIL $N(CN)_2$ - 20 IL $N(CN)_2$ membrane was taken from Tomé et al.[53]

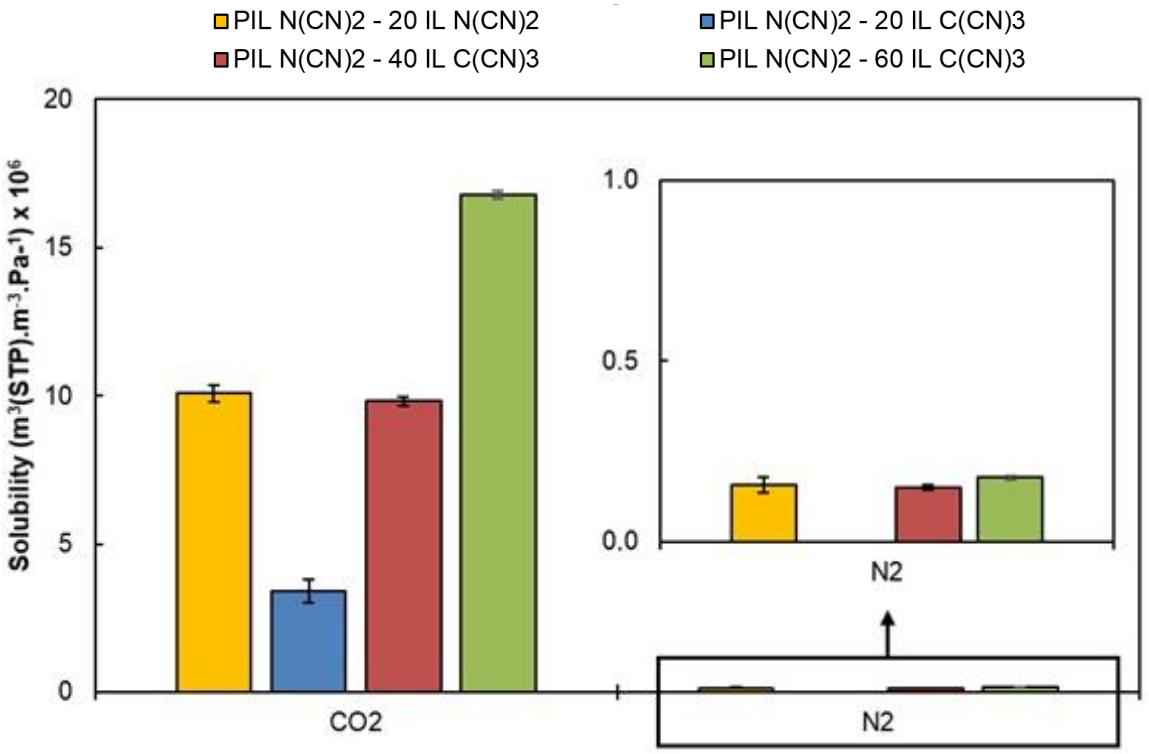

Figure 27 - Gas solubilities in the composite membranes bearing the PIL $N(CN)_2$. The data regarding the PIL $N(CN)_2$ - 20 IL $N(CN)_2$ membrane was taken from Tomé et al.[53]

The CO_2 and N_2 permeabilities for the membranes PIL $N(CN)_2$ – 20 IL $N(CN)_2$ and PIL $N(CN)_2$ – 20 IL $C(CN)_3$ are practically the same, meaning that the influence of the ILs with different cyano functionalized anions is not significant in this case. At 20 wt% of free IL incorporated, the PIL has the main contribution for gas permeability. From Figures 26 and 27, it can be observed that both gas diffusivity and gas solubility in these two membranes are also almost the same.

3.2.2 PIL $C(CN)_3$

As observed for membranes containing the PIL $N(CN)_2$ (section 3.2.1), the composite bearing PIL $C(CN)_3$ also exhibit the same two trends: $P_{CO_2} >> P_{N_2}$ and both CO_2 and N_2 permeabilities increase with the increased amount of free IL incorporated (Figures 28 and 31). Once again, the higher CO_2 permeabilities can be essentially attributed to the higher CO_2 solubility values when compared to those of N_2 (Figures 30 and 33). Also, quicker gas diffusivities through the composites are achieved by increasing the amount of free IL incorporated due to enhanced polymer chain mobility (Figures 29 and 32).

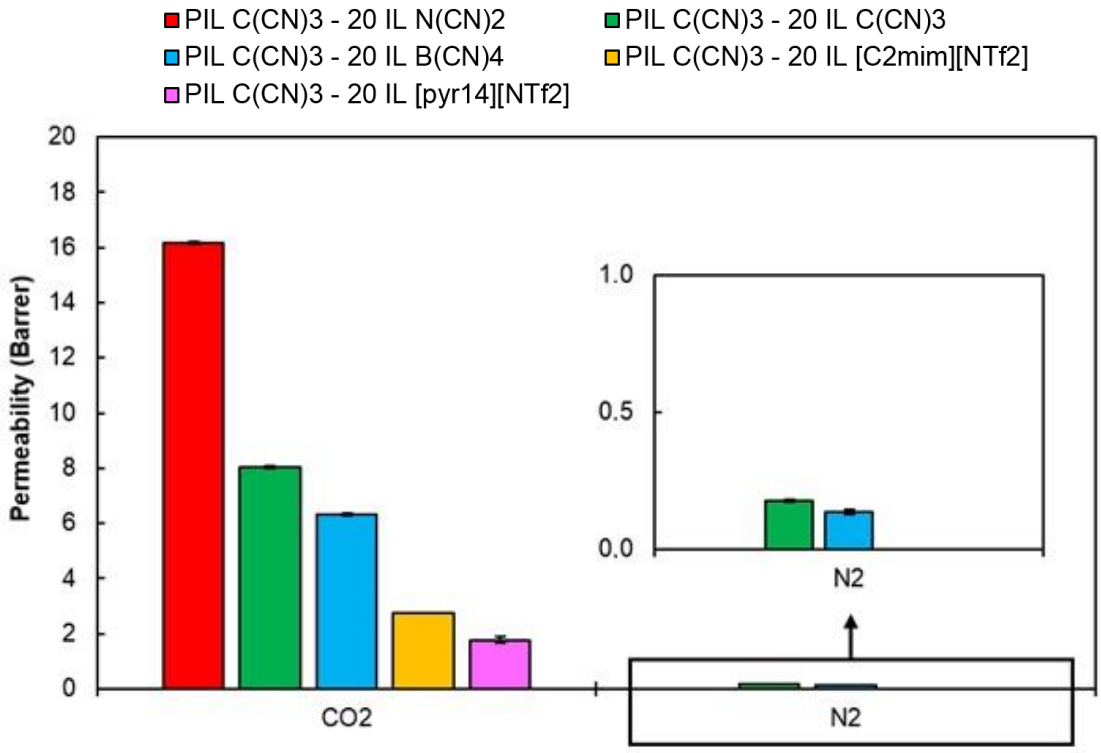

Figure 28 - Gas permeabilities through composite membranes bearing the PIL $C(CN)_3$. Sensitivity of the time-lag apparatus prevented a reliable measurement of the N_2 flux through some of the composites prepared with the following ILs: IL $N(CN)_2$, IL $[C_2mim][NTf_2]$ and IL $[Pyr_{14}][NTf_2]$.The data regarding PIL $C(CN)_3$ - 20 IL $C(CN)_3$ membrane was taken from Tomé et al.[53]

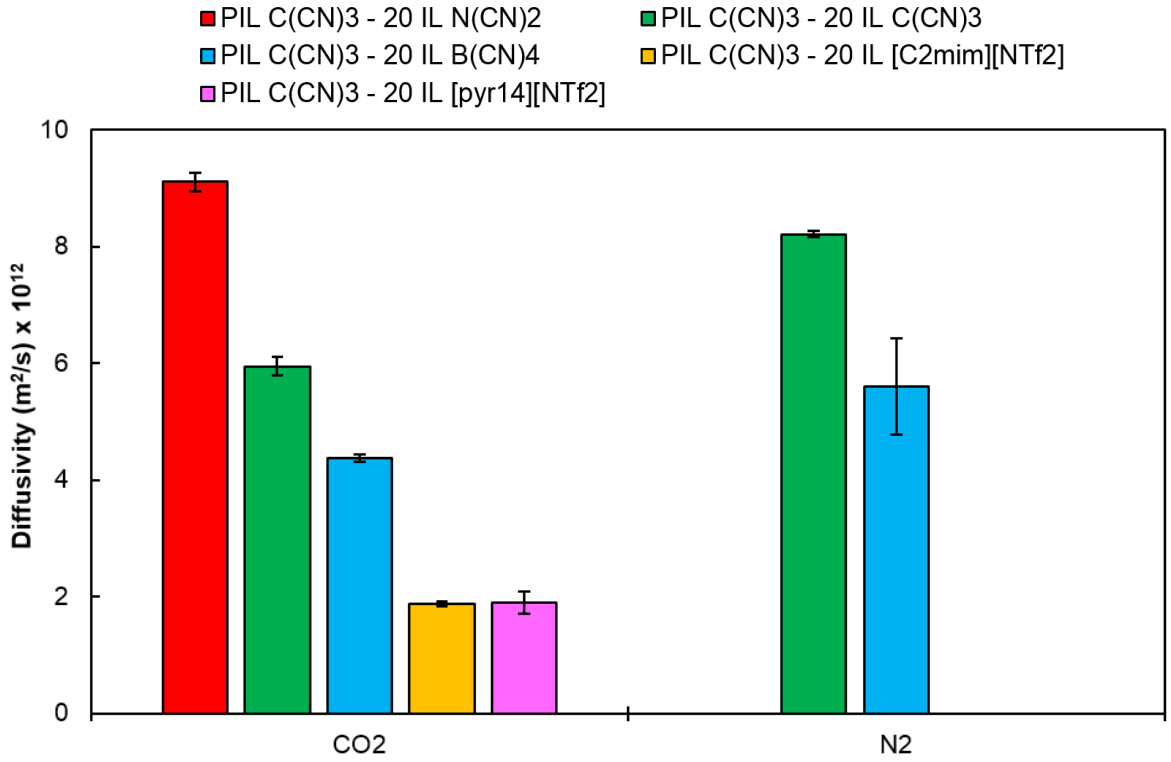

Figure 29 - Gas diffusivities through composite membranes bearing the PIL $C(CN)_3$. Sensitivity of the time-lag apparatus prevented a reliable measurement of the N_2 time-lag through some of the composites prepared with the following ILs: IL $N(CN)_2$, IL $[C_2mim][NTf_2]$ and IL $[Pyr_{14}][NTf_2]$ and, consequently, the determination of diffusivity and the estimation of solubility. The data regarding the PIL $C(CN)_3$ - 20 IL $C(CN)_3$ membrane was taken from Tomé et al.[53]

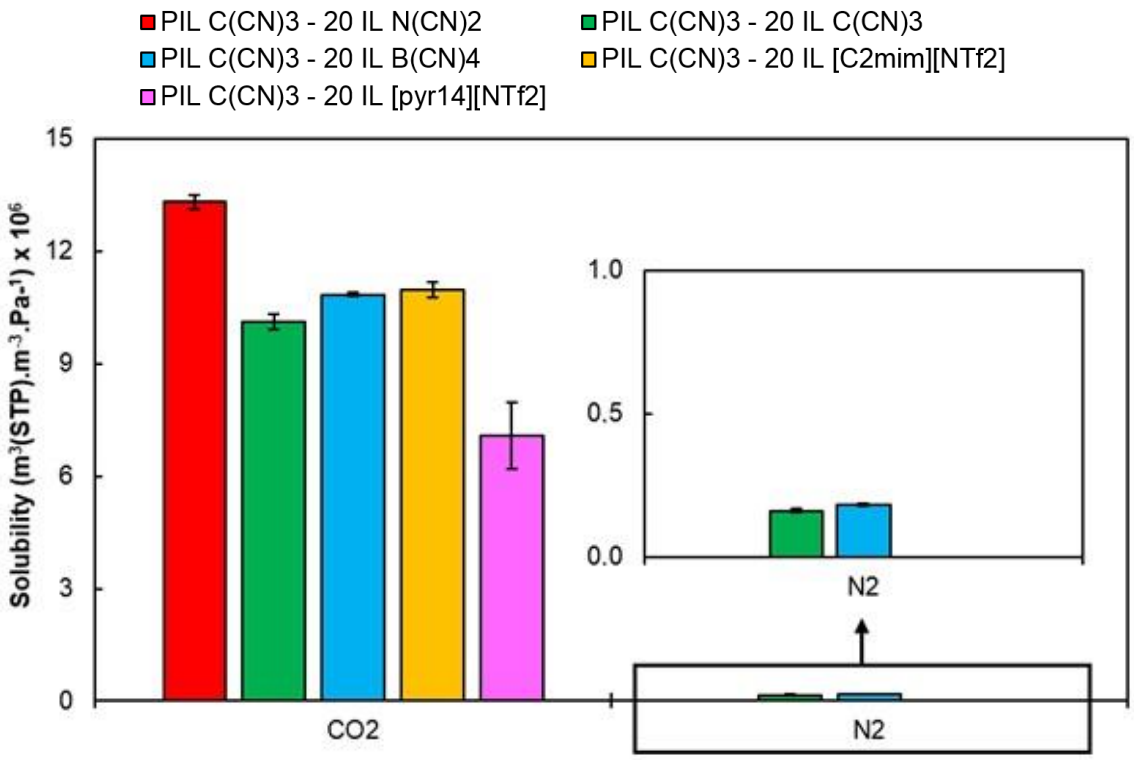

Figure 30 - Gas solubilities through composite membranes bearing the PIL $C(CN)_3$. The data regarding the membrane with the free IL $C(CN)_3$ was taken from Tomé et al.[53]

Table 6 shows that the gas permeabilities through a SILM impregnated with the pure IL $B(CN)_4$ are higher than those of IL $(CN)_3$-based SILM and higher than those of the IL $N(CN)_2$-based SILM. Taking into account these results and analyzing Figures 28 and 31, it can be seen that a non-expected trend was obtained. For the composite membranes prepared with PIL $C(CN)_3$ and each one of the three cyano-functionalized ILs (see Figure 28 for composites with 20 wt% of free IL, and Figure 31 for the composites with 40 wt% of free IL), the opposite trend can be observed: composite having the free IL $C(CN)_3$ have higher permeabilities than those of IL $B(CN)_4$, while the composites with the free IL $N(CN)_2$ have higher permeabilities than both the formers. A possible explanation for this reverse trend can be related with the membrane preparation method and the ILs molecular weight (M). The composite membranes were prepared on a mass basis, meaning that, due to differences on the molecular weight of the free ILs, membranes with different ILs but the same amount of free IL will have a different number of moles of free IL. For example, even though both the PIL $C(CN)_3$ – 20 IL $N(CN)_2$ and the PIL $C(CN)_3$ – 20 IL $B(CN)_4$ membranes have the same amount of free IL in wt% basis, the molecular weight of IL $N(CN)_2$ is lower than that of IL $B(CN)_4$ (Table 6), consequently the first membrane has more moles of free IL than the second one. Moreover, the same trend can be observed in Figures 29 and 32, where the diffusivity values obtained through these membranes also support this explanation. Membranes with free IL $N(CN)_2$ exhibit the highest diffusivity values due to the higher number of free ions present, increasing polymer chain mobility, thus creating lower resistance to gas diffusivity. The gas solubility in these membranes remain nearly the same (Figures 30 and 33), in particular for membranes with 20 wt% of free IL (Figure 30), showing, once again, that the decrease or increase in gas permeability is mainly a diffusivity controlled mechanism. Accordingly,

the results obtained for the composite membranes bearing free ILs with $[NTf_2]^-$ anion, namely $[C_2mim][NTf_2]$ and $[Pyr_{14}][NTf_2]$, present exactly the same trend. In addition to the free IL moles difference, $[C_2mim][NTf_2]$-based SILMs are known to have higher CO_2 permeabilities than $[Pyr_{14}][NTf_2]$-based SILMs (Table 6).

Regarding IL $C(CN)_3$ and IL $B(CN)_4$, it has been reported that their SILMs have higher CO_2 permeabilities than those of $[C_2mim][NTf_2]$ and $[Pyr_{14}][NTf_2]$-based SILMs (Table 6). This behavior was also observed in this work for the composite membranes of PIL $C(CN)_3$ and 20 and 40 wt% of the corresponding free ILs incorporated (Figures 28 and 31). However, the $[C_2mim][NTf_2]$ SILM generally has higher CO_2 permeabilities than that of the IL $N(CN)_2$ (Table 6), which could not be verified in this work for the composite membranes, as it can be seen in Figures 28 and 31. The same explanation regarding the differences in the molecular weight of the ILs supports this result, as the molecular difference between these two ILs is the second largest, only after the difference between the molecular weights of the IL $N(CN)_2$ and the IL $[Pyr_{14}][NTf_2]$. Both ILs with the $[NTf_2]^-$ anion have higher molar volumes than the ILs combining cyano-functionalized anion (Table 6), which should result in less packed membranes and, consequently, more permeable materials. However, the $[NTf_2]^-$ anion is known to have a high conformational structural flexibility,[22] and both ILs with $[NTf_2]^-$ anions also present higher viscosities (Table 6). At the end, composite membranes prepared with free ILs having this anion are denser and more packed, which hinders gas diffusion, resulting in lower permeabilities than those generally observed in this work for composite membranes containing free ILs with cyano-functionalized anions.

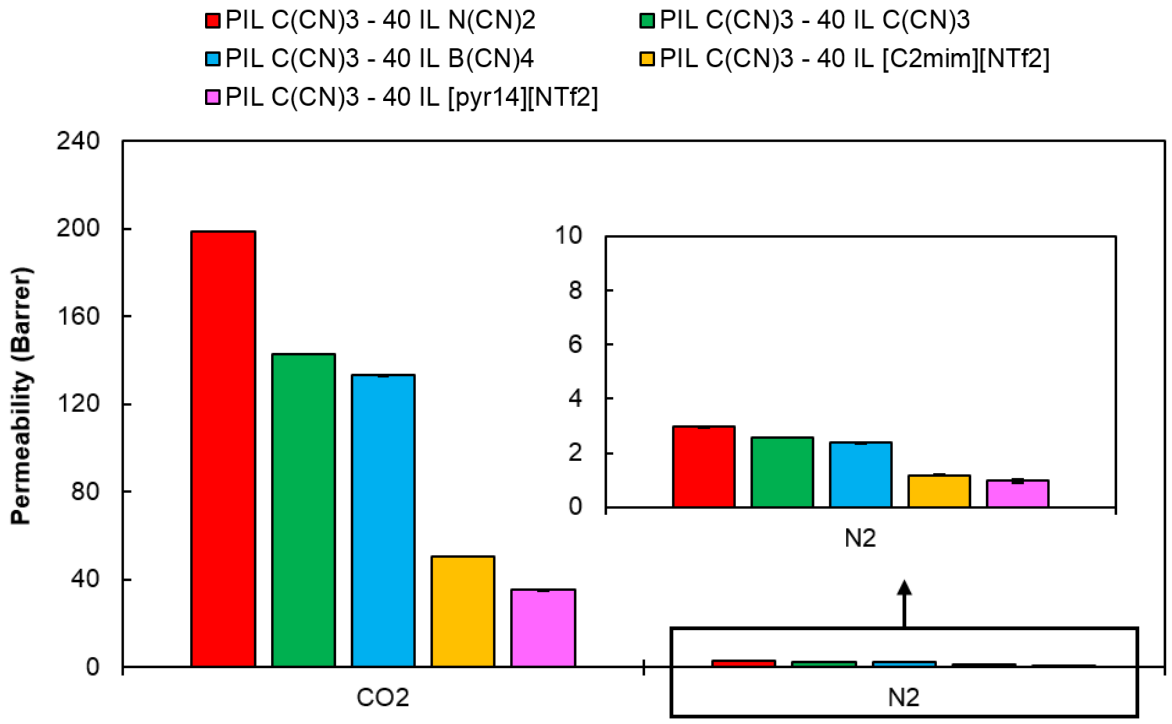

Figure 31 - Gas permeabilities through composite membranes bearing the PIL $C(CN)_3$. The data regarding PIL $C(CN)_3$ - 20 IL $C(CN)_3$ membrane was taken from Tomé et al.[53]

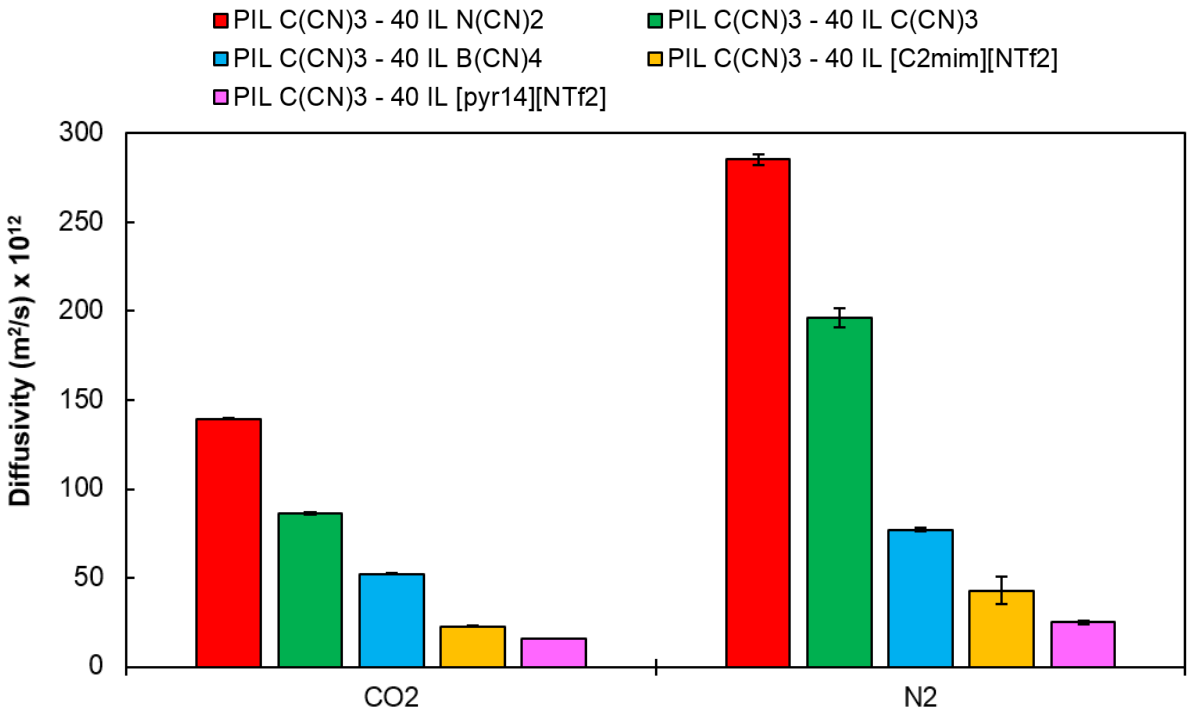

Figure 32 - Gas diffusivities through composite membranes bearing the PIL $C(CN)_3$. The data regarding the PIL $C(CN)_3$ - 20 IL $C(CN)_3$ membrane was taken from Tomé et al.[53]

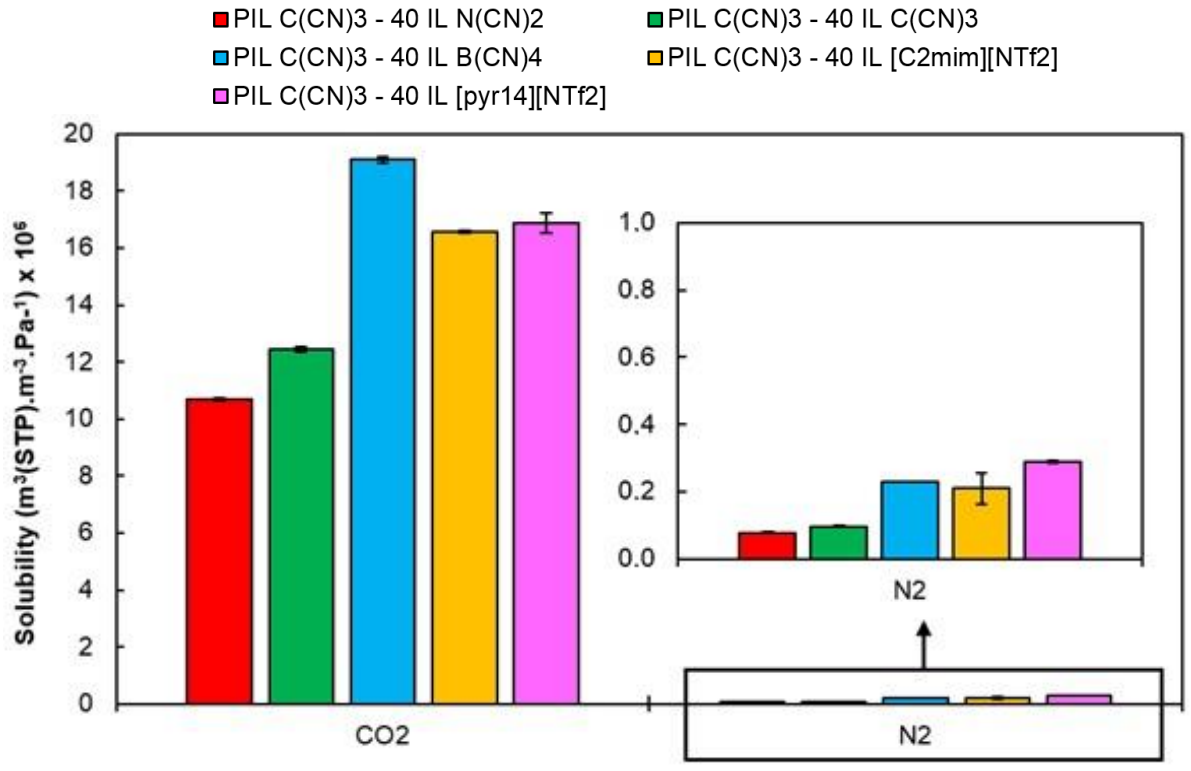

Figure 33 - Gas solubilities through composite membranes bearing the PIL $C(CN)_3$. The data regarding the PIL $C(CN)_3$ - 20 IL $C(CN)_3$ membrane was taken from Tomé et al.[53]

3.2.3 PIL $B(CN)_4$

In this case, only four composite membranes bearing PIL $B(CN)_4$ were obtained. Once again, and as for the composite membranes bearing the PIL $N(CN)_2$ and PIL $C(CN)_3$, an increase in the amount of free IL incorporated into the membrane leads to high gas diffusivities (Figure 35) and permeabilities (Figure 34). Major differences between CO_2 and N_2 permeabilities can also be attributed to their respective differences in gas solubility (Figure 36).

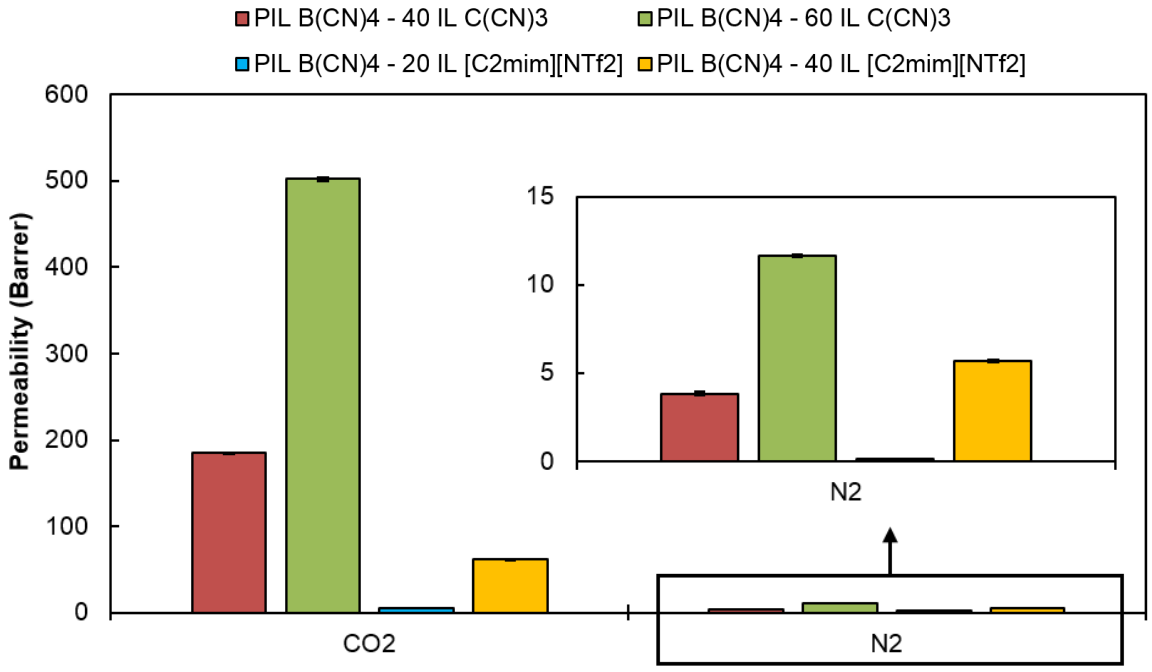

Figure 34 - Gas permeabilities through composite membranes bearing the PIL $B(CN)_4$.

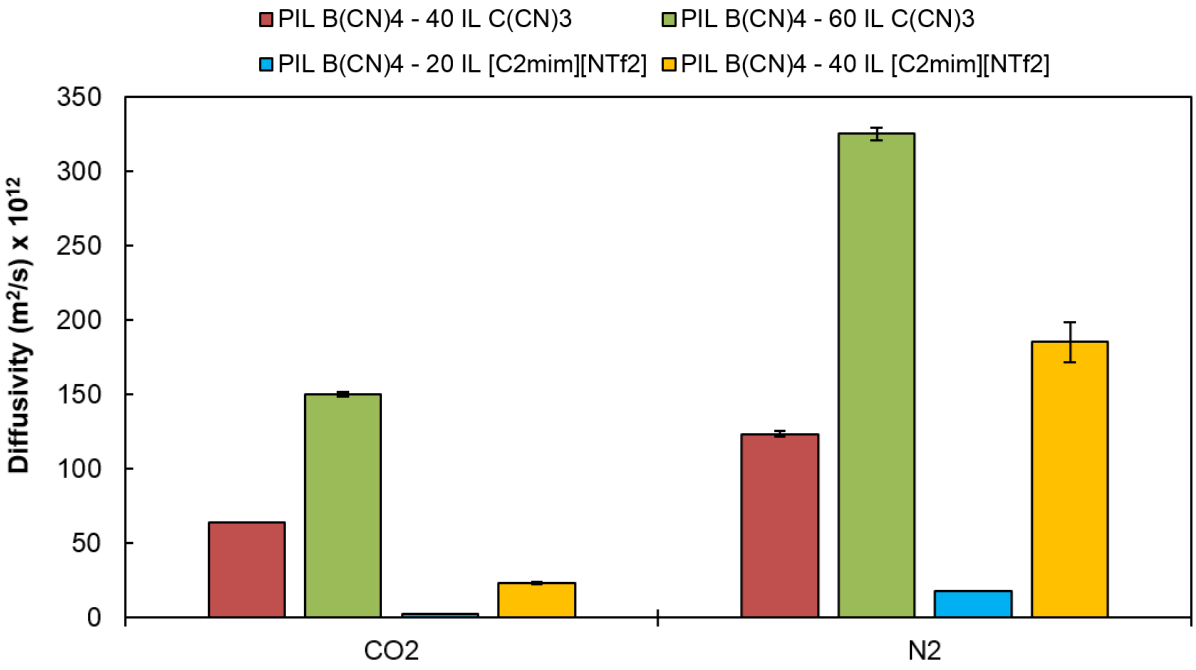

Figure 35 - Gas diffusivities through composite membranes bearing the PIL $B(CN)_4$.

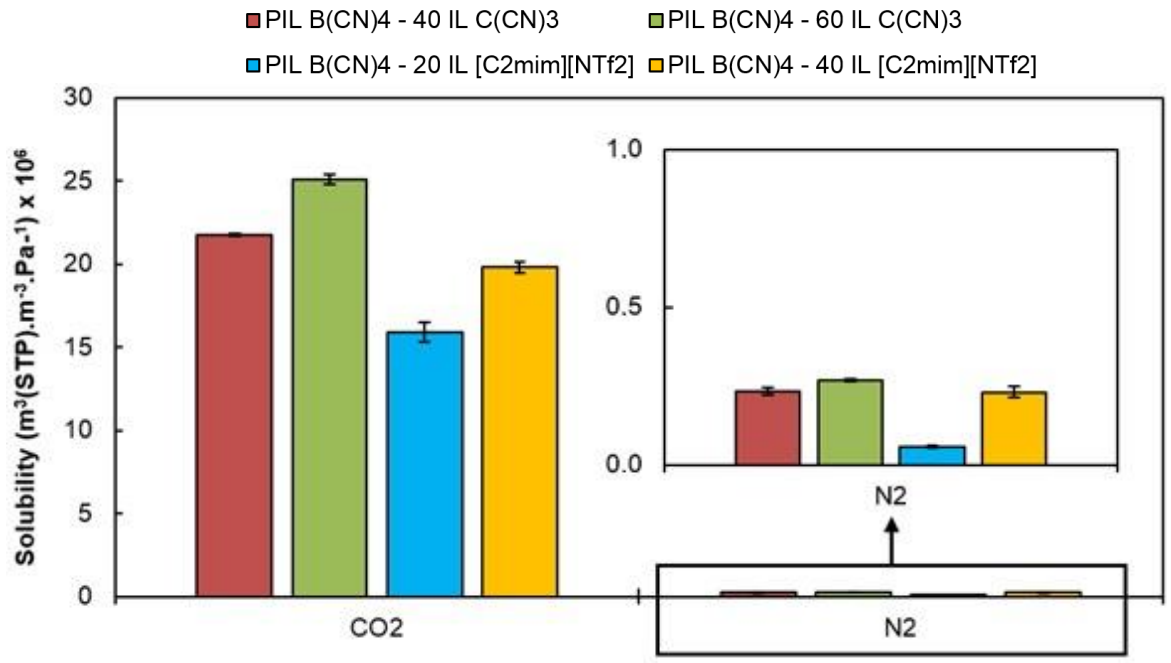

Figure 36 - Gas solubilities through composite membranes bearing the PIL $B(CN)_4$.

The trend observed for gas permeabilities in SILMs, where the permeability of the IL $C(CN)_3$ is higher than the permeability of the IL $[C_2mim][NTf_2]$ (Table 6), is also observed for the composite membranes PIL $B(CN)_4$ – 40 IL $C(CN)_3$ and PIL $B(CN)_4$ – 40 IL $[C_2mim][NTf_2]$, where the gas permeability of the first membrane is higher than the gas permeability of the second membrane (Figure 34). At 40 wt% of free IL incorporated, the influence of the IL is as important as the influence of the PIL. The difference in gas permeabilities between these two membranes is, once again, governed by the difference of their respective gas diffusivity values (Figure 35). The difference between the IL's viscosity values (Table 6) might justify the diverse diffusivity values obtained. Moreover, it can be seen from Figure 36 that the gas solubility values in these membranes are very similar.

3.2.4 PIL NTf_2

The permeability values shown in Figure 37 indicate that the composite membranes bearing PIL NTf_2 with 20 and 40 wt% of IL $[C_2mim][NTf_2]$ out perform their respective analogue membranes PIL NTf_2 with 20 and 40 wt% of IL $[Pyr_{14}][NTf_2]$, as expected from these ILs gas permeabilities measured through their respective SILMs (Table 6). It should be noted that PIL NTf_2 – 40 IL $[C_2mim][NTf_2]$ and PIL NTf_2 – 60 IL $[Pyr_{14}][NTf_2]$ composite membranes have almost the same CO_2 permeability value (Figure 37). Even though it is generally observed that the IL's anion has a bigger influence in CO_2 solubility[63] than that of the IL's cation, in these composite membranes PIL and IL's anions are the same, making the difference in the PIL and IL's cations the most important differentiating factor in this case. It was already reported by other authors that cations with delocalized charges (either in the PIL or in the free IL), such as the $[C_2mim]^+$ cation, result in more CO_2 permeable membranes than membranes containing localized cations as the case of $[Pyr_{14}]^+$ cation.[22] On top of

that, the viscosity of the IL [Pyr_{14}][NTf_2] is twice that of the IL [C_2mim][NTf_2] (Table 6). Ionic liquids with higher viscosities compromise the gas diffusivity through the composite membranes (Figure 38), though allowing for gas solubilities around the same order as membranes containing free ILs with lower viscosities (Figure 39).

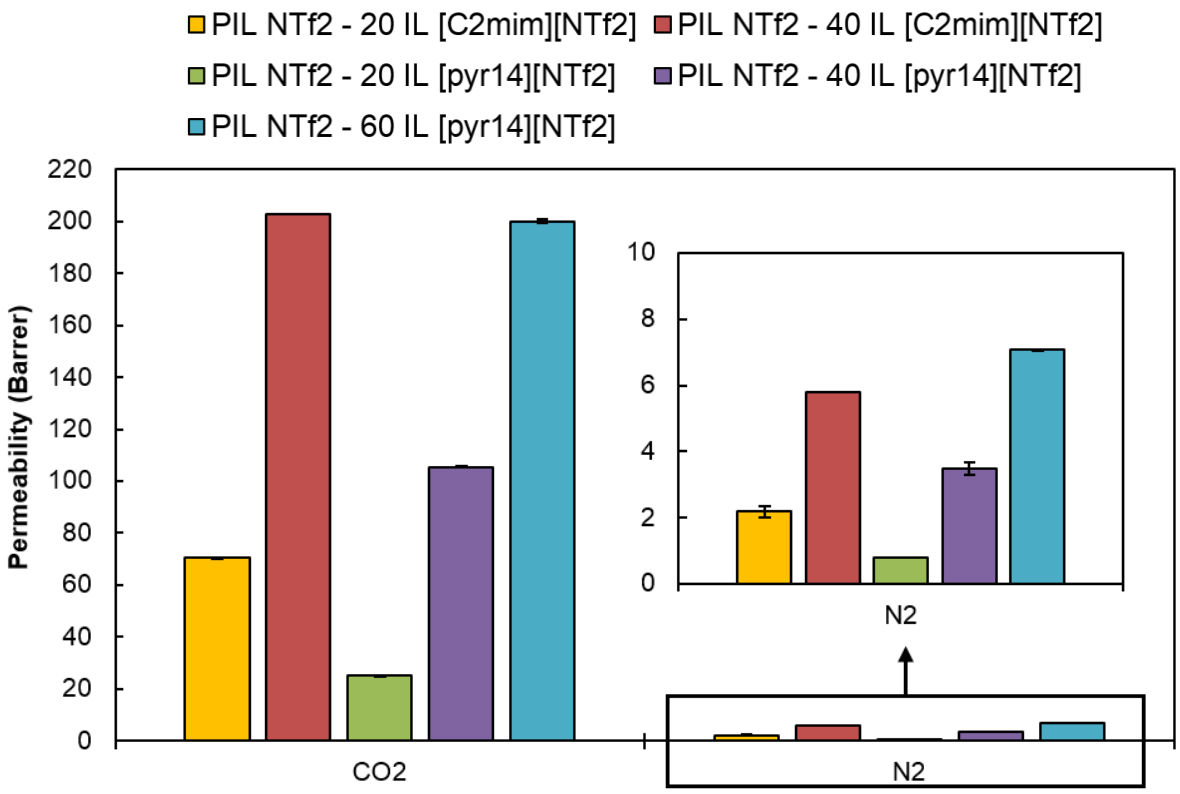

Figure 37 - Gas permeabilities through composite membranes bearing the PIL NTf_2. The data regarding membranes bearing the IL [Pyr_{14}][NTf_2] was taken from Tomé et al.[55]

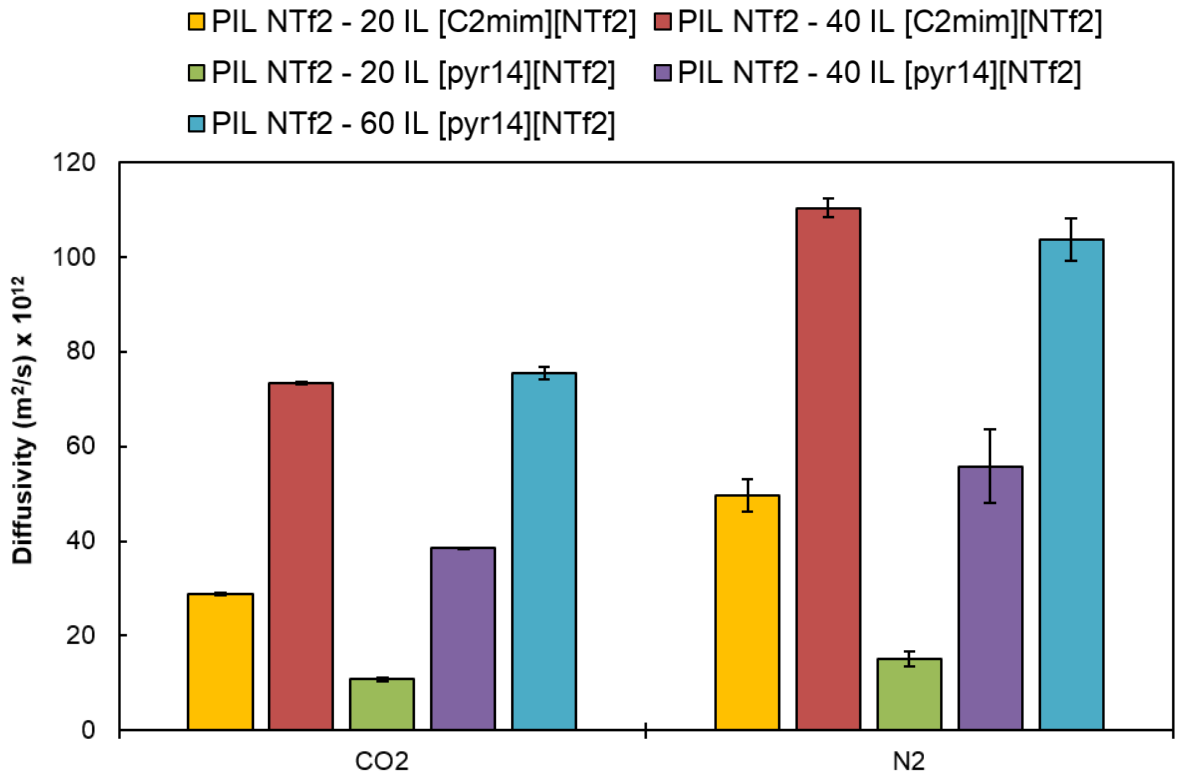

Figure 38 - Gas diffusivities through composite membranes bearing the PIL NTf_2. The data regarding membranes bearing the IL $[Pyr_{14}][NTf_2]$ was taken from Tomé et al.[55]

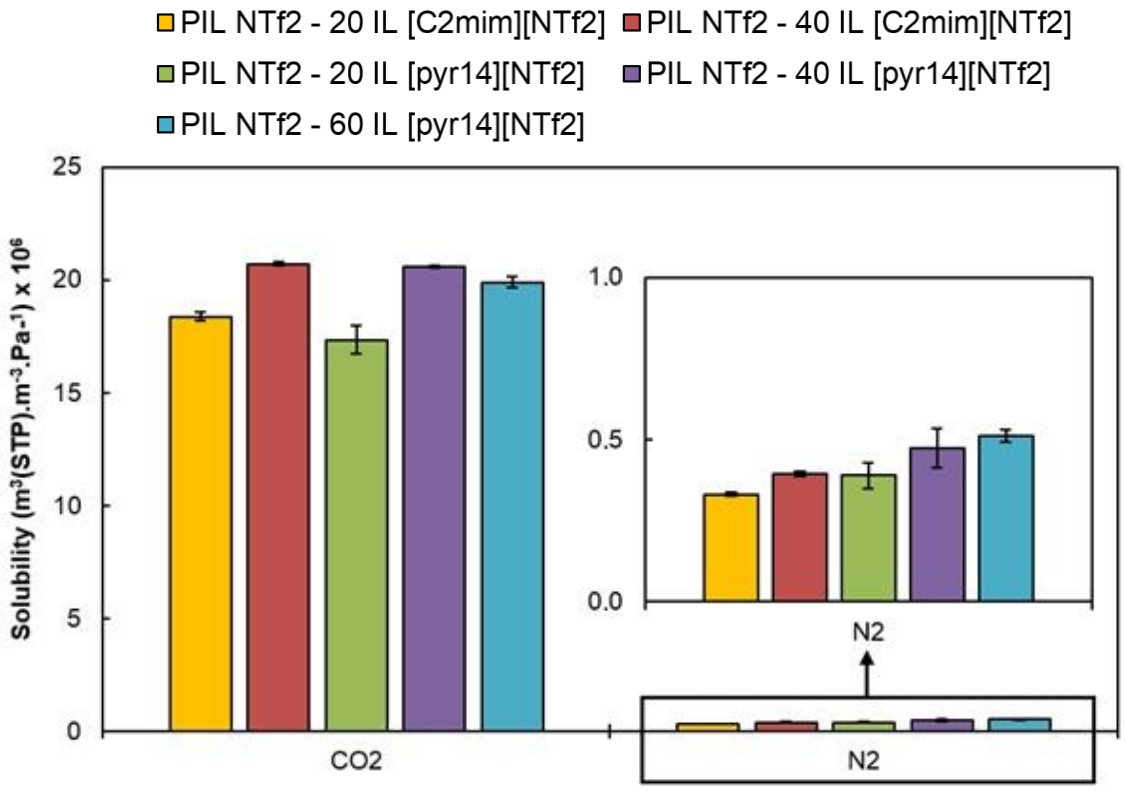

Figure 39 - Gas solubilities through composite membranes bearing the PIL NTf_2. The data regarding membranes bearing the IL $[Pyr_{14}][NTf_2]$ was taken from Tomé et al.[55]

Once again, the gas permeability increases with the increase of free IL incorporated into the PIL (Figure 37), thanks to an increase in diffusivity (Figure 38) and the difference in CO_2 and N_2 permeabilities, which allows for CO_2/N_2 selective gas separation, is due to their differences in solubilities (Figure 39).

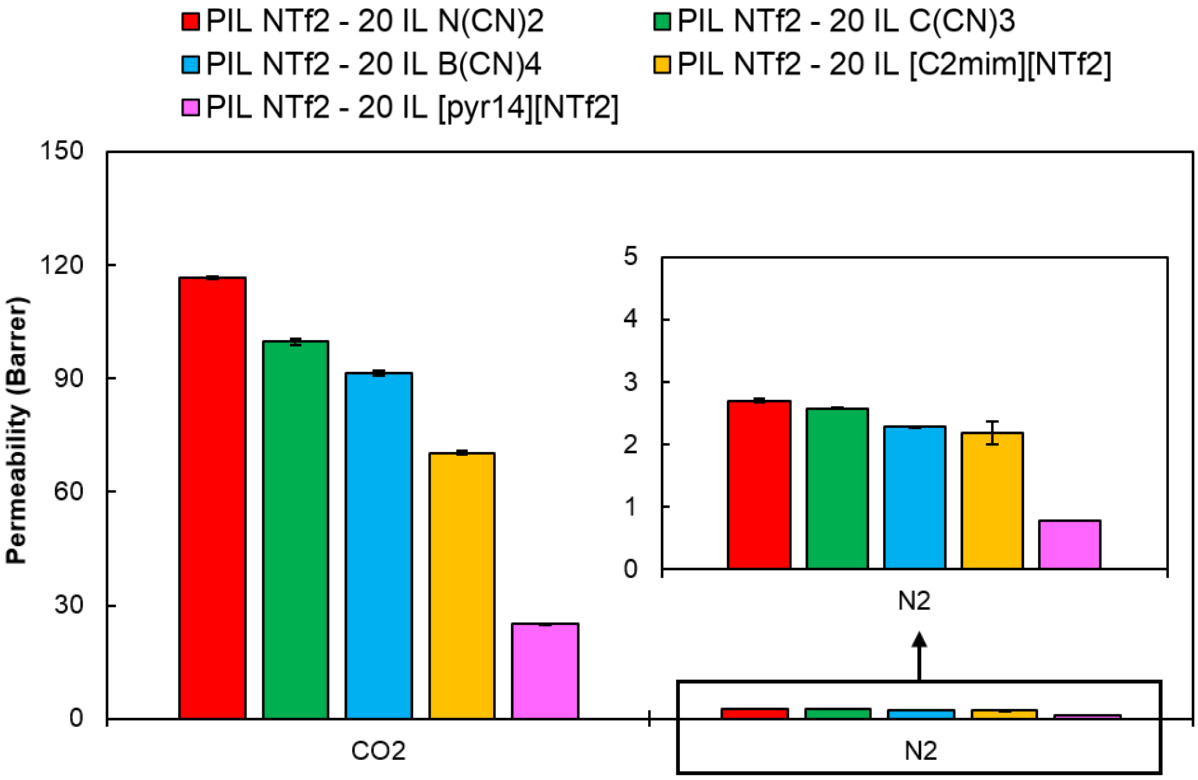

Figure 40 - Gas permeabilities through composite membranes bearing the PIL NTf_2. The data regarding the membrane bearing the IL $[Pyr_{14}][NTf_2]$ was taken from Tomé et al.[55]

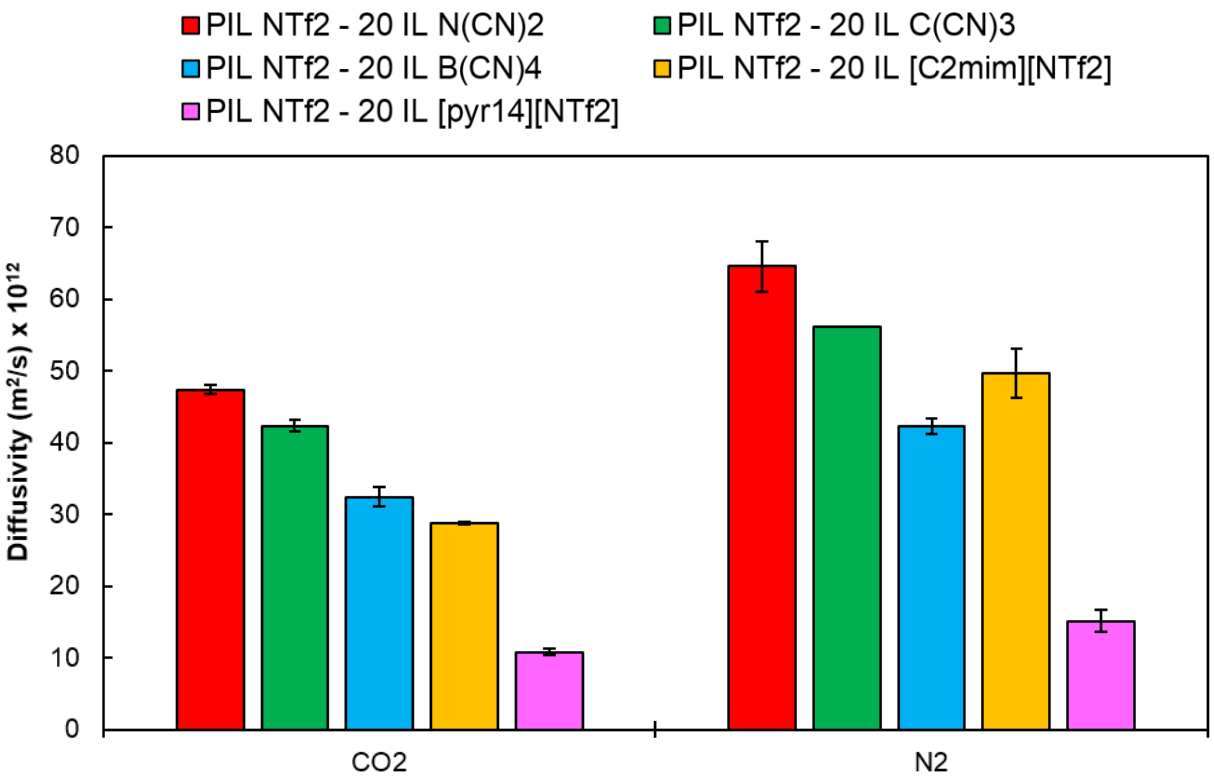

Figure 41 - Gas diffusivities through composite membranes bearing the PIL NTf_2. The data regarding the membrane bearing the IL $[Pyr_{14}][NTf_2]$ was taken from Tomé et al.[55]

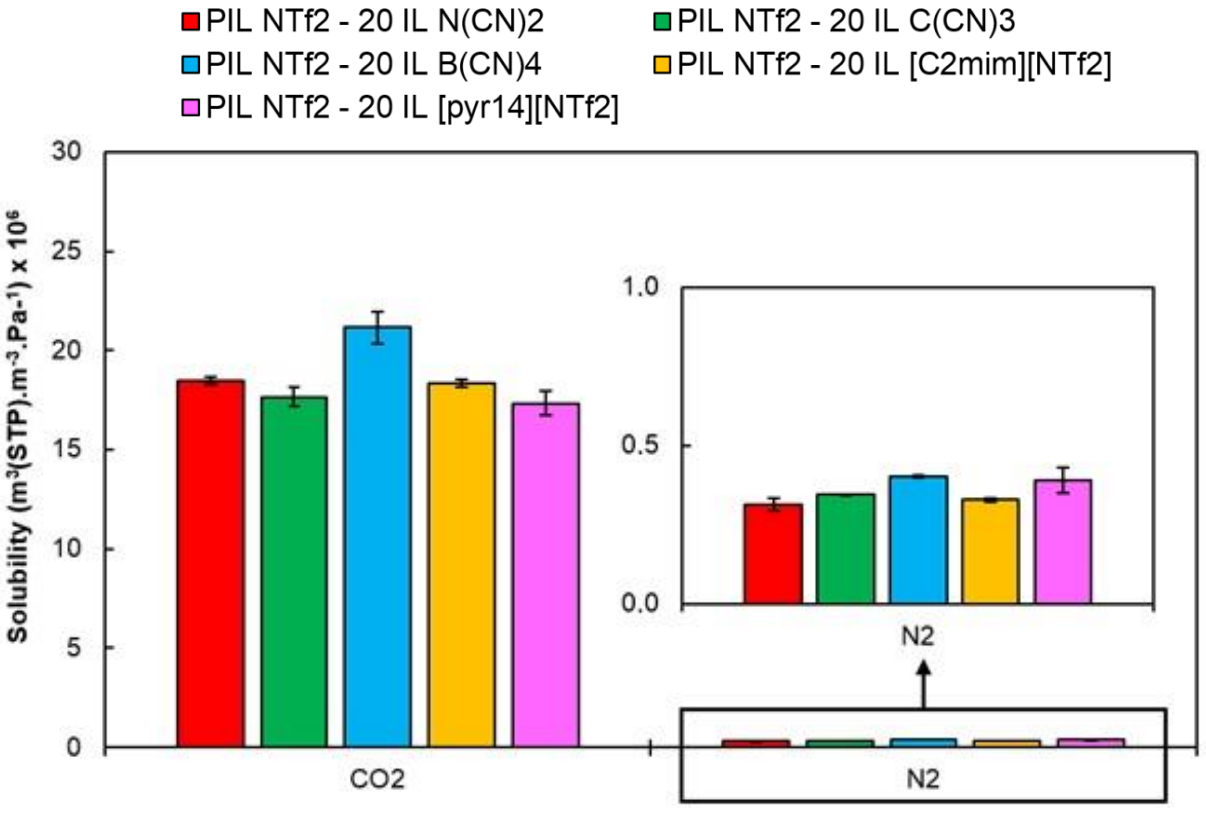

Figure 42 - Gas solubilities through composite membranes bearing the PIL NTf_2. The data regarding the membrane bearing the IL $[Pyr_{14}][NTf_2]$ was taken from Tomé et al.[55]

The gas permeability trend observed in Figure 40 is similar that found for the composite membranes bearing PIL $C(CN)_3$ with 20 and 40 wt% of each one of the five free ILs used (Figures 28 and 31). This behavior was not initially expected, but the differences in the ILs molecular weight also supports these results. Just like it happened with the analogue composite membranes based on PIL $C(CN)_3$ (Figures 29 and 32), the gas diffusivity trend follows that of the gas permeability (Figure 41), indicating a diffusivity regulated mechanism for gas transport through these PIL-IL composite membrane, while gas solubilities remain nearly the same (Figure 42).

3.2.5 IL $N(CN)_2$, IL $C(CN)_3$ and IL $B(CN)_4$

To better understand the role of the PIL and the free IL in the CO_2 gas permeation properties of the prepared PIL-IL composite membranes, it is important to discuss the influence of different free ILs, as well and their amount in wt% basis, across different PILs.

Figure 43 shows the CO_2 permeabilities through several composite membranes bearing different PILs (PIL $N(CN)_2$, PIL $C(CN)_3$ and PIL NTf_2) and 20 wt% of different ILs (IL $N(CN)_2$, IL $C(CN)_3$ and IL $B(CN)_4$). It can be clearly seen that the CO_2 permeabilities of the composite membranes containing PIL NTf_2 are significantly higher than those of their respective analogues membranes with PIL $N(CN)_2$ and PIL $C(CN)_3$, for all three cyano-functionalized ILs tested. At this wt% of free IL (20 wt%), the influence of the polymer has undoubtedly the major role when compared to the influence of the free IL. Since neat membranes of both PIL $N(CN)_2$ and PIL $C(CN)_3$ are very brittle and easily broke,[53] their gas permeation properties could not be measured in order to evaluate their properties and better discuss the polymer role among the different PILs contemplated. On the other hand, the neat PIL NTf_2 membrane was reported to be homogenous and free standing and its gas permeation properties could be measured. [55]

When analyzing the values provided in Table 7, it can be clearly seen that gas diffusivity has great influence in the CO_2 permeability behavior (Figure 43), especially for PIL NTf_2 composites where the flexibility of the $[NTf_2]^-$ anion allows for a higher diffusivity of the CO_2 molecules inside the membrane. The different roles of the anions as they come from the PIL or the IL component can also be discussed. It can be seen from Table 6 that the IL $C(CN)_3$ has a higher CO_2 permeability than that of the ILs containing the $[NTf_2]^-$ anion, whereas the IL $N(CN)_2$ has a higher CO_2 permeability than that of the IL $[Pyr_{14}][NTf_2]$. However, it can be seen from Figure 43 that the membranes with PIL NTf_2 are more permeable than the membranes with PIL $C(CN)_3$ or PIL $B(CN)_4$, for low (20 wt%) concentrations of the same three free IL with cyano-functionalized anions. This can only be explained by the fact that these two cyano anions are present in the PIL, instead of the IL.

Table 7 – Gas diffusivity and solubility values of several PIL - 20 IL composite membranes. Data regarding the membranes PIL $N(CN)_2$ – 20 IL $N(CN)_2$ and PIL $C(CN)_3$ – 20 IL $C(CN)_3$ was taken from Tomé et al.[53]

Free 20 wt% IL	PIL	D_{CO_2} (m^2/s) x 10^{12}	S_{CO_2} ($m^3(STP).m^{-3}.Pa^{-1}$) x 10^6
IL $N(CN)_2$	PIL $N(CN)_2$	2.8 ± 0.1	10.1 ± 0.3
	PIL $C(CN)_3$	9.1 ± 0.2	13.3 ± 0.2
	PIL NTf_2	47.4 ± 0.7	18.5 ± 0.2
IL $C(CN)_3$	PIL $N(CN)_2$	3.5 ± 0.3	3.4 ± 0.4
	PIL $C(CN)_3$	6.0 ± 0.2	10.1 ± 0.2
	PIL NTf_2	42.4 ± 0.8	17.7 ± 0.5
IL $B(CN)_4$	PIL $N(CN)_2$	-	-
	PIL $C(CN)_3$	4.4 ± 0.1	10.8 ± 0.1
	PIL NTf_2	32.4 ± 1.3	21.2 ± 1.0

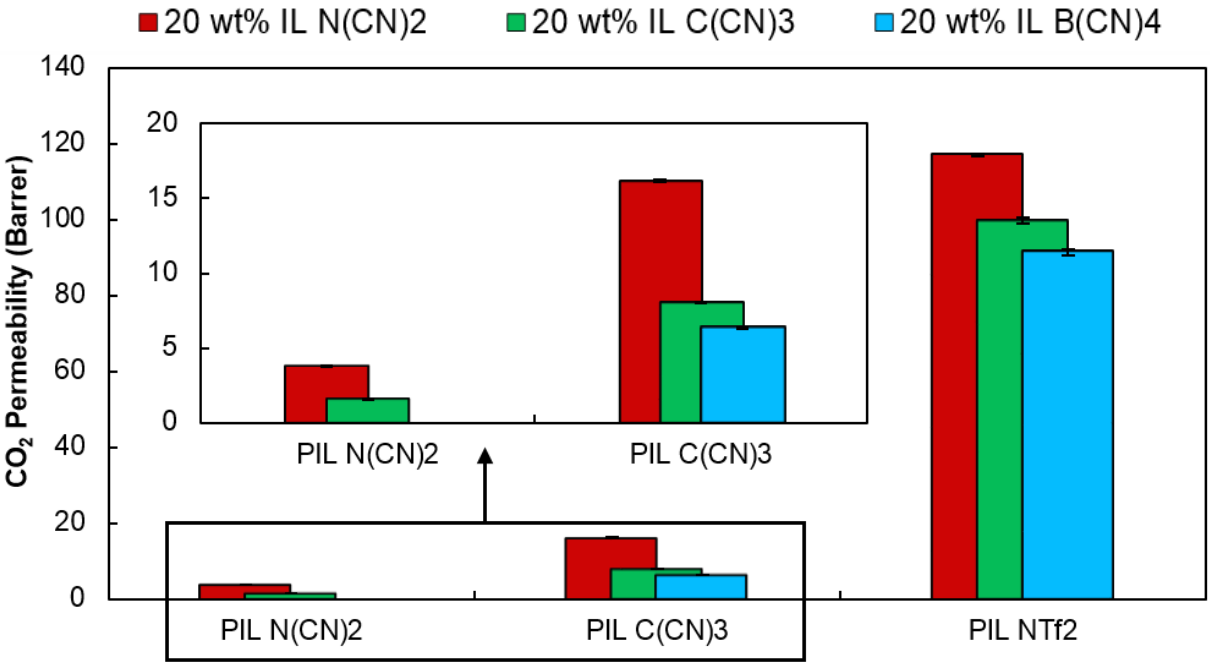

Figure 43 – CO_2 permeabilities through several composite membranes. The data regarding the membranes PIL $N(CN)_2$ – 20 IL $N(CN)_2$ and PIL $C(CN)_3$ – 20 IL $C(CN)_3$ was taken from [53].

Among the three studied ILs bearing cyano-functionalized anions, IL $C(CN)_3$ was the one whose use resulted in a higher number of stable and homogenous membranes, fit for gas permeation experiments. Therefore, it is interesting to discuss the influence of IL $C(CN)_3$ across composite membranes containing different PILs. The results presented in Figure 44 of the composite membranes with 40 wt% or 60 wt% of the free IL $C(CN)_3$ embedded into PIL $N(CN)_2$, PIL $C(CN)_3$ or PIL $B(CN)_4$ show the same trend which was previously observed for ILs in their SILMs configuration (Table 6): P_{CO_2} IL $B(CN)_4$ > P_{CO_2} IL $C(CN)_3$ > P_{CO_2} IL $N(CN)_2$, except that in this case the trend is observed for the PILs, since the IL $(CN)_3$ is the same for all composite membranes. At 40 wt% of free IL $(CN)_3$, the

influence of the PIL and IL is practically the same, whereas at 60 wt% the influence of the free IL is greater. Notwithstanding, and considering that the same IL was used for all the composites, PIL characteristics are the differentiating factor for CO_2 permeability in these membranes. According to Table 8, the CO_2 permeability increase between PIL $N(CN)_2$ – (40 and 60) IL $C(CN)_3$ and PIL $C(CN)_3$ – (40 and 60) IL $C(CN)_3$ membranes is primarily due to an increase in CO_2 diffusivity. However, between both these last membranes and PIL $B(CN)_4$ – (40 and 60) IL $C(CN)_3$ membranes, the CO_2 diffusivity decreases and the CO_2 solubility considerably increases. This trade-off suggests that changing IL $C(CN)_3$ by IL $B(CN)_4$ results in a membrane with higher chemical affinity for CO_2 molecules but, due to the rigid nature of the $[B(CN)_4]^-$ anion, with a higher resistance to gas diffusion. This result is important when designing new PIL-IL composite membranes for CO_2 separation since it allows for the improvement of the performance of innovative membranes with tunable properties by careful selection of anions and their source (whether they come from the PIL and/or the free IL).

Table 8 – Gas diffusivity and solubility values of several PIL - (40 and 60) IL $C(CN)_3$ composite membranes. Data regarding the membranes PIL $C(CN)_3$ – (40 and 60) IL $C(CN)_3$ was taken from Tomé et al.[53]

Free IL C(CN)₃	**PIL**	**D_{CO_2} (m^2/s) x 10^{12}**	**S_{CO_2} ($m^3(STP).m^{-3}.Pa^{-1}$) x 10^6**
40 wt%	PIL $N(CN)_2$	23.6 ± 0.5	9.8 ± 0.1
	PIL $C(CN)_3$	86.2 ± 0.6	12.4 ± 0.1
	PIL $B(CN)_4$	63.8 ± 0.1	21.7 ± 0.1
60 wt%	PIL $N(CN)_2$	111.2 ± 1.1	16.8 ± 0.1
	PIL $C(CN)_3$	189.5 ± 0.2	17.4 ± 0.1
	PIL $B(CN)_4$	150.1 ± 1.3	25.1 ± 0.3

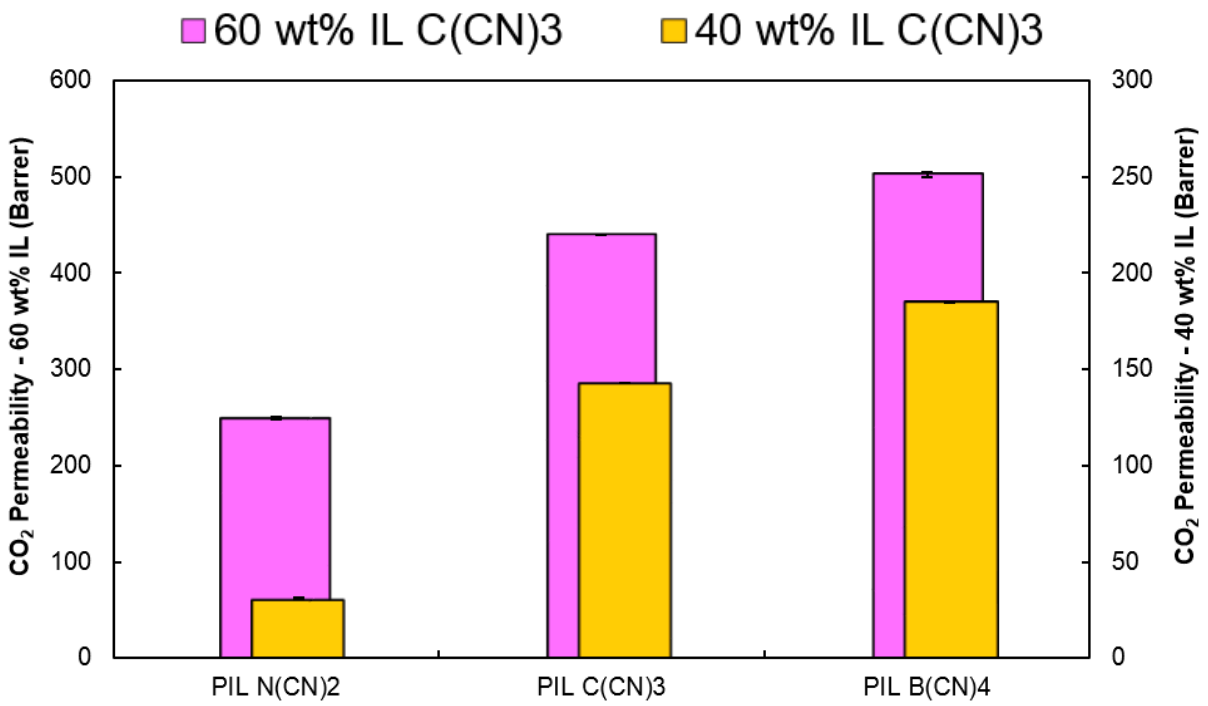

Figure 44 - CO_2 permeabilities through several composite membranes. The data regarding the membranes PIL $C(CN)_3$ – (20 and 40) IL $C(CN)_3$ was taken from [53].

3.2.6 IL [C_2mim][NTf_2] and IL [Pyr_{14}][NTf_2]

The results depicted in Figure 45 present the same behavior previously observed before for composite membranes containing either PIL $N(CN)_2$, PIL $C(CN)_3$ or PIL NTf_2 and 20 wt% of the free IL $N(CN)_2$, IL $C(CN)_3$ or IL $B(CN)_4$ (Figure 43). In these membranes only 20 wt% of the free IL [C_2mim][NTf_2] or IL [Pyr_{14}][NTf_2] was incorporated into the PIL $C(CN)_3$, PIL $B(CN)_4$ or PIL NTf_2, meaning the PIL has the largest influence in gas permeability. For the same membranes, but at 40 wt% of free IL, the same behavior can also be observed in Figure 46, even though the influence of the free IL in these membranes is larger when compared to their analogues with 20 wt% of free IL. Over again, the increased CO_2 permeability obtained through the composite membranes of PIL NTf_2 seems to be controlled by gas diffusivity (Table 9 and Table 10).

Table 9 - Diffusivity and solubility values for several PIL - 20 IL composite membranes. Data regarding the membrane PIL NTf_2 – 20 IL $[Pyr_{14}][NTf_2]$ was taken from [55].

Free 20 wt% IL	PIL	D_{CO_2} (m^2/s) x 10^{12}	S_{CO_2} ($m^3(STP).m^{-3}.Pa^{-1}$) x 10^6
IL $[C_2mim][NTf_2]$	PIL $C(CN)_3$	1.9 ± 0.1	11.0 ± 0.2
	PIL $B(CN)_4$	2.7 ± 0.1	15.9 ± 0.6
	PIL NTf_2	28.8 ± 0.2	18.4 ± 0.2
IL $[Pyr_{14}][NTf_2]$	PIL $C(CN)_3$	1.9 ± 0.2	7.1 ± 0.9
	PIL $B(CN)_4$	-	-
	PIL NTf_2	10.8 ± 0.4	17.3 ± 0.6

Table 10 - Diffusivity and solubility values for several PIL - 40 IL composite membranes. Data regarding the membrane PIL NTf_2 – 40 IL $[Pyr_{14}][NTf_2]$ was taken from [55].

Free 40 wt% IL	PIL	D_{CO_2} (m^2/s) x 10^{12}	S_{CO_2} ($m^3(STP).m^{-3}.Pa^{-1}$) x 10^6
IL $[C_2mim][NTf_2]$	PIL $C(CN)_3$	22.8 ± 0.1	16.6 ± 0.1
	PIL $B(CN)_4$	14.7 ± 0.6	23.8 ± 0.4
	PIL NTf_2	73.4 ± 0.3	20.7 ± 0.1
IL $[Pyr_{14}][NTf_2]$	PIL $C(CN)_3$	15.7 ± 0.2	16.6 ± 0.4
	PIL $B(CN)_4$	-	-
	PIL NTf_2	38.4 ± 0.2	19.9 ± 0.1

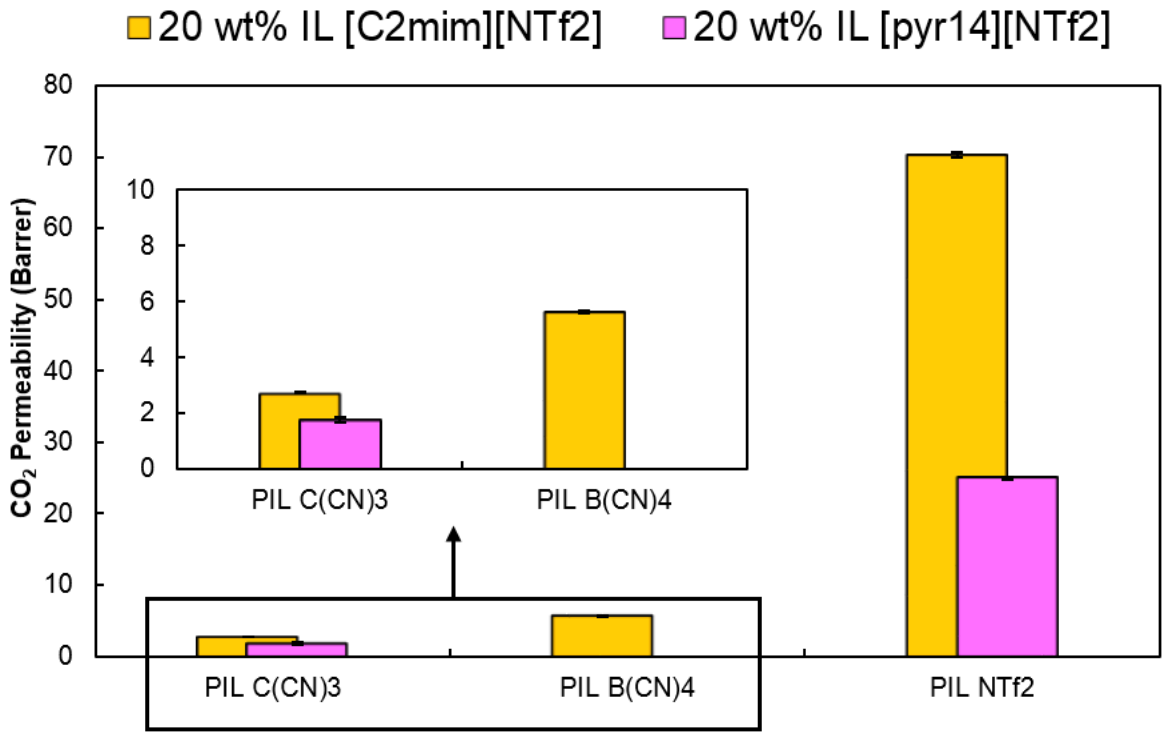

Figure 45 - CO_2 permeabilities through several composite membranes. The data regarding the membrane PIL NTf_2 – 20 IL $[Pyr_{14}][NTf_2]$ was taken from [55].

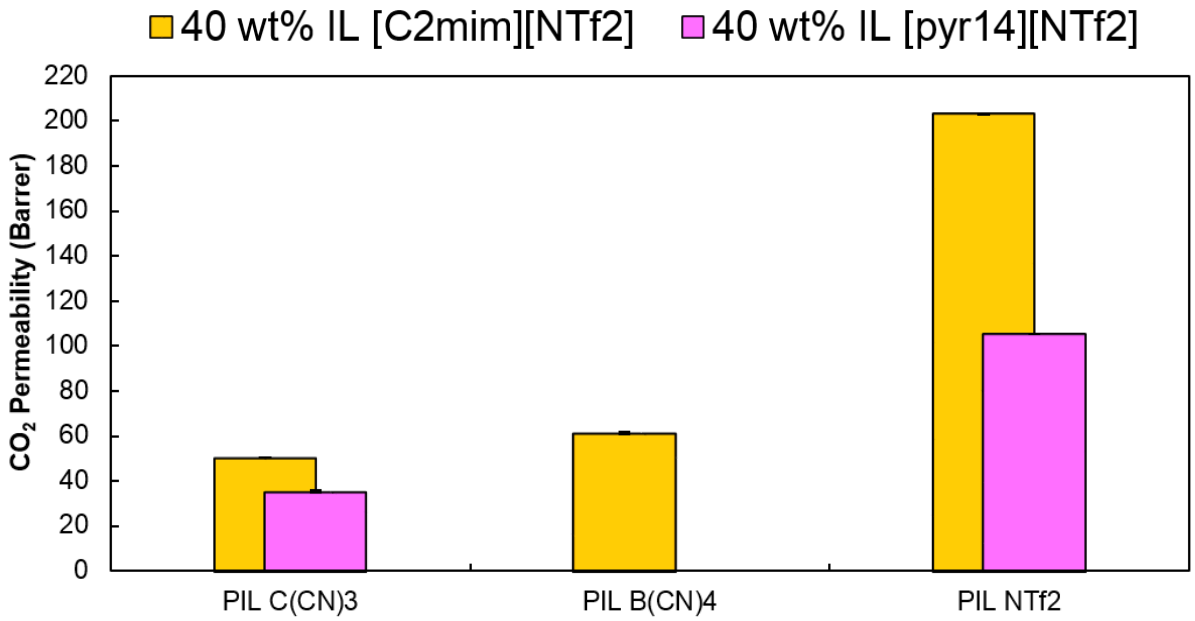

Figure 46 - CO_2 permeabilities through several composite membranes. The data regarding the membrane PIL NTf_2 – 40 IL $[Pyr_{14}][NTf_2]$ was taken from [55].

3.2.7 CO_2 Separation Performance

From all the composite membranes studied in this work, three can be considered to have high CO_2 separation performances, and so they will be further discussed in this final section.

Figure 47 illustrates the CO_2 permeabilities through these membranes, along with the previously reported PIL $C(CN)_3$ – 60 IL $C(CN)_3$ membrane.[53] The presence of free IL $C(CN)_3$ in three of the four membranes shows the great versatility and compatibility of this IL with other anions and cations. The $[C(CN)_3]^-$ anion is also the counter anion present in the PIL of two membranes, meaning that the presence of this anion, either in the free IL or PIL, leads to high CO_2 separation performance.

The three membranes with the best CO_2 separation performance (PIL $C(CN)_3$ – 60 IL $C(CN)_3$, PIL $C(CN)_3$ – 60 IL $B(CN)_4$ and PIL $B(CN)_4$ – 60 IL $C(CN)_3$) combine two cyano-functionalized anions, whose respective ILs present the highest CO_2 permeabilities through SILMs (Table 6). The chemical similarity of these anions makes them compatible and allows the preparation of stable and homogenous membranes. The CO_2 diffusivity through PIL $C(CN)_3$ – 60 IL $C(CN)_3$ is slightly higher than that of the other membranes (Figure 48), while the two membranes with the $[B(CN)_4]^-$ anion present slightly higher CO_2 solubility values (Figure 49). This trade-off was aforementioned and discussed for the composite membranes presented in Table 8 and Figure 44. By changing either the PIL $C(CN)_3$ or the IL $C(CN)_3$ of the membrane PIL $C(CN)_3$ – 60 IL $C(CN)_3$ by PIL $B(CN)_4$ or IL $B(CN)_4$, respectively, an increase in CO_2 permeability is always achieved (Figure 7), mainly due to an increase in the CO_2 solubility (Figure 49), which in turn compensates the decrease in CO_2 diffusivity (Figure 48). This result shows that the source component (PIL or IL) of the $[B(CN)_4]^-$ is not so relevant here since the CO_2 permeability, diffusivity and solubility values of the two membranes having this anion

are very similar. The increase in CO_2 solubility for SILMs containing the $[B(CN)_4]^-$ anion, which resulted in higher CO_2 permeabilities, was already reported.[71] The strong CO_2 molecules – $[B(CN)_4]^-$ anion interactions, as well as the weak cation-anion interactions, may be the main key factor for increased CO_2 solubilities.[71] In addition, it has also been observed that the increasing number of cyano groups of the IL's anion leads to higher CO_2 permeabilities.[61]

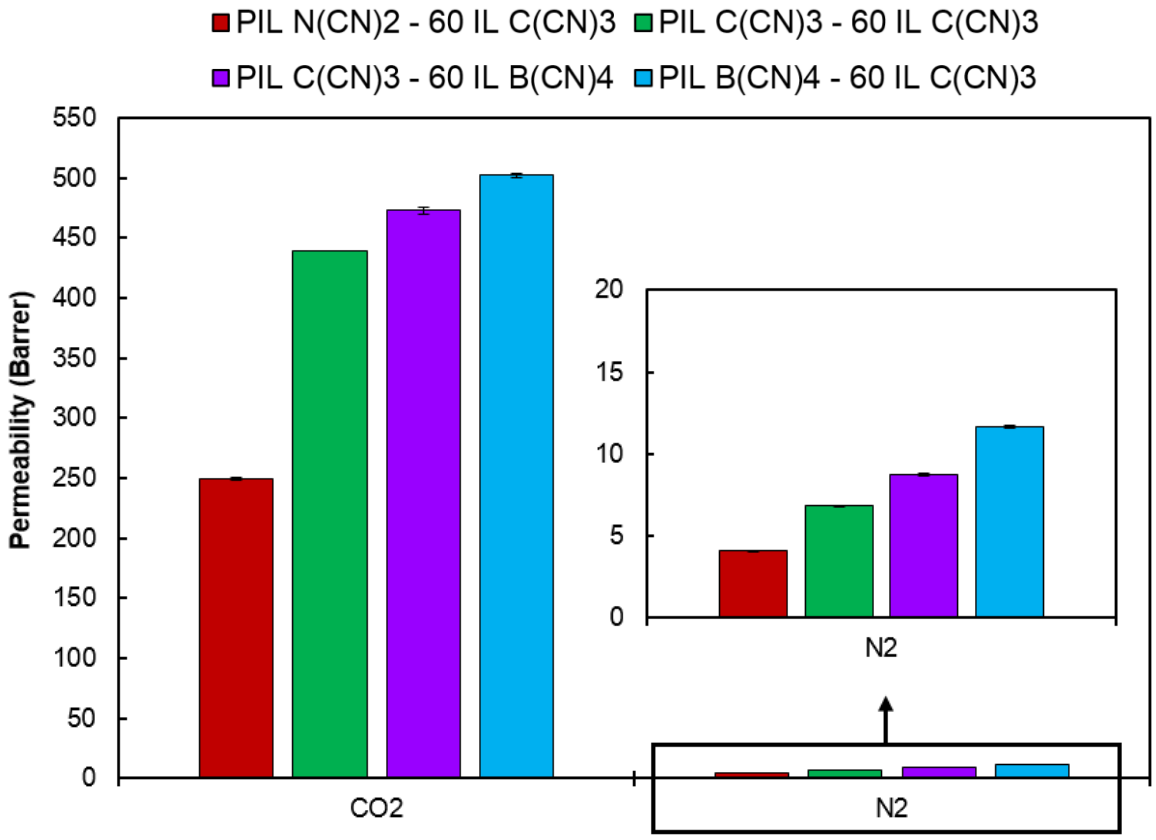

Figure 47 - Gas permeabilities through several composite membranes. The data regarding the membrane PIL $C(CN)_3$ – 60 IL $C(CN)_3$ was taken from [53].

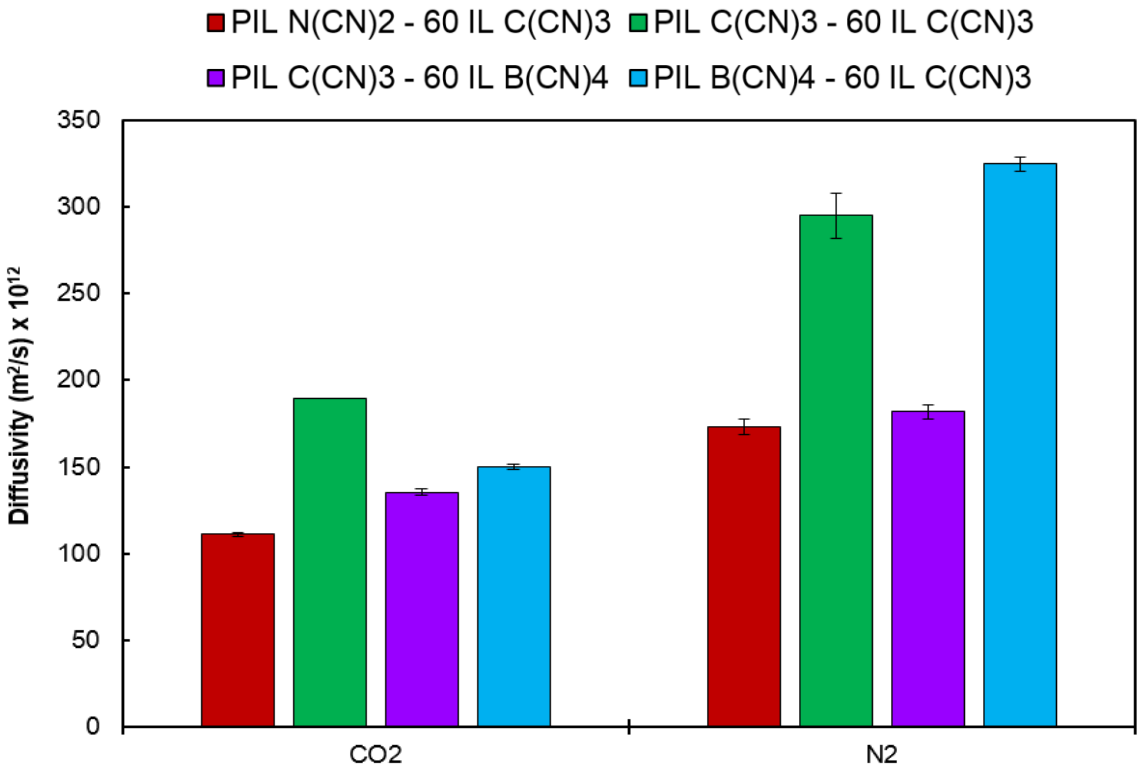

Figure 48 - Gas diffusivities through several composite membranes. The data regarding the membrane PIL $C(CN)_3$ – 60 IL $C(CN)_3$ was taken from [53].

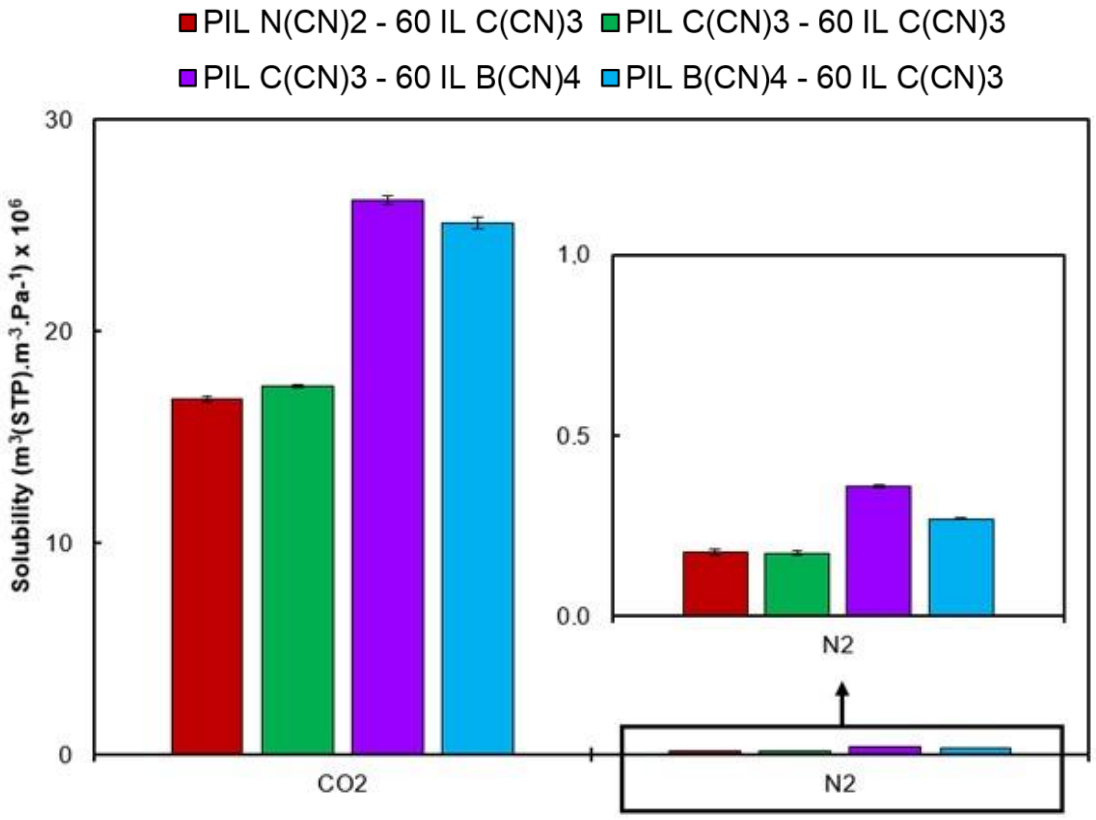

Figure 49 - Gas solubilities through several composite membranes. The data regarding the membrane PIL $C(CN)_3$ – 60 IL $C(CN)_3$ was taken from [53].

In order to better evaluate the CO_2 separation performance of these composite membranes, a Robeson Plot is used. In this plot the four above mentioned membranes are compared against other membranes reported in the open literature (Figure 50). The membranes with the highest CO_2 separation performances (Table 11) fall above or on top the upper bound, on the upper-right corner of the Robeson plot.

The results provided in Table 11 display a trade-off between the CO_2 permeability and the CO_2/N_2 permselectivity values, in other words, when the CO_2 permeability increases the permselectivity value decreases. This trade-off follows the same previously observed permeability vs permselectivity trend through SILMs (Table 6). The increase/decrease in CO_2/N_2 permselectivity can be attributed to a solubility controlled mechanism since the diffusivity selectivity (D CO_2/N_2) values fall in the 0.5 – 0.7 range, while the solubility selectivity (S CO_2/N_2) values range from 73.0 to 100.2 (Table 11). The same behavior was also observed for the previously reported composite membranes bearing PIL $C(CN)_3$ with 20, 40 and 60 wt% of the free IL $C(CN)_3$ composite membranes.[53] This solubility controlled selectivity mechanism applies for all membranes measured in this work (Table 13 and Table 14, Appendixes).

In sum, it can be concluded that the increase of CO_2 permeability is generally controlled by gas diffusivity, while the increase in CO_2/N_2 permselectivity is due to contributions of a solubility controlled mechanism.

Table 11 – CO_2 permeability and permselectivity values obtained for the four PIL-IL composite membranes with the best CO_2 separation performance. The data of PIL $C(CN)_3$ – 60 IL $C(CN)_3$ membrane was taken from Tomé et al.[53]

Composite Membranes	P_{CO_2} *(Barrer)*	α_{CO_2/N_2}
PIL $N(CN)_2$ – 60 IL $C(CN)_3$	249.0 ± 1.0	61.3 ± 0.8
PIL $C(CN)_3$ – 60 IL $C(CN)_3$	439.3 ± 0.1	55.9 ± 0.1
PIL $C(CN)_3$ – 60 IL $B(CN)_4$	472.7 ± 3.0	54.4 ± 0.8
PIL $B(CN)_4$ – 60 IL $C(CN)_3$	502.1 ± 1.9	43.1± 0.4

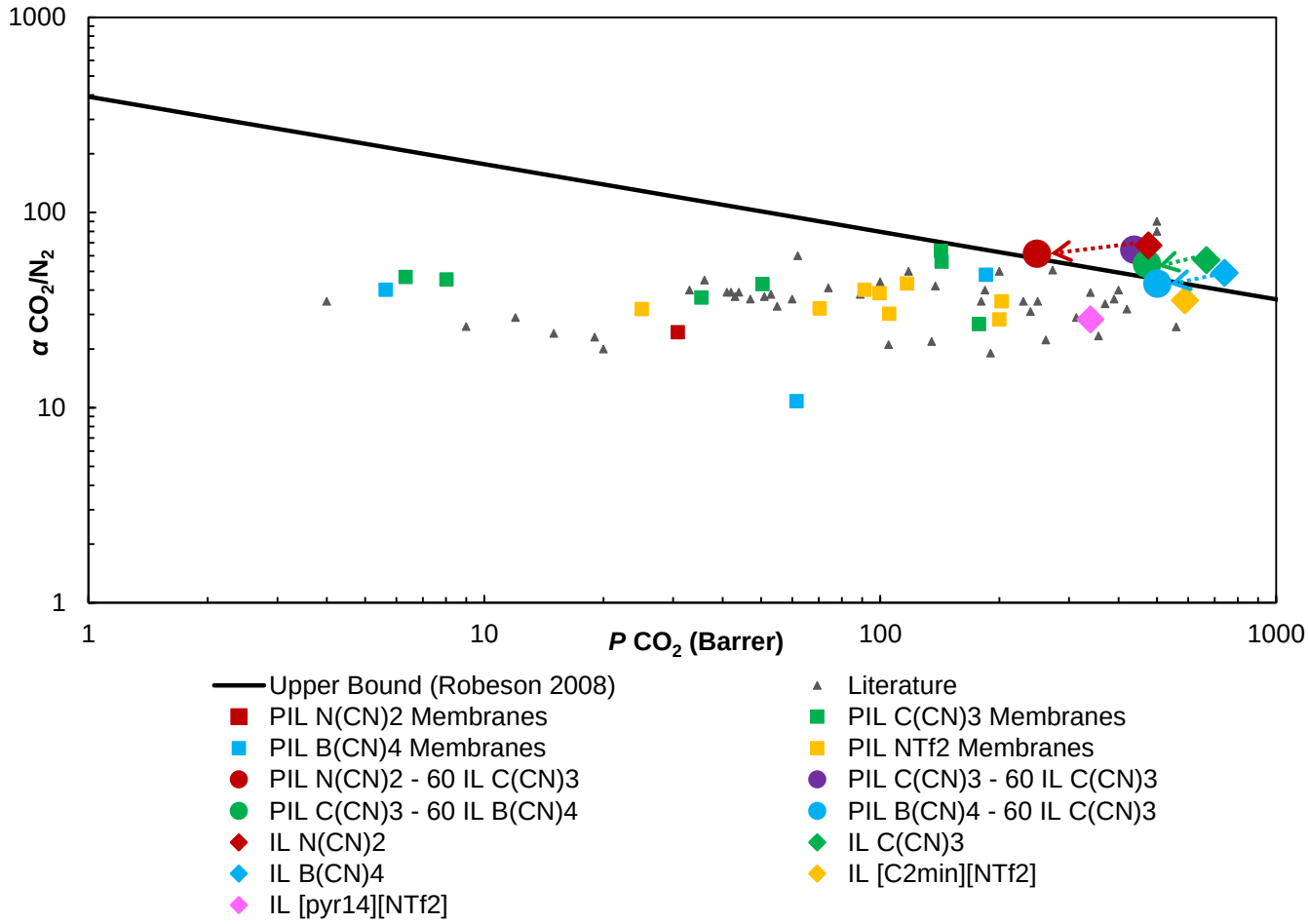

Figure 50 - CO_2 separation performance of the PIL-IL composite membranes studied in this work, plotted on a CO_2/N_2 Robeson plot. "Literature" stand for several neat PIL and PIL-IL composite membranes previously reported by other research groups.[38, 40-42, 45-47, 49, 53, 55, 64-67] "PIL $N(CN)_2$, PIL $C(CN)_3$, and PIL $B(CN)_4$ Membranes" stand for the PIL-IL composites studied in this work. The data for the membrane PIL $C(CN)_3$ – 60 IL $C(CN)_3$ was taken from reference[53] while the SILMs data came from references[61, 62]. The different data are plotted on a log-log scale and the upper bound is adapted from Robeson[21]. It should be noted that the two "Literature" membranes (gray triangles) above the upper bound were measured at low CO_2 partial pressure and 95% RH.

All the results obtained for the four composite membranes shown in Table 11 fall right above or on top the upper-bound (Figure 50). Interestingly, the distance between the membranes PIL $N(CN)_2$ – 60 IL $C(CN)_3$, PIL $C(CN)_3$ – 60 IL $B(CN)_4$ and PIL $B(CN)_4$ – 60 IL $C(CN)_3$ somewhat mimics the distance between the IL $N(CN)_2$, IL $C(CN)_3$ and IL $B(CN)_4$. In other words, each CO_2 separation performance of the composite membranes falls back to slightly lower permeability and permselectivity values than that of the respective SILMs, due to the presence of polymeric PIL chains in the membrane (Figure 50, the fall backs are represented by arrows). Nevertheless, these composite membranes have very good CO_2 separation performances, in addition to their robustness advantages when compared to SILMs. With further research on their chemical and physical properties these PIL-IL composite membranes may hold a great promise for gas membrane technology, in particular for CO_2/N_2 separation.

4. Conclusions and Future Work

The main goal of this work was the evaluation of the CO_2/N_2 separation performance of several PIL-IL composite membranes. All membranes here prepared have cyano-functionalized counter anions ($[N(CN)_2]^-$, $[C(CN)_3]^-$ or $[B(CN)_4]^-$) or an $[NTf_2]^-$ counter anion, which are different in the PIL and IL.

For this purpose, four PILs with a pyrrolidinium polycation backbone having either cyano-functionalized (the three mentioned above) or $[NTf_2]^-$ as counter anions, were synthesized via anion exchange reactions, which guaranties a uniform polymer molecular weight, an important variable in membrane preparation. The PILs were obtained by mixing the commercially available poly(diallydimethyammonium chloride) and the corresponding salt in a water solution. The PIL $C(CN)_3$, PIL $B(CN)_4$ and PIL NTf_2 precipitated in the aqueous solution, and after filtration and drying procedures, high pure PILs were obtained. The PIL $N(CN)_2$ did not precipitate in water and thus it was further purified by re-dissolution in ethanol, where it precipitated, and then it was finally filtered and dried.

The four PILs were then used to prepare 42 PIL-IL composite membranes by blending the PILs with different weight percentages (20, 40 and 60 wt%) of five commercially available free ILs. The free ILs have an imidazolium ($[C_2mim]^+$) or a pyrrolidinium ($[Pyr_{14}]^+$) based cation and either a cyano (the same three already mentioned) anion or an $[NTf_2]^-$ anion. The composite membranes were prepared by a solvent casting process and different casting conditions (different solvents, PIL and IL (w/v)% concentrations, evaporation times and temperatures, as well as different plate materials) were tested in order to obtain the maximum number of homogenous and free standing membranes possible.

From all 42 tested membranes, 21 were free standing and homogenous while the other 21 were either heterogeneous, non-stable or both. Membranes with $[C(CN)_3]^-$ anion (either in the PIL or IL) had a membrane formation success rate of 71%, while membranes with the $[N(CN)_2]^-$ anion (either in the PIL or IL) had the lowest formation success rate, 33%. The chemical and structural compatibility of $[C(CN)_3]^-$ anion with the other cyano anions and with the $[NTf_2]^-$ anion may be the reason why most membranes containing this anion are homogenous and free standing. Due to the hydrophilic nature of $[N(CN)_2]^-$ anion, their membranes generally are gel-like materials, which makes them impossible to handle. Membranes with $[B(CN)_4]^-$ or $[NTf_2]^-$ anions had formation success rates of 44% and 45%, respectively. The chemical incompatibility of the $[NTf_2]^-$ anion with the other cyano counter anions, as well as the rigid nature of the $[B(CN)_4]^-$ anion may explain these lower success numbers. In general, it was more difficult to obtain homogenous and free standing membranes containing higher amounts of free IL (only 3 homogenous and free standing membranes with 60 wt% of free IL were obtained), while 18 suitable membranes with lower amounts of IL (20 and 40 wt%) were prepared. The only exception was the heterogeneous membrane bearing PIL $B(CN)_4$ and 20 wt% of the free IL $C(CN)_3$, while the 40 wt% and 60 wt% membranes equivalents were homogenous and stable.

Concerning the gas permeation experiments carried out to evaluate the CO_2/N_2 separation performance of the 21 suitable membranes several conclusions could be drawn. For all membranes tested, the CO_2 permeability was always higher than the N_2 permeability thanks to a correspondingly difference between these two gases solubilities. When increasing the free IL content of the membranes, both CO_2 and N_2 permeabilities also increased. This increment in gas permeability was attributed to an increase in gas diffusivity, which means that membranes with higher content of free IL have higher polymer chain mobility and the gas molecules can more easily move within these polymer chains. It was also observed that, while the increase/decrease of CO_2 and N_2 permeability is a diffusivity controlled mechanism, the increase/decrease of CO_2/N_2 permselectivity is a solubility controlled mechanism.

Composite membranes with the same PIL containing either free IL $C(CN)_3$ or IL $B(CN)_4$ always out performed composite membranes containing one of the two ILs bearing $[NTf_2]^-$ anion. This trend was already reported for SILMs-based on these ILs,[61, 62] and the difference in the ILs viscosity (being the ILs with $[NTf_2]^-$ anion more viscous) is suggested as the main possible reason for this trend. SILMs-based on the IL $N(CN)_2$ do not outperform SILMs-based on the IL $[C_2mim][NTf_2]$,[61, 62] but the opposite behaviour was observed in this work for the composite membranes bearing the same PIL with these two ILs. The mass basis from which all composite membranes were prepared and the lower molecular weight of the IL $N(CN)_2$ result in membranes with a higher number of free IL ions. SILMs-based on the IL $[C_2mim][NTf_2]$ are reported to outperform SILMs-based on the IL $[Pyr_{14}][NTf_2]$.[62] This trend was also verified for composite membranes bearing either PIL $C(CN)_3$ or PIL NTf_2[55] with these two ILs incorporated. The high viscosity of the IL $[Pyr_{14}][NTf_2]$ (twice that of the IL $[C_2mim][NTf_2]$) and the localized charge of the pyrrolidinium based cation are possible explanations for the less efficient CO_2 separation performance of composite membranes bearing this IL.

The three composite membranes with 60 wt% of free IL mentioned before, more precisely PIL $N(CN)_2$ – 60 IL $C(CN)_3$, PIL $C(CN)_3$ – 60 IL $B(CN)_4$ and PIL $B(CN)_4$ – 60 IL $C(CN)_3$, were on top or even surpassed the Robeson 2008 upper bound for CO_2/N_2 separation. It was found that replacing IL $C(CN)_3$ or PIL $C(CN)_3$ from the previously reported[53] composite membrane PIL $C(CN)_3$ – 60 IL $C(CN)_3$, by IL $B(CN)_4$ or PIL $B(CN)_4$, respectively, decreases gas diffusivity while increasing gas solubility. The increase in gas solubility compensates the decrease in gas diffusivity resulting in more permeable membranes. The two composite membranes bearing the $[B(CN)_4]^-$ anion, PIL $C(CN)_3$ – 60 IL $B(CN)_4$ and PIL $B(CN)_4$ – 60 IL $C(CN)_3$, hold the most promise for efficient CO_2/N_2 separation membranes.

The membrane preparing method followed a mass basis. To better understand the dynamics between the PIL and the IL and their influence in gas permeation proprieties it would be interesting to further study these membranes using a molar basis. In this work and consequent discussion it is not considered that an interchange of anions between the PIL and IL happens. This topic has never been studied before but deserves to be explored in future works. Further research of the composite membranes with the best CO_2 separation performance under real industrial conditions should also be considered. The evaluation of the behavior of these membranes under different pressure, temperature, compositions of binary gas mixtures (including the exposure to different impurities) and humidity contents is crucial for their application in CO_2 separation processes.

5. References

1. S. D. Kenarsari, D. Yang, G. Jiang, S. Zhang, J. Wang, A. G. Russell, Q. Wei and M. Fan, *RSC Adv.*, 2013.
2. M. Z. Jacobson, *Energ. Environ. Sci.*, 2009, 2, 148-173.
3. M. E. Boot-Handford, J. C. Abanades, E. J. Anthony, M. J. Blunt, S. Brandani, N. Mac Dowell, J. R. Fernandez, M.-C. Ferrari, R. Gross, J. P. Hallett, R. S. Haszeldine, P. Heptonstall, A. Lyngfelt, Z. Makuch, E. Mangano, R. T. J. Porter, M. Pourkashanian, G. T. Rochelle, N. Shah, J. G. Yao and P. S. Fennell, *Energ. Environ. Sci.*, 2014, 7, 130-189.
4. http://www.ccsassociation.org/ (15 April 2016)
5. N. MacDowell, N. Florin, A. Buchard, J. Hallett, A. Galindo, G. Jackson, C. S. Adjiman, C. K. Williams, N. Shah and P. Fennell, *Energ. Environ. Sci.*, 2010, 3, 1645-1669.
6. C. A. Scholes, G. W. Stevens and S. E. Kentish, *Fuel*, 2012, 96, 15-28.
7. Deanna M. D'Alessandro, Berend Smit and Jeffrey R. Long, *Angew. Chem. Int. Ed7.*, 2010, 49, 6058 – 6082.
8. http://www.globalccsinstitute.com/ (1 May 2016)
9. J. Adanez, A. Abad, F. Garcia-Labiano, P. Gayan and F. Luis, *Progress in Energy and Combustion Science*, 2012, 38, 215-282.
10. B. P. Spigarelli and S. K. Kawatra, *J. CO_2 Util.*, 2013, 1, 69-87.
11. J. Wang, L. Huang, R. Yang, Z. Zhang, J. Wu, Y. Gao, Q. Wang, D. O'Hare and Z. Zhong, *Energ. Environ. Sci.*, 2014, 7, 3478-3518.
12. R. W. Baker, *Membrane Technology and Applications, 2nd ed.*, John Wiley & Sons Ltd., Chischester, England, 2004.
13. J. W. Phair and S. P. S. Badwal, *Science and Technology of Advanced Materials*, 2006, 7(8), 792-805.
14. D. F. Sanders, Z. P. Smith, R. Guo, L. M. Robeson, J. E. McGrath, D. R. Paul and B. D. Freeman, *Polymer*, 2013, 54, 4729-4761.
15. Brunetti, F. Scura, G. Barbieri and E. Drioli, *J. Membr. Sci.*, 2010, 359(1), 115-125.
16. G. Dong, H. Li and V. Chen, *J. Mater. Chem. A*, 2013, 1, 4610-4630.
17. T. S. Chung, L. Y. Jiang, Y. Li and S. Kulprathipanja, *Prog. Polym. Sci.*, 2007, 32(4), 483-507.
18. J. G. Wijmans and R. W. Baker, *J. Membr. Sci.*, 1995, 107, 1-21.
19. B. D. Freeman, *Macromolecules*, 1999, 32, 375-380.
20. L. M. Robeson, *J. Membr. Sci.*, 1991, 62, 165-185.
21. L. M. Robeson, *J. Membr. Sci.*, 2008, 320, 390-400.
22. L. C. Tomé and I. M. Marrucho, *Chem. Soc. Rev.*, 2016, 45, 2785-2824.
23. P. Walden, *Bull. Russian Acad. Sci.*, 1914, 405-422.
24. N. V. Plechkova and K. R. Seddon, *Chem. Soc. Rev.*, 2008, 37, 123-150.

25. Z. Dai, R. D. Noble, D. L. Gin, X. Zhang and L. Deng, *J. Membr. Sci.*, 2016, 497, 1–20.

26. M. A. Malik, M. A. Hashim and F. Nabi, *Chem. Eng. J.*, 2011, 171, 242–254.

27. L.A. Blanchard, Z. Y. Gu, J. F. Brennecke, *J. Physical Chem*., 2001, B105(12), 2437–2444.

28. Z. G. Lei, C. N. Dai, B. H. Chen, *Chem. Rev.*, 2014, 114(2), 1289–1326.

29. M. Hasib-ur-Rahman, M. Siaj and F. Larachi, *Chem. Eng.Process.: Process Intensification*, 2010, 49, 313-322.

30. S. Zulfiqar, M. I. Sarwar and D. Mecerreyes, *Polym. Chem*., 2015, 6, 6435–6451

31. L.J. Lozano, C. Godinez, A.P. de los Rios, F.J. Hernandez-Fernandez, S. Sanchez-Segado and F.J. Alguacil, *J. Membr. Sci*., 2011, 376, 1–14.

32. J. Yuan, D. Mecerreyes and M. Antonietti, *Progress in Polymer Science*, 2013, 38.7, 1009-1036.

33. J. Yuan and M. Antonietti, *Polymer*, 2011, 52 1469-1482.

34. T. D. Ho, A. J. Canestraro and J. L. Anderson, *Anal. Chim. Acta*, 2011, 695, 18-43.

35. S. T. Hemp, M. H. Allen, M. D. Green and T. E. Long, *Biomacromolecules*, 2012, 13, 231-238.

36. Y. Kohno and H. Ohno, *Aust. J. Chem*., 2012, 65, 91-94.

37. L. C. Tomé, D. Mecerreyes, C. S. R. Freire, L. P. N. Rebelo and I. M. Marrucho, *J. Mater. Chem. A*, 2014, 2, 5631-5639.

38. J. E. Bara, S. Lessmann, C. J. Gabriel, E. S. Hatakeyama, R. D. Noble and D. L. Gin, *Ind. Eng. Chem. Res*., 2007, 46, 5397-5404.

39. K. Simons, K. Nijmeijer, J. E. Bara, R. D. Noble and M. Wessling, *J. Membr. Sci*., 2010, 360, 202-209.

40. J. E. Bara, C. J. Gabriel, E. S. Hatakeyama, T. K. Carlisle, S. Lessmann, R. D. Noble and D. L. Gin, *J. Membr. Sci*., 2008, 321, 3-7.

41. J. E. Bara, E. S. Hatakeyama, C. J. Gabriel, X. Zeng, S. Lessmann, D. L. Gin and R. D. Noble, *J. Membr. Sci*., 2008, 316, 186-191.

42. T. K. Carlisle, E. F. Wiesenauer, G. D. Nicodemus, D. L. Gin and R. D. Noble, *Ind. Eng. Chem. Res.*, 2013, 52, 1023-1032.

43. http://www.co2crc.com.au/ (15 May 2016)

44. H. Cong, B. Yu, J. Tang and X. Zhao, *J. Polym. Res.*, 2012, 19, 1-6.

45. J. E. Bara, E. S. Hatakeyama, D. L. Gin and R. D. Noble, *Polym. Adv. Technol*., 2008, 19, 1415-1420.

46. J. E. Bara, D. L. Gin and R. D. Noble, *Ind. Eng. Chem. Res*., 2008, 47, 9919-9924.

47. J. E. Bara, R. D. Noble and D. L. Gin, *Ind. Eng. Chem. Res*., 2009, 48, 4607-4610.

48. L. C. Tomé, A. S. L. Gouveia, C. S. R. Freire, D. Mecerreyes and I. M. Marrucho, *J. Membr. Sci*., 2015, 486, 40-48.

49. P. Li, K. P. Pramoda and T.-S. Chung, *Ind. Eng. Chem. Res*., 2011, 50, 9344-9353.

50. S. M. Mahurin, J. S. Lee, G. A. Baker, H. Luo and S. Dai, *J. Membr. Sci*., 2010, 353, 177-183.

51. J. Yuan, D. Mecerreyes and M. Antonietti, *Prog. Polym. Sci*., 2013, 38, 1009-1036.

52. Y. C. Hudiono, T. K. Carlisle, J. E. Bara, Y. Zhang, D. L. Gin and R. D. Noble, *J. Membr. Sci*., 2010, 350, 117-123.

53. L. C. Tome, M. Isik, C. S. R. Freire, D. Mecerreyes and I. M. Marrucho, *J. Membr. Sci*., 2015, 483, 155-165.

54. R. D. Noble, D. L. Gin, *J. Membr. Sci*., 2011, 369, 1–4.

55. L. C. Tomé, D. Mecerreyes, C. S. R. Freire, L. P. N. Rebelo, I. M. Marrucho, *J. Membr. Sci*., 2013, 428, 260–266.

56. R. M. Felder, *J. Membr. Sci*., 1978, 3 15-27

57. P. Taveira, A. Mendes and C. Costa, *J. Membr. Sci*., 2003, 221, 123–133.

58. H.A. Daynes, *Proc. Roy. Soc. Lond*. 1920, 497, 286-307.

59. X. Q. Nguyen, Z. Brož, P. Uchytil and Q. T. Nguyen, *J. Chem. Soc. Faraday Trans*., 1992, 88(24), 3553-3560.

60. S. W. Rutherford, and D. D. Do, *Adsorption 3*, 1997, 4, 283-312.

61. L. C. Tomé, C. Florindo, C. S. R. Freire, L. P. N. Rebelo and I. M. Marrucho, *Phys. Chem. Chem. Phys.*, 2014, 16, 17172-17182.

62. H. Tokuda, S. Tsuzuki, M. A. B. H Susas, K. Hayamizu, and M. Watanabe, *J. Phys. Chem. B*, 2006, 110(39), 19593-19600.

63. M. J. Muldoon, S. N. V. K. Aki, J. L. Anderson, J. K. Dixon and J. F. Brennecke, *J. Phys. Chem. B*, 2007, 111, 9001–9009.

64. P. Li, D. R. Paul and T. S. Chung., *Green Chem*., 2012, 14, 1052-1063.

65. T. K. Carlisle, J. E. Bara, A. L. Lafrate, D. L. Gin, R. D. Noble, *J. Membr. Sci*., 2010, 359, 37-43.

66. L. C. Tomé, M. A. Aboudzadeh, L. P. N. Rebelo, C. S. R. Freire, D. Mecerreyes and I. M. Marrucho, *J. Mater. Chem. A*, 2013, 1, 10403-10411.

67. W. S. Chi, S. U. Hong, B. Jung, S. W. Kang, Y. S. Kang and J. H. Kim, *J. Membr. Sci*., 2013, 443, 54-61.

68. http://www.ico2n.com/ (15 May 2016)

69. http://www.netl.doe.gov/ (15 May 2016)

70. http://www.jisf.or.jp/ (15 May 2016)

71. H. Liu, S. Dai and D. Jiang, *Phys.Chem.Chem.Phys.*, 2014, 16, 1909-1913.

72. P. R. Bevington and D. K. Robinson, *Data reduction and error analysis for the physical sciences,* McGraw-Hill, 2003.

6. Appendixes

Table 12 – CO_2 and N_2 permeability and CO_2/N_2 permselectivity values for all the PIL-IL composite membranes measured in this work. Sensitivity of the time-lag apparatus prevented a reliable measurement of the N_2 time-lag for some membranes and, consequently, the determination of N_2 permeability and CO_2/N_2 permselectivity.

Composite Membrane	**Permeability (Barrer)**		**$\alpha CO_2/N_2$**
	CO_2	**N_2**	
PIL $N(CN)_2$ - 20 IL $C(CN)_3$	1.6	-	-
PIL $N(CN)_2$ - 40 IL $C(CN)_3$	30.8	1.4	24.3
PIL $N(CN)_2$ - 60 IL $C(CN)_3$	249.0	4.1	61.3
PIL $C(CN)_3$ - 20 IL $N(CN)_2$	16.2	-	-
PIL $C(CN)_3$ - 40 IL $N(CN)_2$	198.8	3.0	67.0
PIL $C(CN)_3$ - 20 IL $B(CN)_4$	6.3	0.1	46.7
PIL $C(CN)_3$ - 40 IL $B(CN)_4$	133.4	2.4	56.3
PIL $C(CN)_3$ - 60 IL $B(CN)_4$	472.7	8.7	54.4
PIL C(CN)3 - 20 IL $[C_2mim][NTf_2]$	2.8	-	-
PIL C(CN)3 - 40 IL $[C_2mim][NTf_2]$	50.4	1.2	42.9
PIL $C(CN)_3$ - 20 IL $[Pyr_{14}][NTf_2]$	1.8	-	-
PIL $C(CN)_3$ - 40 IL $[Pyr_{14}][NTf_2]$	35.4	1.0	36.6
PIL $B(CN)_4$ - 40 IL $C(CN)_3$	184.9	3.9	48.0
PIL $B(CN)_4$ - 60 IL $C(CN)_3$	502.1	11.6	43.1
PIL B(CN)4 - 20 IL $[C_2mim][NTf_2]$	5.6	0.1	40.1
PIL B(CN)4 - 40 IL $[C_2mim][NTf_2]$	46.7	2.1	22.5
PIL NTf_2 - 20 IL $N(CN)_2$	116.8	2.7	43.2
PIL NTf_2 - 20 IL $C(CN)_3$	99.7	2.6	38.6
PIL NTf_2 - 20 IL $B(CN)_4$	91.4	2.3	40.1
PIL NTf2 - 20 IL $[C_2mim][NTf_2]$	70.4	2.2	32.2
PIL NTf2 - 40 IL $[C_2mim][NTf_2]$	202.7	5.9	35.0

Table 13 - CO_2 and N_2 diffusivity and CO_2/N_2 diffusivity selectivity values for all the PIL-IL composite membranes measured in this work. Sensitivity of the time-lag apparatus prevented a reliable measurement of the N_2 time-lag for some membranes and, consequently, the determination of N_2 diffusivity and CO_2/N_2 diffusivity selectivity.

Composite Membrane	**Diffusivity (m^2/s) x 10^{12}**		**D CO_2/N_2**
	CO_2	**N_2**	
PIL $N(CN)_2$ - 20 IL $C(CN)_3$	3.5	-	-
PIL $N(CN)_2$ - 40 IL $C(CN)_3$	23.6	64.0	0.4
PIL $N(CN)_2$ - 60 IL $C(CN)_3$	111.2	173.0	0.6
PIL $C(CN)_3$ - 20 IL $N(CN)_2$	9.1	-	-
PIL $C(CN)_3$ - 40 IL $N(CN)_2$	139.5	285.2	0.5
PIL $C(CN)_3$ - 20 IL $B(CN)_4$	4.4	5.6	0.8
PIL $C(CN)_3$ - 40 IL $B(CN)_4$	52.4	77.1	0.7
PIL $C(CN)_3$ - 60 IL $B(CN)_4$	135.4	181.8	0.7
PIL C(CN)3 - 20 IL [C_2mim][NTf_2]	1.9	-	-
PIL C(CN)3 - 40 IL [C_2mim][NTf_2]	22.8	42.9	0.5
PIL $C(CN)_3$ - 20 IL [Pyr_{14}][NTf_2]	1.9	-	-
PIL $C(CN)_3$ - 40 IL [Pyr_{14}][NTf_2]	15.7	25.1	0.6
PIL $B(CN)_4$ - 40 IL $C(CN)_3$	63.8	123.5	0.5
PIL $B(CN)_4$ - 60 IL $C(CN)_3$	150.1	324.9	0.5
PIL B(CN)4 - 20 IL [C_2mim][NTf_2]	2.7	18.2	0.1
PIL B(CN)4 - 40 IL [C_2mim][NTf_2]	14.7	31.1	0.5
PIL NTf_2 - 20 IL $N(CN)_2$	47.4	64.6	0.7
PIL NTf_2 - 20 IL $C(CN)_3$	42.4	56.2	0.8
PIL NTf_2 - 20 IL $B(CN)_4$	32.4	42.3	0.8
PIL NTf2 - 20 IL [C_2mim][NTf_2]	28.8	49.7	0.6
PIL NTf2 - 40 IL [C_2mim][NTf_2]	73.4	110.4	0.7

Table 14 - CO_2 and N_2 solubility and CO_2/N_2 solubility selectivity values for all the PIL-IL composite membranes measured in this work. Sensitivity of the time-lag apparatus prevented a reliable measurement of the N_2 time-lag for some membranes and, consequently, the determination of N_2 solubility and CO_2/N_2 solubility selectivity.

Composite Membrane	**Solubility (m^3(STP).m^{-3}.Pa-1) x 10^6**		**S CO_2/N_2**
	CO_2	**N_2**	
PIL $N(CN)_2$ - 20 IL $C(CN)_3$	3.4	-	-
PIL $N(CN)_2$ - 40 IL $C(CN)_3$	9.8	0.1	66.0
PIL $N(CN)_2$ - 60 IL $C(CN)_3$	16.8	0.2	95.3
PIL $C(CN)_3$ - 20 IL $N(CN)_2$	13.3	-	-
PIL $C(CN)_3$ - 40 IL $N(CN)_2$	10.7	0.1	136.8
PIL $C(CN)_3$ - 20 IL $B(CN)_4$	10.8	0.2	59.7
PIL $C(CN)_3$ - 40 IL $B(CN)_4$	19.1	0.2	83.2
PIL $C(CN)_3$ - 60 IL $B(CN)_4$	26.2	0.4	73.0
PIL C(CN)3 - 20 IL [C_2mim][NTf_2]	11.0	-	-
PIL C(CN)3 - 40 IL [C_2mim][NTf_2]	16.6	0.2	78.6
PIL $C(CN)_3$ - 20 IL [Pyr_{14}][NTf_2]	7.1	-	-
PIL $C(CN)_3$ - 40 IL [Pyr_{14}][NTf_2]	16.9	0.3	58.3
PIL $B(CN)_4$ - 40 IL $C(CN)_3$	21.7	0.2	92.9
PIL $B(CN)_4$ - 60 IL $C(CN)_3$	25.1	0.3	93.3
PIL B(CN)4 - 20 IL [C_2mim][NTf_2]	15.9	0.1	274.2
PIL B(CN)4 - 40 IL [C_2mim][NTf_2]	23.8	0.50	47.6
PIL NTf_2 - 20 IL $N(CN)_2$	18.5	0.3	58.7
PIL NTf_2 - 20 IL $C(CN)_3$	17.7	0.3	51.2
PIL NTf_2 - 20 IL $B(CN)_4$	21.2	0.4	52.3
PIL NTf2 - 20 IL [C_2mim][NTf_2]	18.4	0.3	55.6
PIL NTf2 - 40 IL [C_2mim][NTf_2]	20.7	0.4	52.6